

Methods and Principles in Medicinal Chemistry Series

CASE STUDY SAMPLER

INCLUDING

Chapter 21: **GPR81 HTS Case Study** by Eric Wellner and Ola Fjellström from
Lead Generation: Methods, Strategies, and Case Studies edited by Jörg Holenz

Chapter 22: **The Integrated Optimization of Safety and DMPK Properties Enabling
Preclinical Development: A Case History with S1P₁ Agonists** by Simon Taylor from
Early Drug Development: Bringing a Preclinical Candidate to the Clinic edited by
Fabrizio Giordanetto.

Chapter 14: **BACE Inhibitors** by Daniel F. Wyss, Jared N. Cumming, Corey O. Strickland,
and Andrew W. Stamford from **Fragment-based Drug Discovery: Lessons and Outlook**
edited by Daniel A. Erlanson and Wolfgang Jahnke

21

GPR81 HTS Case Study

Eric Wellner and Ola Fjellström

21.1

General Remarks

One of the key lead generation strategies to identify new chemical entities against a certain target is high-throughput screening (HTS). Running an HTS requires a clear line of sight regarding the pharmacodynamic (PD) and pharmacokinetic (PK) profile of the compounds one is interested in. This means that there has to be a clear screening and deconvolution strategy in place to successfully assess the hits from an HTS output. The intended outcome of an HTS is the identification of compounds that both engage the appropriate target and produce the desired effect. It is based on serendipity; running a large number of structurally diverse compounds will usually favor the identification of novel hit structures. The screening cascade has to match this demand and the assay performance has to be closely monitored and should provide a highly reliable signal.

HTS stands at the interface between target biology and chemistry space, and the chemist assessing an HTS output will need a detailed understanding of (a) each readout from the screening cascade, (b) the possible interferences, and (c) the selection criteria at hand. In other words, what signal is measured in the assay, what would lead to a false positive signal and finally is the measured signal significant? In the hit evaluation phase (HE) of the HTS, structure–activity relationships (SARs) and structure–property relationships (SPRs) will be established and matched with the desired *in vitro* PD and PK properties of the hits. All these steps require excellent feedback loops between chemistry and biology to achieve a successful HTS campaign.

In the following chapters, the case study of a GPR81 agonist campaign will outline the key principles of an HTS process from a medicinal chemistry perspective. Rather than presenting a glossy success story, the aim of this case study is to provide a more nuanced picture about a “real-life” HTS campaign with all its dead ends, difficulties, and opportunities.

21.2

The Target

The G-protein-coupled receptor 81 (GPR81), also known as hydroxycarboxylic acid receptor 1 (HCA1), is highly homologous to GPR109a and GPR109b. All three receptors are activated by hydroxycarboxylic acid ligands originating from energy metabolism [1] and they display a high selectivity for their endogenous ligands (lactate for GPR81, 3-hydroxy-butyrate for GPR109a, and 3-hydroxy-octanoate for GPR109b) as shown in Diagram 21.1.

GPR81 is highly expressed in adipose tissue and has been identified as a G_i -type receptor coupled to a decrease in the cellular concentration of cAMP [1,2]. Early on, there was some evidence that lactate leads to an antilipolytic effect resulting in inhibition of free fatty acid (FFA) release from adipocytes [3]. Excess circulating FFA is a metabolic defect commonly seen in type 2 diabetic (T2D) patients and the scientific rationale for GPR81 agonism is based on lowering plasma FFA. GPR81 is thought to have a main role in regulating insulin's inhibitory effect on FFA release from adipose tissue. A GPR81 agonist will lower plasma FFA and switch energy substrate utilization from fat to carbohydrate. Inhibiting the high FFA flux seen in patients with insulin resistance and diabetes should improve insulin sensitivity in muscle and liver by reducing ectopic lipid storage. Inhibition of lipolysis should also in the long term result in reduced cardiovascular (CV) morbidity and mortality in T2D patients with multiple CV

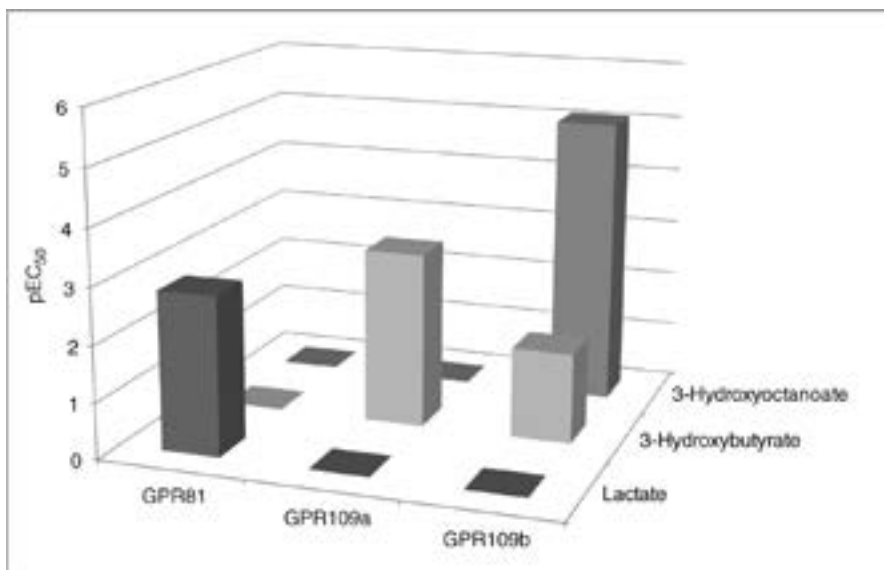


Diagram 21.1 pEC_{50} values of endogenous ligands for the HCA receptor family in human GTP γ S binding assays.

risk factors. Similar effects are well documented for drugs targeting the GPR109a receptor. However, the beneficial antilipolytic effect in clinical trials seen for GPR109a agonism is offset by the severe flushing side effects caused by the activation of Langerhans cells in the skin [4]. Another drawback is that GPR109a receptor internalization [5] is thought to be the underlying cause for the tachyphylactic effect of many known GPR109a agonists making it a more difficult druggable target [6]. Since GPR81 is mainly expressed in adipocytes, the unfavorable profile of GPR109a agonists might not be shared by GPR81 agonists.

21.3

Screening Cascade

Several considerations have to be made to ensure that the profile of a compound matches the desired pharmacodynamic outcome. The bioscientist and the medicinal chemist have to ensure that the screening cascade is predictive and that all decisions, whether to progress a compound or not, are well understood. The screening cascade and the progression criteria are designed to prioritize compounds with the most favorable hit profile. In the GPR81 campaign, the following selection criteria were initially considered:

- Compounds should be agonists of both the human and the rat GPR81 receptor.
- Compounds should engage the receptor in a G_i -signaling manner leading to inhibition of adenylyl cyclase activity.
- G_i -activation should be achieved solely through the GPR81 receptor and not by another target or background signal.
- False positive technology hitters should be removed using an orthogonal assay.
- Compound purity should be >85%.

Each compound passing these initial filters will be considered to enter the secondary screening cascade.

In detail, the primary activity assay is run as a single-point HTS screen at 10 μ M compound concentration. GPR81 is a $G_{\alpha i}$ -coupled receptor overexpressed in CHO-TREx cells. Upon receptor activation, the G_{α} -unit dissociates from the heterotrimeric $G_{\alpha\beta\gamma}$ -protein leading to inhibition of the adenylyl cyclase (AC) and a reduction of cAMP ($G_{\text{inhibition}}$ -type coupling). To measure the inhibition of AC, the cAMP levels in the cells are increased by forskolin stimulation of AC and the cAMP production can be inhibited by agonist activation of the GPR81 receptor. The effect of the compound is determined by the time resolved-FRET (TRF) signal at 665 nm where cAMP competes with an Eu-labeled cAMP for a FRET partner and alternates the FRET signal at 665 nm. Residual energy from the europium chelate will produce light at 615 nm that is also measured and used for signal ratio calculation (see Figure 21.1a and b). The ratio is translated

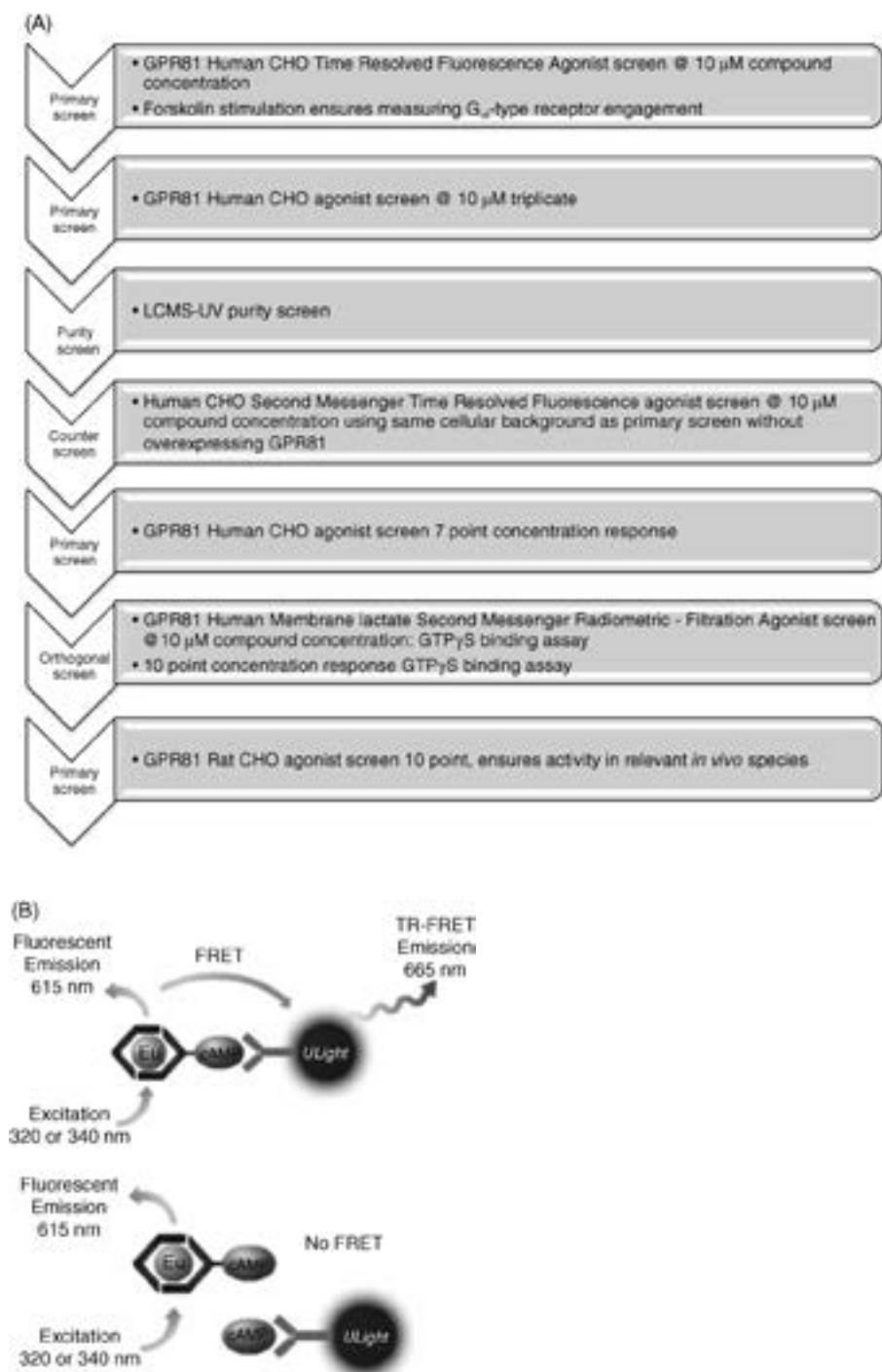


Figure 21.1 (a) Initial screening cascade of the GPR81 campaign was designed to identify hits producing a signal on the GPR81 receptor not related to off-target activity or technology. (b) LANCE cAMP assay principle.

into a % effect value. Compounds with an effect > 4 times the interquartile range were considered to be active. This corresponds to an activity cutoff at 15% effect.

There are some general pitfalls for the medicinal chemist to consider when running and evaluating a cellular GPCR agonist single-point screen.

- The cutoff criteria are biased and mainly designed to avoid too many false positives.
- Effect data do not necessarily reflect the potency of the compounds. It is tempting for the chemist to interpret high-effect values as high potency and vice versa. There is no linear correlation between effect data in a single-point screen and the % effect values generated in a full curve concentration response assay.
- Compounds having an EC_{50} around 3–30 μ M are probed in the steep part of their EC_{50} curves. In a single-point experiment, small concentration shifts inside the well due to titration can lead to big changes in the observed effect in a retest.
- Overexpression of the receptor in a transfected cell line is artificial and leads to a high receptor reserve in case of GPCRs that might exaggerate the effect of a compound leading to a left shift of the concentration response curve. A straight 1:1 potency translation into more relevant or endogenous cell line might be compromised.
- Partial versus full agonism is hard to assess. Receptor overexpressing cell lines might not show partial agonism, and a low effect in the single point could still be a very potent partial agonist. A partial agonist in an overexpressing cell line might act as a functional antagonist in a more relevant cell line.
- Technology hitters will lead to false positive signals, that is, fluorescent compounds might interfere with the FRET technology.
- Low solubility in the buffer can result in loss of compound effect due to precipitation.
- Permeability can be an issue since, although GPCRs are membrane-bound receptors and represent an extracellular target, the binding site can still be buried deep in the membrane.
- Cellular assay systems often require BSA. Since most of HTS compound collections are historically grown, many compounds might have poor overall physicochemical properties leading to high protein binding. While 0.1% w/v BSA might appear low, it still means that the solution has a concentration of about 15 μ M BSA. Depending on the affinity of a compound for BSA, this can significantly lower the fraction unbound in the assay.
- Aggregators might lead to physical phase transition and affect the target interaction.

21.4

Compound Selection (10 k Validation Set)

It is good practice as part of any HTS to perform a critical evaluation of a test set comprising about 10 000 diverse compounds (10 k validation set). This set should contain a representative selection of the overall compound collection. Other hypotheses, not based on serendipity, can also be assessed. Usually, reference compounds from patents and literature are included and nearest neighbours (NN) are selected or designed to expand the knowledge around these known structures. Another approach is to consider the endogenous ligand and identify NN to the natural ligand present in the compound collection. The third approach is to look at the phylogenetic tree of the target, identify compounds known to act on related targets, and include them in the initial 10 k set screen. This approach is based on the selective optimization of side activities (SOSA) principle [7] where structurally related targets might bind a pool of related compounds. Virtual screening, using a model or a known structure of the target, can also be applied to identify a rational hypothesis to include certain compound structures into a screen. There are many examples in the literature where these rational approaches have replaced an HTS campaign. However, an internal analysis of several HTS campaigns against a variety of targets showed that the hit rates derived from focused or selected libraries are often lower compared to a full HTS. An exception is where compounds share a very high similarity to known ligands [8].

The use of physicochemical properties for compound selection has also been widely discussed in the industry and literature [9]. There is no doubt that compounds with inflated physicochemical properties such as high lipophilicity, basicity, and/or number of hydrogen bonds are more likely to encounter poor metabolic stability [10], low permeability [11], high degree of promiscuity [9a], and toxicity issues. Today's hit evaluation is a far cry from potency-driven campaigns. Evaluation of compounds includes a balanced view on physicochemical properties, ADME properties, efficacy, and potency. There are strong arguments to start with small leads or even fragments and use various indices to maintain their fitness through the hit expansion and lead generation phase [12]. Another approach would be to start with a potent hit and evaluate if it's possible to expand the SAR into a favorable physicochemical and ADME property space. It is our experience that hit expansion and evaluation should not limit itself to one or the other approach. In the case of campaigns with access to structural information, the first approach has a clear rationale of how to maintain fitness. Still, any fragment-based lead generation [13] (FBLG) campaign profits significantly if it is supported by an HTS and uses confirmed hits as a template for fragment expansion. In case where no structural information is available and hit expansion relies on a ligand-based strategy, the second approach is often easier and more successful.

One advantage of evaluating a 10 k selection before running the full HTS is that the set can be used to ensure the quality of the screen and to estimate the

Table 21.1 A short checklist on the use of the 10 k set in an HTS campaign.

Information extracted from 10 K set	Comments
Hit rate	Should reflect the hit rate of the HTS
Single-concentration effect	Can later be correlated with the HTS output to ensure quality of the screen
Early hits	Can be used as tool compounds for further evaluation, e.g. counterscreen or performance of secondary screens
Possible off-target or technology-dependent activities	The assays propensity to identify off-target-related hits or technology hitters can be assessed
Potency	Provides information in which potency range compounds will be identified by the HTS

hit rate. For example, a hit rate above 5% might indicate that there will be limitations in running the hit evaluation screening cascade successfully. Additionally, early tool compounds can often be identified that can be used for further evaluation of the target and additional assays. Table 21.1 provides a short checklist on how the 10 k set can be used in an HTS campaign.

The 10 k set should always be retested as part of the full HTS campaign to assess reproducibility.

In the case of GPR81, only two ligands were known to activate the receptor at the time we started the campaign. The endogenous ligand, lactate, itself has a rather low affinity to the receptor [14]. Arena Pharmaceuticals has also published a series of imidazopyridines and provided potency both data of several compounds tested in a GTP γ S- and HTRF-cAMP assay as well as the antilipolytic effect of compound **1** *in vivo*. The potency of the compounds was in the medium-to-low nM range [15]. Two representatives (**1**, **2**) were dosed orally in a rat model at up to 100 mg/kg. The FFA levels were determined and compared with those of animals only dosed with the formulation or niacin **3**, and showed a significant effect on FFA lowering (Figure 21.2).

This data provided a clear rationale to include imidazopyridines into the 10 k set and expand the series with an additional five representatives known from the publication. The 10 k set also included 900 lactate analogs with a MW cutoff below 450, mimicking the natural ligand. The remainder of the set contained a 2000 SOSA compound set that included privileged structures against a series of targets, a set of frequent/technology hitters (3000 compounds, FH set) and about 4000 compounds randomly chosen from the compound collection. The rationale behind this set of compounds was that compounds with good drug-like properties are good starting points for new drugs. Developing target selectivity is often possible, to adjust the pharmacology of the compounds, while keeping the favorable pharmacokinetic properties. The cutoff criterion for an active hit was set to 15% effect in a single concentration screen at 10 μ M. The results are summarized in Figure 21.3.

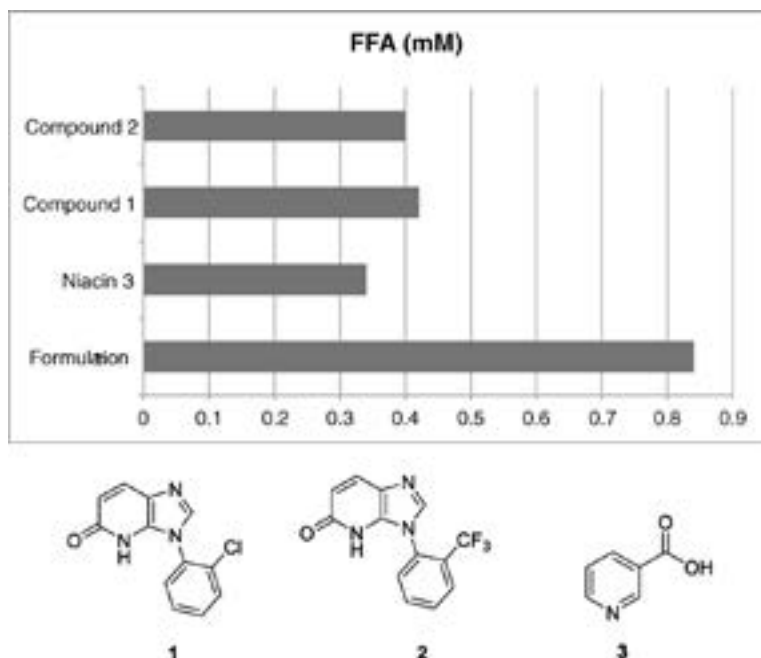


Figure 21.2 *In vivo* effect of imidazopyridin-5-ols (1,2) and niacin 3 (GPR109a agonist) on FFA lowering. Compounds are reported to be dosed at 100 mg/kg.

The overall hit rate of the 10 k set was 0.66% (66 actives). The hit rates for the subsets were 1.2% for the FH set, 0.55% for the SOSA set, and 0.43% for the randomly chosen set. No actives were found among the lactate mimetics. This was not too surprising considering the low potency of the natural agonist. However, it also indicated that expanding the search around the natural ligand using analogs would probably be difficult. Further, looking at the high hit rate coming from the FH set (blue in Figure 21.3), it was apparent that the screen had some propensity to respond to fluorescent compounds and/or GPCR ligands. The counterscreen using the same technology and cellular background was designed to filter this out. Another observation from the 10 k set was that compounds from the SOSA or randomly chosen compound set could be found in the lower range of the effect data. This indicated that finding strong full agonists would be a challenge. Overall, the results suggested that the hit rate of the full deck would be between 0.5 and 1% indicating that the capacity of the counter- and secondary screens would be sufficient.

Examining the reference compound **1**, it was particularly surprising that compound **1** gave only a 30% effect signal at 10 μ M concentration. The EC_{50} value of the compound was determined in a 10-point triplicate concentration response experiment on nine different occasions. The compound behaved as a partial agonist in our hands with a mean potency of 340 ± 40 nM and a mean top effect of

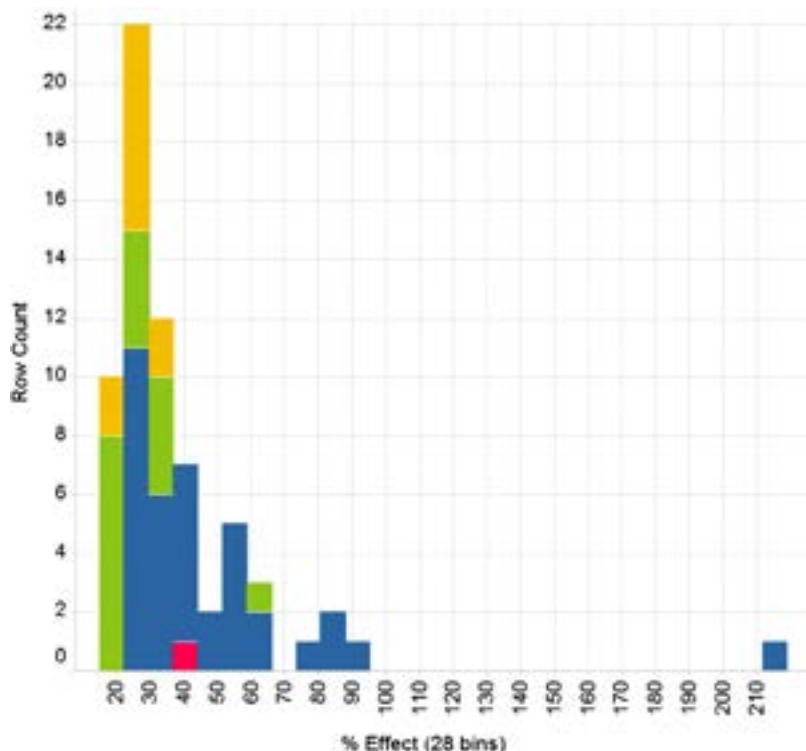


Figure 21.3 Outcome of the 10 k screen. Only compounds assigned as actives are presented. Inactives are not shown. The row count gives the number of compounds active for a certain % effect range. The bars are stacked. The color coding depicts the origin of

the compounds. Red represents compound 1, yellow are compounds from the SOSA set, and green and blue bars represent compounds derived from the random and frequent/technology hitter set, respectively.

$56 \pm 3\%$. The curve-fits of compound **1** are given in Figure 21.4. Looking at the spread of effect values for the baseline and the top efficacy, it becomes very clear why an HTS readout is in most cases not a quantitative assessment of an effect at a single concentration. This is the challenge many medicinal chemists face when confronted with HTS data. Compound **1** shows at $10 \mu\text{M}$ concentration for single-point data a variation in effect between 36 and 69%. Looking at the steep part of the curve, the variation of effect values at 300 nM is between 3 and 49%. This illustrates the risk of overinterpreting HTS results.

In fact, all compounds of the imidazopyrimidine series behaved in our hands as partial agonists, which is one reason why they were so hard to detect in the single-point screen. Results are given in Table 21.2. This limited their use as possible tools for target validation since it is a well-described phenomenon that partial agonist competing with the endogenous full agonist can behave as functional antagonists [16].

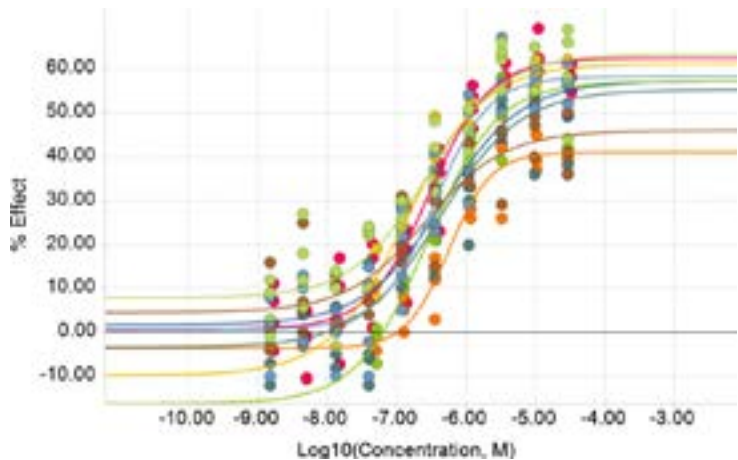
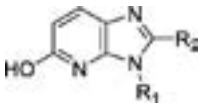


Figure 21.4 The color of the curves represents the various test occasions. All points were measured in triplicates. Compound **1** behaved in this cell line and under these assay conditions as a partial agonist.

Table 21.2 In-house efficacy and potency data of imidazopyrimidines.

Compound		Mean EC ₅₀ [μM]	Mean top effect%	N
1	R ₁ = <i>o</i> -Cl-phenyl; R ₂ = H	0.31	55	9
2	R ₁ = <i>c</i> -Heptyl; R ₂ = H	0.20	46	5
3	R ₁ = Adamant-1-yl; R ₂ = H	0.11	60	9
4	R ₁ = <i>c</i> -Heptyl; R ₂ = Methyl	0.19	52	6
5	R ₁ = Tetrahydropyran-4-yl; R ₂ = H	3.65	17	3

N = number of times tested.

In contrast to the reported literature data [15], we could not confirm an anti-lipolytic effect of compound **1** *in vivo* despite good oral exposure.

21.5
HTS

In the GPR81 human CHO lactate second messenger TRF agonist screen, 941 439 compounds were tested. The cutoff criterion for an active hit was set to 15%. Corresponding to a hit rate of 0.57%, 5345 primary actives were identified. All actives were retested at 10 μM single concentration in triplicates. In this

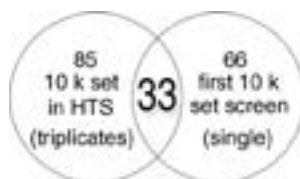


Figure 21.5 Overlap between the two 10 k set screening occasions. The numbers represent the active hits.

retest, 2882 compounds were identified as actives having an average effect above 15%, resulting in an overall hit rate of 0.31%. The initial 10 k set was included in the HTS run and both readouts were compared. Only 50% of the initial hits coming from the 10 k set could be recovered from the HTS output, while 52 new hits coming from the 10 k set were discovered in the HTS (Figure 21.5).

The % effect correlation between the two different occasions at which the 10 k set was run was limited possibly due to the fact that single data points are compared with the mean value of a triplicate data point in Figure 21.6. Interestingly,

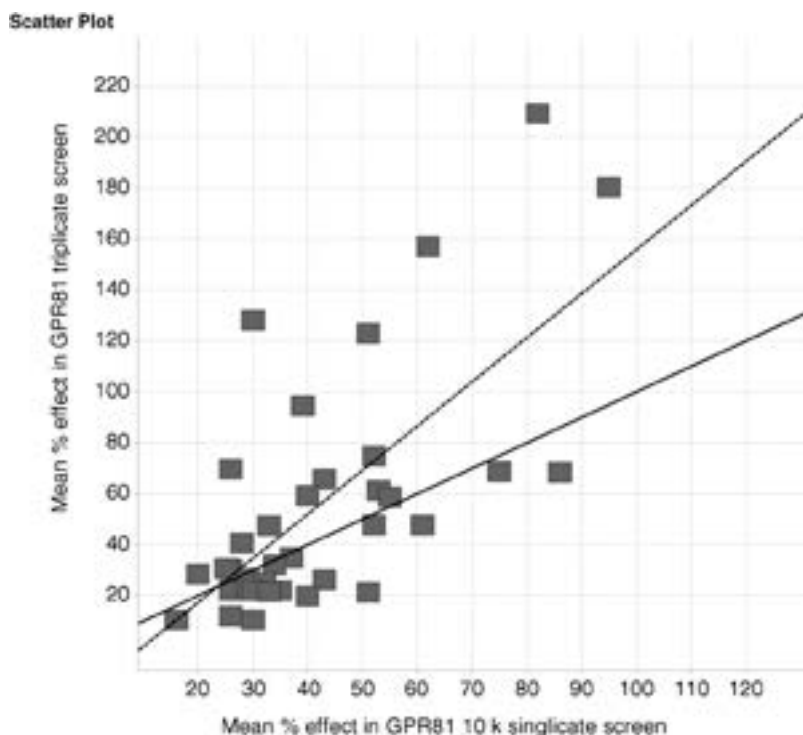


Figure 21.6 Comparison between the mean retest triplicate % effect of the 10 k set hits coming from the HTS and the initial % effect of the 10 k data set (single-point data). The

dotted line represents the straight line fit of the overlapping active hits. The R^2 of the regression is 0.465. The solid line represents the line of unity.

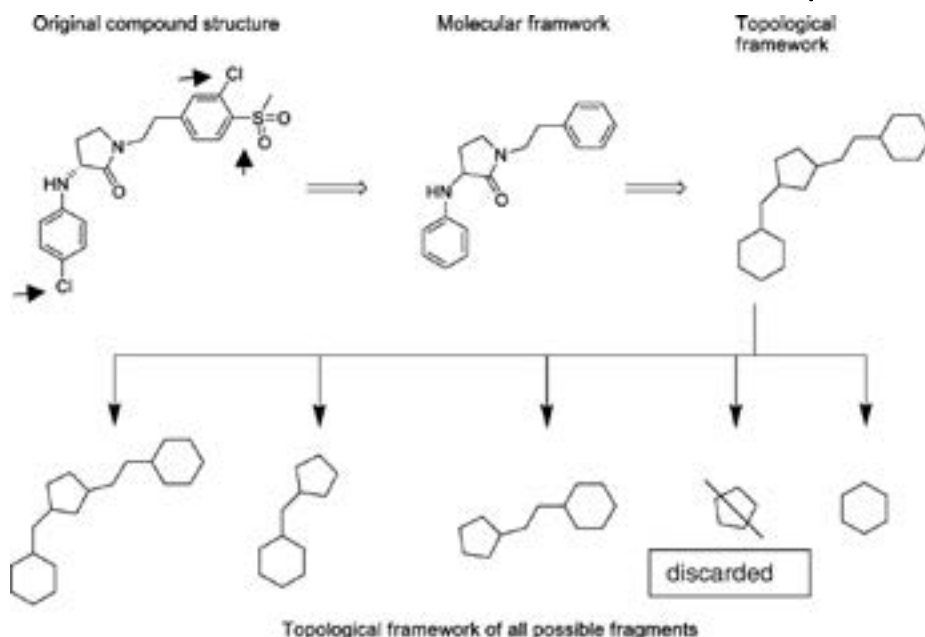


Figure 21.7 Side chains (arrow) are defined as atoms not connected via a linker to another ring system. In the first step, side chains and chiral information are removed leading to a molecular framework. In the next step, all functional groups are removed and heteroatoms are replaced by carbon atoms leading to

the topological framework. In the final step, the topological framework is fragmented by breaking all possible linker parts yielding a series of various subfragments. Fragments smaller than six-membered ring systems were discarded.

of all compounds in the HTS. To assess the activity of a certain scaffold, the two distributions were plotted as empirical cumulative distribution functions against each other and the maximum D shifts were calculated. Negative D -values indicate that the activity distribution of a cluster of compounds is shifted to lower effect values compared to the distribution of all compounds. Positive D shifts indicate that the distribution of the compounds associated with the fragment is shifted to higher % effect values than the background distribution. Negative D -shifted fragments could be interpreted as compound clusters with a possible inverse agonistic effect. This was however not followed up (Figure 21.9).

Due to the low hit rate in the GPR81 HTS, we were more concerned about false negatives rather than false positives. Therefore, we considered even compound clusters with small D_{\max} shifts, few compounds and therefore lower significance level. One point made in the literature regarding CSE [20] is that this method compensates for the lack of replicates in the HTS by pooling compounds into groups and makes a statistical signal evaluation of the group

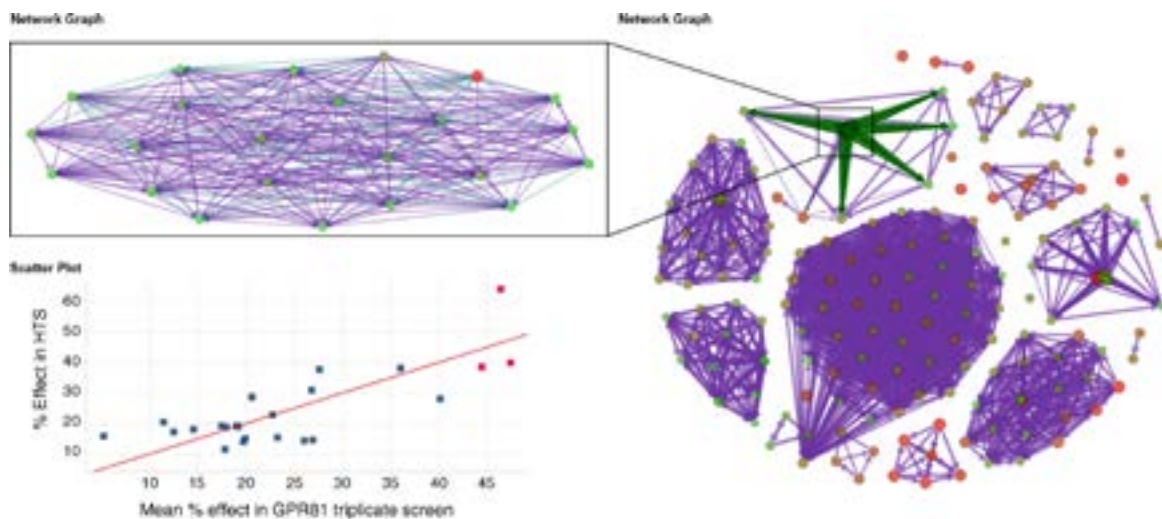


Figure 21.8 The right network map represents the Murcko fragments as nodes. There are islands with nodes that are closely related to each other surrounded by unrelated nodes. The left network plot in the box zooms in on an island of related nodes and maps the intercorrelation of the nodes to each other based on the Tanimoto overlap. The colors in the plot represent the D_{\max} values for a positive shift resulting from the KS statistics. Red indicates a low

D_{\max} shift, while green indicates a larger positive shift. The scatter plot zooms in on the compound activity of molecules that are associated with a certain fragment. % Effect is the effect of the compound in the HTS screen, while the triplicate data represent the effect data from the triplicate confirmation screen. Compounds classified as actives and inactives from the HTS are marked red and blue, respectively.

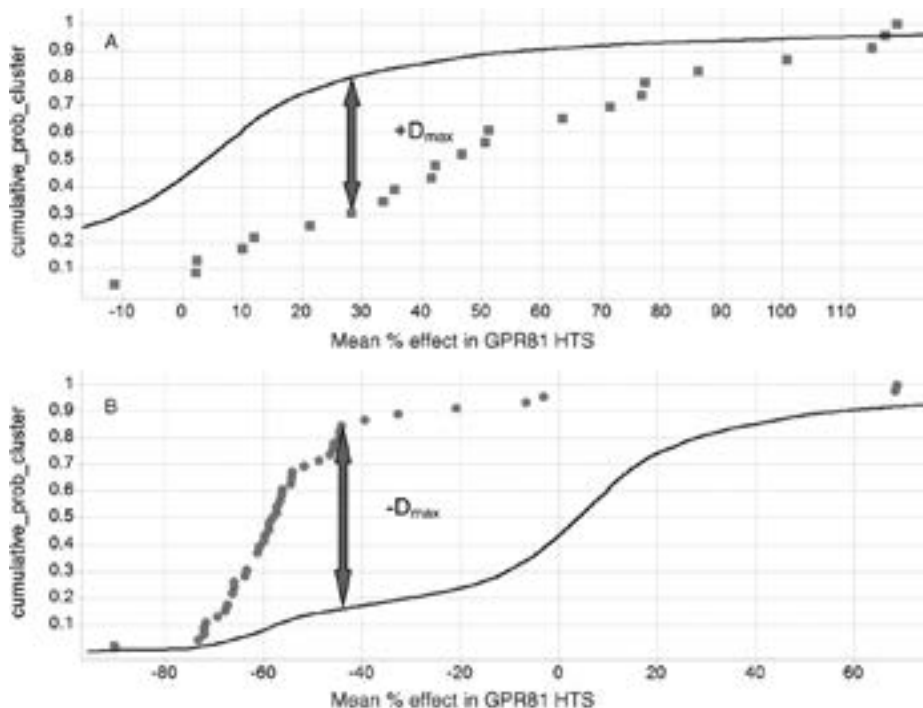


Figure 21.9 Both graphs plot the cumulative probability function of all compounds (black line) and the cumulative probability function of the fragments (A: squares, B: circles) against the % effect seen in the HTS. In graph A, a “positive” D_{max} shift results from fragment distribution versus the HTS distribution. In graph B, a “negative” D_{max} shift results from the fragment distribution compared to the HTS distribution.

rather than of a single compound. This is powerfully demonstrated in the example shown in Figure 21.10. All fragments relate to a molecular framework containing a benzothiazoleacylurea core structure **A**. All fragments show a strong Tanimoto overlap of >0.7 . Furthermore, all fragments have a D_{max} shift >0.64 (0 being the minimum and 1 the maximum possible value). There is an excellent correlation between triplicate and HTS data for this scaffold confirming the significance of this methodology.

One could argue that most of these compounds would have been picked up by the usual HTS evaluation due to their rather high effect data. A different picture emerges when looking at fragments associated with compounds having a low % effect in the HTS. The molecular scaffold **B** in Figure 21.11 was identified from two fragments with $0.51 < D_{max} < 0.61$.

Pushing these compounds with borderline and below cutoff criteria effect into the triplicate screen revealed that they were true actives. This exemplifies how

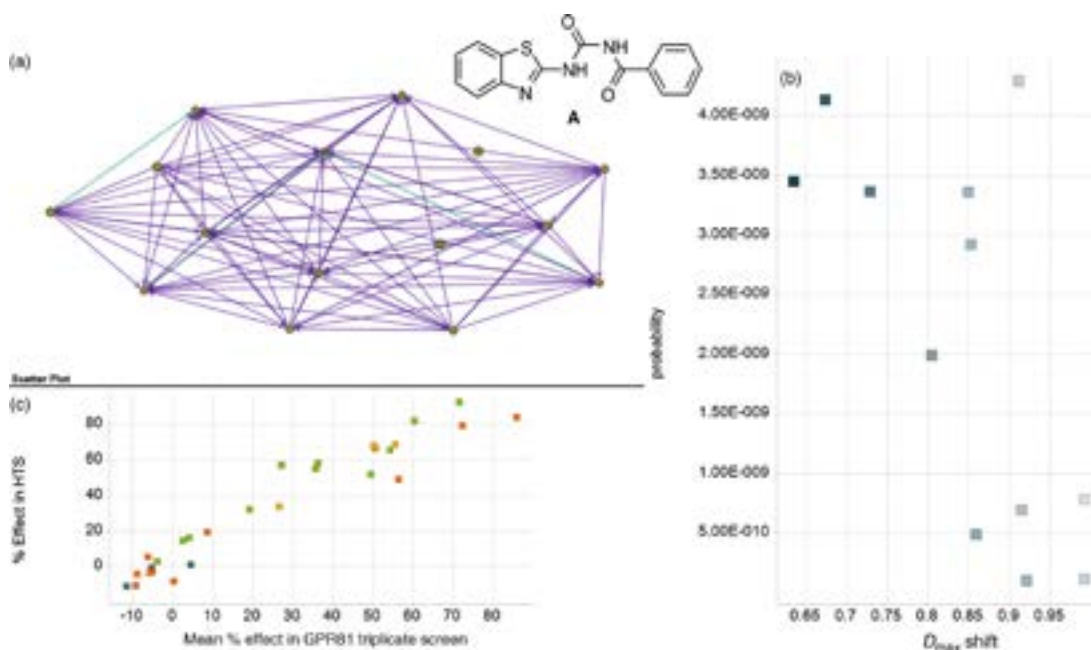


Figure 21.10 The network map in (a) shows the connections between the Murcko scaffolds. All fragments contain compounds with a significantly shifted activity distribution in the HTS screen versus the entire compound collection (green nodes). The D_{\max} shift and the probability (p -value of the shift) of the fragment is plotted in (b). The color gives the number of compounds associated

with the Murcko scaffold (darkest color, 25; lightest color, 11 compounds). Plot (c) shows the correlation between primary data and triplicates. The color indicates no activity (green) or x-flaged activity (triplicate measurement: two inactive one active = orange; one inactive two active = yellow) in the empty cell counterscreen.

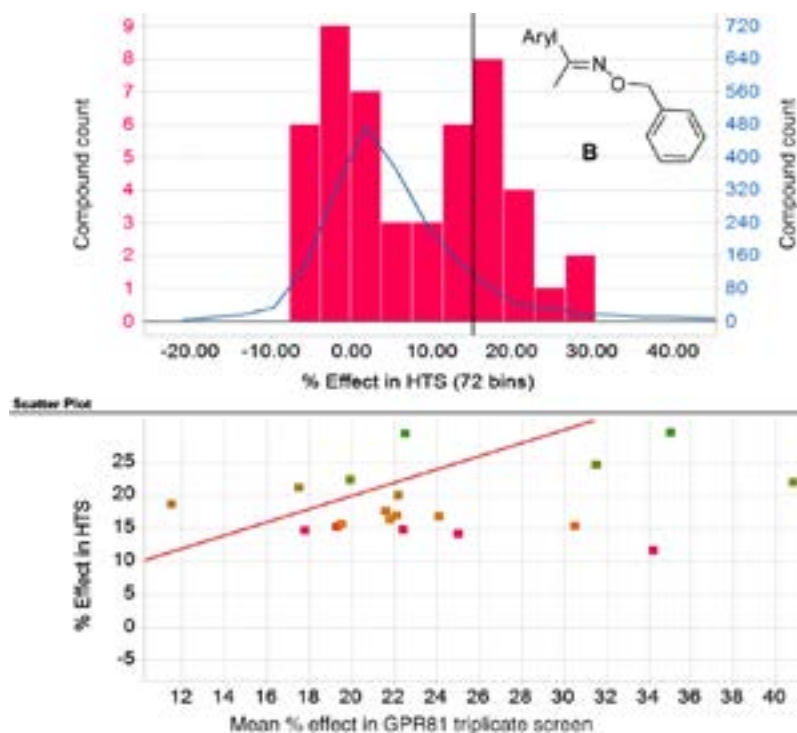


Figure 21.11 The upper combination chart shows the distribution of all the compounds in the HTS (blue line) and the distribution of compounds associated with scaffold **B** (red bars). It appears that the distribution of effect data for scaffold **B** reaches one maximum at around -4% effect and another around 15%, just borderline to the cutoff criteria.

Rescreening of compounds in the triplicate screen just below and above the cutoff criteria confirmed that compounds were true positives. This is visualized in the lower scatter plot. The line of unity is represented in red. The colors reflect the effect range in the HTS (15% < % effect < 20%, orange to green; <15%, red).

this method can be used to offer a survival mechanism for compounds that would have been discarded otherwise, since CSE provides a rationale to keep compounds in the screening cascade. However, it provides no safeguard against false positives. In Figure 21.12, compounds associated with fragments with a strong D_{\max} shift came back as false positives in the triplicate screen. This was particularly surprising since the % effect data derived from the HTS correlated rather well with the triplicate data. It is not understood why substructure **C** (stars) was identified as strong positive hit in the HTS and then disappeared in the retest. The usual suspects, for example, plate effects, dispense failures, and different compound or cell batches, were excluded.

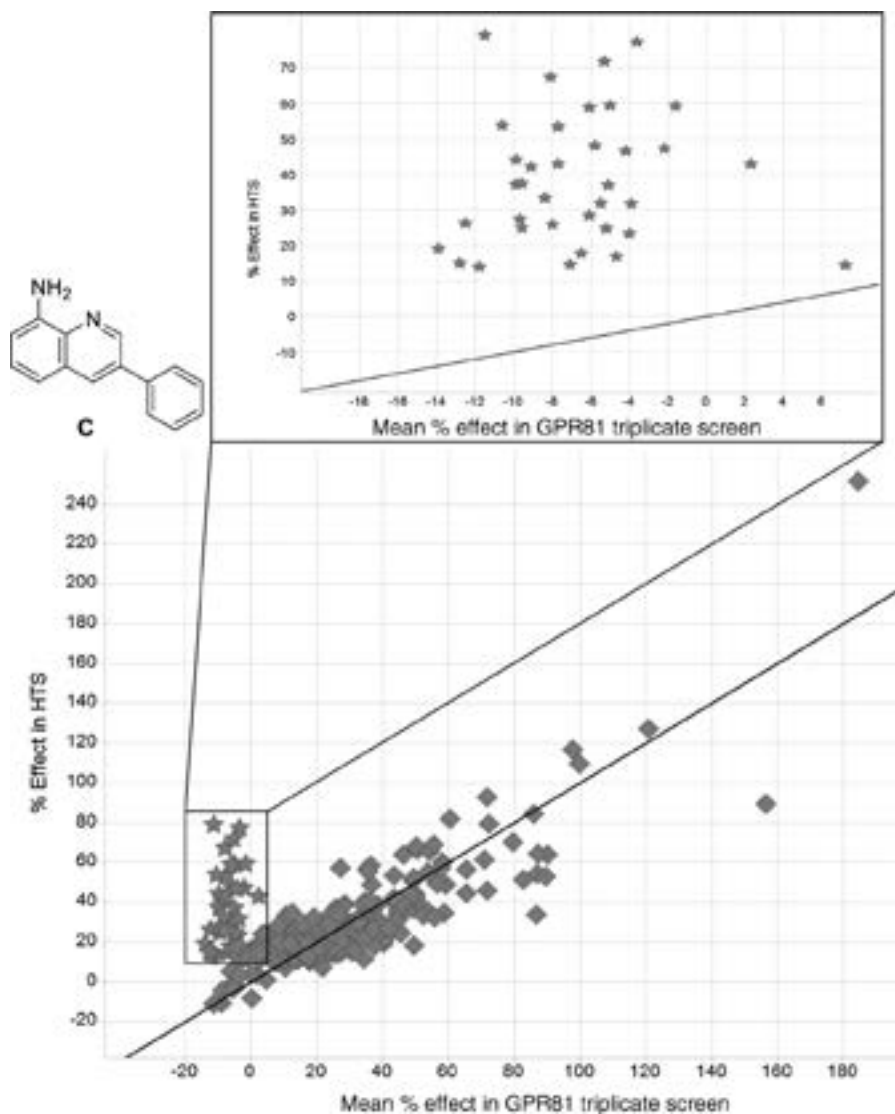


Figure 21.12 The scatter plots show the correlation of the primary data versus the 3-point single-concentration data @ 10 μ M compound concentration. The black line represents the line of unity. The data demonstrates the clear outlier behavior of the scaffold C (stars).

21.5.2

Single-Concentration Counterscreen

While the HTS screen and its evaluation is focused on identifying hits of interest to progress, and the triplicate screen is about confirmation of those hits, the

follow-up screens are all about filtering toward the right PD profile (with exception of the purity screen). At this stage of the screening campaign, all compounds with a UV purity below 85% were removed from the cascade with few exceptions. The next steps in the cascade were designed to confirm hits. A confirmed hit is a compound that exerts its actions most probably via the desired primary target and not through interference or other processes. This is the task of the secondary screens in the cascade after an HTS. They are designed either to remove false positives or unwanted PD effects or to ensure that compounds possess wanted PD effects. It has been suggested to use already at the HTS read-out stage an efficiency index like $PEI = \% \text{ effect} / MW$ [21] to prioritize hits against each other, such that the past HTS evaluations are not solely potency driven [22]. This might have some meaning in case the % effect data are based on a triplicate measurements, but otherwise it is up to the investigator to make a judgment of how meaningful it is to filter based on a binomial readout (active versus inactive) divided by the MW of a compound.

About 2800 actives in the triplicate screen were submitted to the first counterscreen. The artifact screen was performed in the same cellular background to identify compounds that interfere with the assay by absorbance, fluorescence, or a cell-related effect. Compounds were tested at one concentration in triplicate. The cells were stimulated by forskolin to produce cAMP via adenylate cyclase. Measurement of an inhibition of the cell production of cAMP by fluorescent-based methods would be affected by compounds that quench fluorescence or are fluorescent, and would cause a signal change and could be mistaken as actives. Results from the artifact assay were compared with results from the GPR81 triplicate screen to sort out the true actives from the assay artefacts in that test. Originally, the filtration criteria had been set to the following criteria. If the % effect in the GPR81 screen was 1.5 times higher in the retest compared to counterscreen data, the compound was considered active and tested in seven-point concentration response (7 pt CR). As can be seen in Figure 21.13, this resulted in a compound set marked by the yellow area below the orange line.

Examining the straight line fit (dotted line) between counterscreen and triplicate data, it might be the case that the GPR81 screen had a tendency to yield higher effect data than the corresponding counterscreen. To have a more conservative cutoff criteria, it might be advisable to either consider compounds with no counterscreen signal at all (green box) or consider those with a 3.4-fold increase in effect against GPR81. This corresponds to a two-fold increase in effect on GPR81 based on the straight line fit correlation.

21.5.3

Clustering

After the counterscreen, 740 compounds remained with either no or a 1.5-fold lower % effect in untransfected cells. At this point, all hits were clustered using Murcko scaffold preclustering. The resulting clusters were refined by using an additional “k-means”-based clustering procedure. The average cluster size was

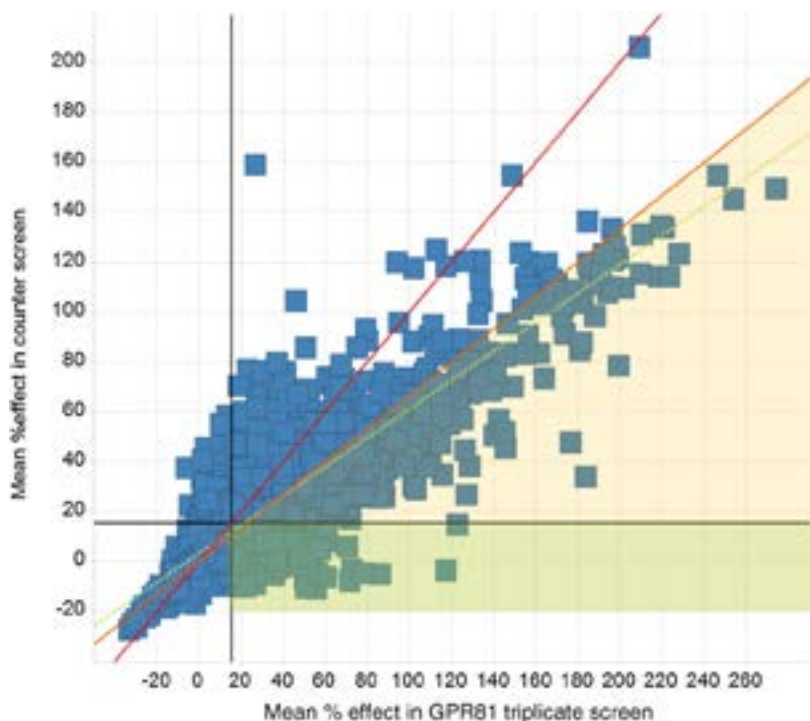


Figure 21.13 The plot shows the counter-screen data versus the triplicate data on the GPR81 receptor. The red line is the line of unity while the orange line represents the “true hit” cutoff criteria. The dotted line is the straight line fit between the counter and the

triplicate data having a slope factor of 0.58. This could mean nonspecific or artifact compounds were performing in the GPR81 screen about 1.7 times better than in the counter-screen. The green box marks the area with no counterscreen signal.

set to 100 compounds/cluster, and compounds within the cluster had a maximum distance of 0.6 from the cluster center. The resulting clusters were either merged or split based on the manual assessment of a medicinal and computational chemist. This resulted in an initial set of 214 clusters containing more than a single compound and 240 singleton clusters, meaning that no other related compound was available and/or active within the compound collection. While the use of a cluster algorithm often provides an initial meaningful clustering of compounds, it is advisable to refine clustering by hand, looking at common substructural motifs, and the possibility of overlap between pharmacophores [23] or existence of possible bioisosteric motifs [24] within the compounds (Figure 21.14).

Clustering fulfils several functions; it aids the HTS evaluator to look at the compound ensemble as a whole, and most significantly, allows the evaluator to identify early trends in data and SAR.

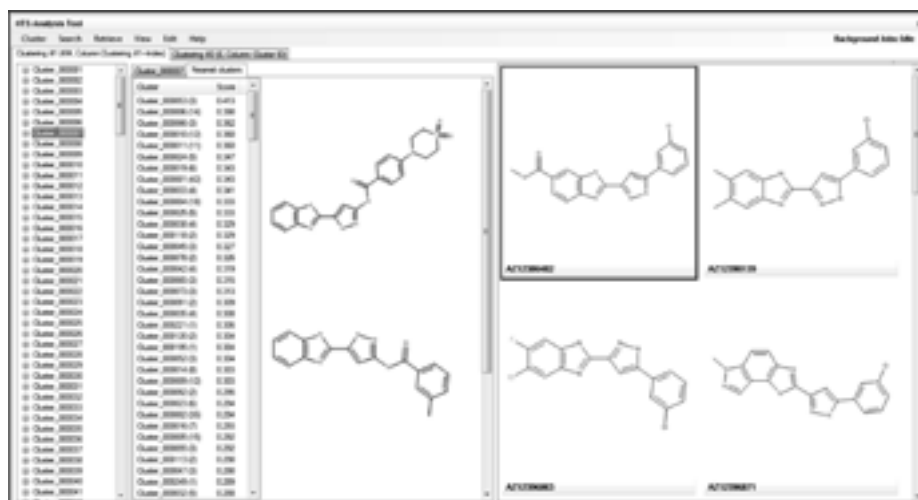


Figure 21.14 Snapshot of the initial GPR81 clustering results. The right panel shows cluster 7 compounds sharing a 3-benzimidazole-5-phenol-substituted pyrazole motif. Cluster 53 compounds are shown in the left panel. This cluster shares a similarity with cluster 7, but only with 0.41 Tanimoto overlap. Examining the structures, however, makes it apparent that both clusters share the benzimidazole-pyrazole moiety. Many clusters contain very few compounds as

indicated by the number in brackets. This is due to the fact that the AZ collection is a historical grown collection containing compounds from old projects, compounds from collection enhancement activities, references, and unique scaffold hops with ongoing compound depletion. Purity deterioration also leads to compound depletion.

21.5.4

Cluster Expansion and Nearest Neighbours

Singletons and clusters containing only a few compounds are usually expanded by adding structurally related compounds and nearest neighbours, if they are available. It is obvious that larger sized clusters are easier to assess compared to singletons and small-sized clusters. It can be noted that singletons should not simply be disregarded and should be usually progressed to full dose–response evaluation. There are several computational solutions available to identify nearest neighbours. In principle, they are mainly based on similarity, pharmacophore, shapeophore [25], or substructural elements. Looking at a variety of HTS campaigns, we found that one method often performs best for a certain target. However, this is usually evident only at a much later stage of the HTS evaluation (HE), and therefore all methods are initially considered equally and applied.

21.6

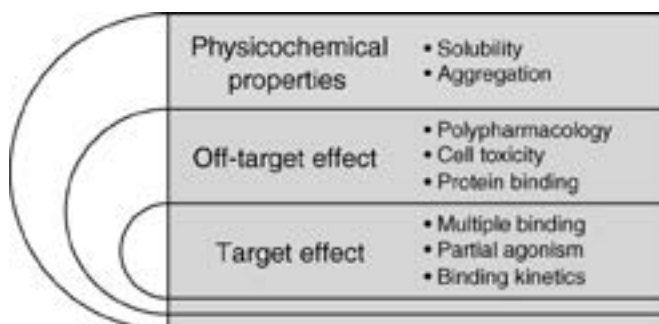
Hit Evaluation

21.6.1

Potency, Efficacy, and Curves

Around 500 compounds representing various clusters were submitted for screen to provide full concentration response curves in the human GPR81 cAMP TRF assay in addition to the described counterscreen. This included most of the singletons and a large number of representatives from larger compound clusters.

The scatter plot in Figure 21.15 reveals the clear lack of correlation between the pEC_{50} data and the triplicate % effect data. This is not due to poor assay performance but rather the detailed behavior of compounds at escalating concentrations. The first effect that can be easily spotted in the plot is the response of partial (gray shaded) versus full agonists (black). Potency data is determined by curve fit and is reported as concentration needed to achieve 50% of the measured maximum efficacy of a compound. If a compound is a partial agonist with a top effect of 60%, the potency is reported as concentration needed to achieve a 30% effect (Figure 21.16). Other factors influencing the dose–response behavior reflected by the curve of a compound are described as follows:



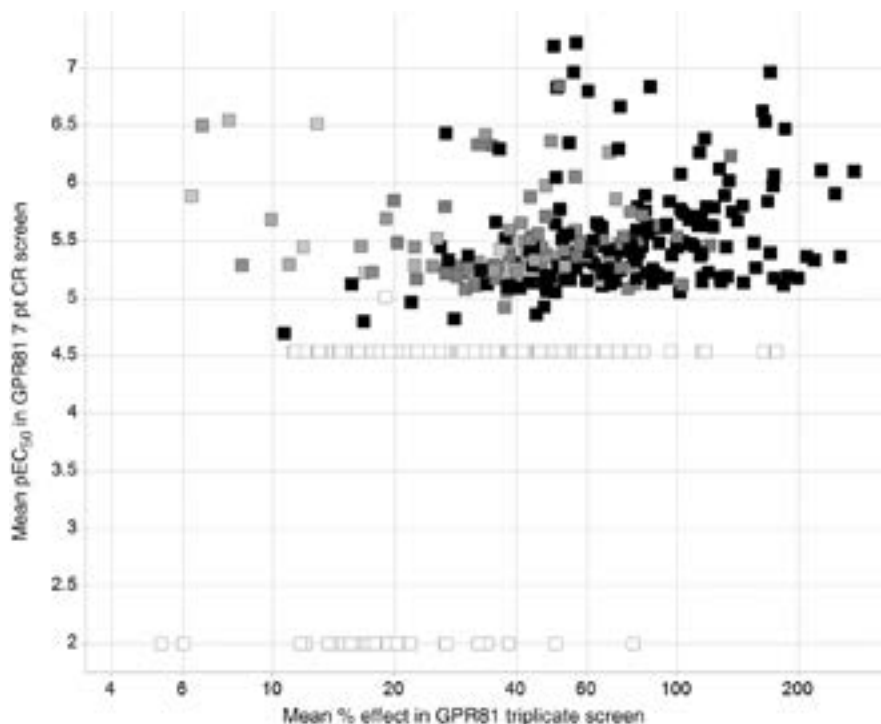


Figure 21.15 Correlation between GPR81 potency and triplicate single-concentration data. The gray shade represents the maximum effect of the compound with gray indicating partial agonism and black full agonism. White colored compounds are either not active in the 7 pt screen (pEC₅₀ assigned to 2) or no plateau was observed (pEC₅₀ assigned to 4.5).

Physicochemical properties have a large impact on all aspects of compound interaction with its environment. High lipophilicity will impact solubility, protein binding, permeability, toxicity, and compound promiscuity. Compounds with high lipophilicity or lattice energy can be poorly soluble in buffer solutions [26]. This might lead to precipitation or incomplete dissolution and consequently to bell-shaped curves (Figure 21.16). Another reason for bell-shaped curve behavior might be cell toxicity leading to a decrease in effect of a compound at high concentration. Irregular curve behavior can also be caused by polypharmacological effects of compounds. The cell response is affected differently at different compound concentrations depending on off-target engagement. Steep curve behavior can be caused by aggregators. For example, compounds with amphiphilic behavior aggregating at high concentration where it is the aggregate formed that causes the observed effect. Even

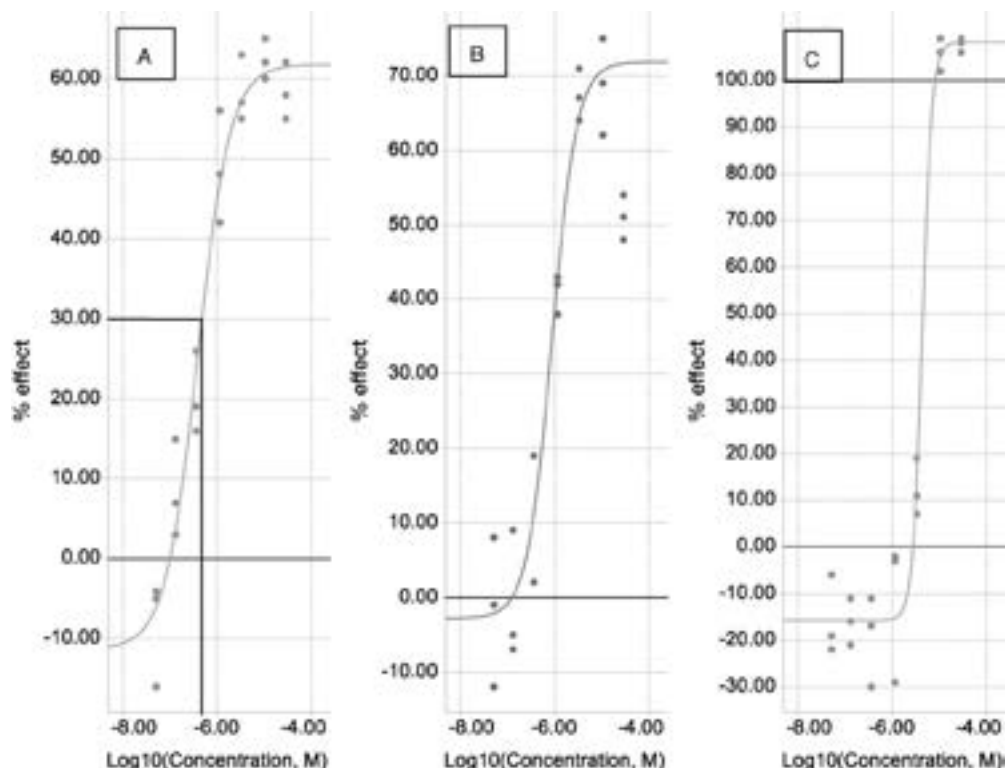


Figure 21.16 Curve A shows a partial agonist curve with a reported potency just below $1 \mu\text{M}$ at around 30% effect. Curve B represents a bell-shaped curve. Curve C is a steep curve with a slope factor far above 1.

molecules with rather low molecular weight can form aggregates and generate false hits. This behavior might be assay dependent and therefore such compounds might not be detected by a counterscreen [27]. Some compounds might form 2:1 or even higher stoichiometry complexes with a target. Multi-site binding can especially be seen for inhibitors of oligomers. The binding of more than a single equivalent of compound might affect target signaling or function [28] and the slope of the concentration response curve will rise with the number of binding sites.

Steep curve behavior can also be seen for covalently binding compounds or very potent inhibitors with the K_d value below the target protein concentration of the assay. For enzymes, this is known as “zone behavior” [28,29]. By applying the mass action law, inhibition becomes a linear function of the enzyme concentration if the K_d value of the inhibitor is far below the enzyme concentration. The steepness of the concentration response curve also increases with the amount of enzyme added.

21.6.2

Binding Kinetics

Binding kinetics and their influence on curve shifts have been heavily discussed in the literature lately [30]. Tight binding effects or slow off rate kinetics can influence the apparent potency of a compound since the assay is not in equilibrium. Some authors suggest that binding kinetics should be taken into account already under HTS evaluation [31]. While the risk that a compound is a false negative due to its binding kinetics in a typical HTS screening setting is minimal, there might be a risk that the real potency of the compound is underestimated. Zhang and Monsma [31] outlined this risk for an inhibitor using short incubation times. Their calculations build on a no tight binding scenario and negligible reporter effect from ligand or substrate. Those calculations take the receptor occupancy into account that controls the effect of a compound on the target. If the equilibrium receptor occupancy is not reached at a certain drug concentration within a certain incubation time, binding and effect data might be misleading. Table 21.3 summarizes the results of the simulation of time-dependent IC_{50} values using a 30 min incubation time. In an effect assay, however, it is not necessarily the binding kinetics that are rate limiting to create the final response since there are possible multiple signal transduction steps occurring before the effect readout.

Although there might be a risk to underestimate potencies dramatically, from an empirical point of view we never encountered k_{on} values $< 10^3$ (Ms) $^{-1}$. The more likely area for k_{on} values in the small molecule area is marked gray in Table 21.3 indicating the potential for up to a four-fold drop-off which is not too dramatic. However, it is very important to keep in mind that potency data will be more stable and relevant if the assay is close to equilibrium, and testing reference compounds using varying incubation times should always be a part of assay development.

An exception occurs for the compounds with extremely long residence time (slow k_{off}). Such compounds behave like or are covalent binders to the target [32]. In the case of reactive compounds, this type of behavior can lead to pan-assay interference (PAINS [33]) since such compounds frequently appear as actives against a broad range of targets. Such compounds are not always detected by a

Table 21.3 Calculated incubation time-dependent IC_{50} values for an inhibitor with no tight binding scenario and negligible reporter effect from natural ligand or substrate.

k_{off}	k_{on}	IC_{50} @ 30 min $K_i = 10$ nM	k_{on}	IC_{50} @ 30 min $K_i = 100$ nM
10^{-6} s $^{-1}$	10^2 Ms $^{-1}$	3800 nM	10^1 Ms $^{-1}$	38 000 nM
10^{-5} s $^{-1}$	10^3 Ms $^{-1}$	380 nM	10^2 Ms $^{-1}$	3800 nM
10^{-4} s $^{-1}$	10^4 Ms $^{-1}$	40 nM	10^3 Ms $^{-1}$	400 nM
10^{-3} s $^{-1}$	10^5 Ms $^{-1}$	10 nM	10^4 Ms $^{-1}$	105 nM

counterscreen since they might still react with specific functional groups in the target protein [34]. In the GPR81 campaign, a database search with known PAINS and a similarity-based risk assessment was performed to flag for possible covalent binders. Four clusters containing 25 compounds were classified as reactive or potentially reactive, some of which were not filtered out by the counterscreen.

In summary, there are many reasons why single concentration triplicate data might not necessarily track the potency of a compound. This is another aspect to keep in mind before filtering compounds solely on single concentration data. Furthermore, it is vital for the HTS evaluator to investigate the curve behavior of compounds. It might be misleading to assess compounds based on their reported potency or efficacy values. While an evolved and validated compound series might behave well in this respect, the normality for compounds coming from an HTS readout is that they can display all kinds of curve behavior within and across series.

21.6.3

Concentration–Response Counterscreen

All compounds that were submitted to pEC₅₀ measurements in the GPR81 cAMP TRF assay were also submitted to full concentration response screen in the counterscreen to determine pEC₅₀ values in a cell line with no expression of GPR81. The results are summarized in Figure 21.17.

There was a strong correlation for most of the compounds between the GPR81 potency and the counterscreen potency. Only compounds within the box were considered of further interest. Clusters containing only inactive compounds or only compounds with an activity of pEC₅₀ >4.5 in the counterscreen (28 clusters) were removed. At this stage, 55 clusters and 115 singletons remained.

21.6.4

Hit Assessment

21.6.4.1 Size and Lipophilicity Efficiency Assessment

At this point of the HTS evaluation, it is up to the evaluator to make a judgment call on which compounds and clusters to progress further into the secondary screening cascade. This is a difficult task since few obvious selection criteria remain. Highly potent compounds with potencies in the low nanomolar range should always be considered. However, potency should not be the sole driver for compound progression. Clusters can contain only highly lipophilic compounds, which diminishes the likelihood of success in the future [35]. While lipophilicity is a well-known driver for both positive and negative properties, other physicochemical and structural properties also play an important role for drug development. Aromatic ring count [36], enthalpic versus entropic contributions [37], basicity [38], sp³ content [39], PAINS [40], synthetic feasibility, and redox recycling compounds [41], to name a few, all might impact on the probability to develop a compound class into a lead series or a clinical candidate. In fact, it is

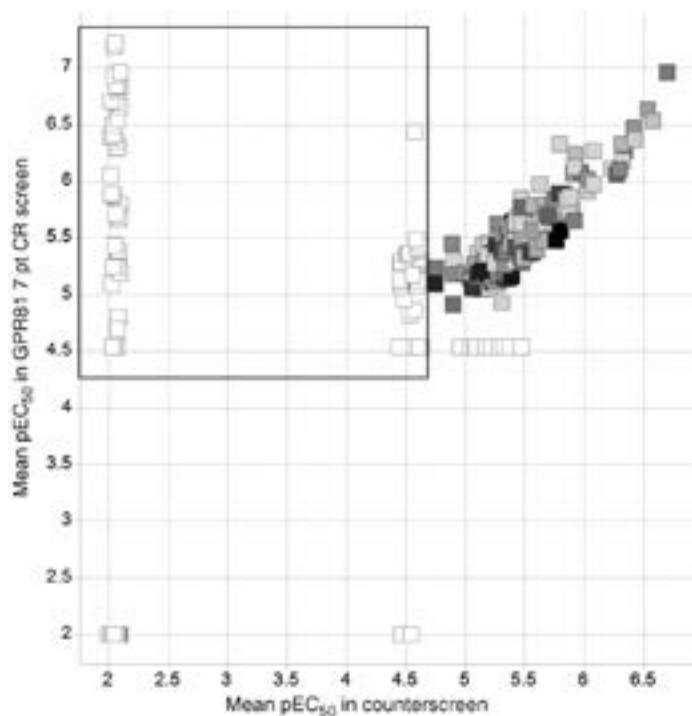


Figure 21.17 Correlation plot between GPR81 pEC_{50} data and pEC_{50} data from the counterscreen. The gray shade represents the delta value between the mean top effect in the GPR81 screen and the mean top effect in the counterscreen. Negative values (light gray)

indicate a higher top effect in the counterscreen compared to the top effect in the GPR81 screen. Positive values (darker gray and black) indicate a higher top effect in the GPR81 overexpressing cells. The box indicates the remaining compounds of interest.

hard to keep track of all the possible rules to consider since Lipinski published the rule-of-five [42]. For a start, looking at the lipophilicity of compounds and assessing the performance of a compound in light of its potency versus its lipophilicity is a straightforward process since lipophilicity is both easy to measure and to calculate. In the GPR81 campaign a battery of composite parameters were used to assess several aspects of lipophilicity, size, and potency. Ligand efficiency (LE) was used to assess the impact of the number of heavy atoms on potency. Fit quality (FQ) values [43] were computed to compensate size-dependent impact on LE [44]. Lipophilicity ligand efficiency (LLE) values [34,45] based on $clogP$ and $\log D$ ($LLE = pEC_{50} - clogP$; $LLE = pEC_{50} - \log D$) were calculated to assess the hydrophilic contribution to the potency of a compound. LLE_{AT} [46] was used to adjust the LLE of a compound with its size. The reason why we use in general all these parameters is that every composite parameter has its own

merits and limitations. We calculated the LE based on the pEC_{50} value from the GPR81 screen ($LE = (1.37/HA) \times pEC_{50}$). Classically, this parameter is interpreted in the way that hits with values above 0.3 are considered highly attractive. However, data from Reynolds, Tounge, and Bembenek [43] as well as in-house data showed a clear size dependency where compounds below a heavy atom count of 25 often show higher LE values compared to compounds above 25. In fact, hit series expansion from fragment-like compounds having a low molecular weight is difficult in the absence of structural information. Adding additional polar groups to grow the fragment often leads to loss in potency within the concentration response window of the assay. While a small fragment might be able to position a polar group in an optimal geometry to the target, it becomes increasingly difficult to adopt an optimal fit for additional specific interactions. Further, increase in size results in reduction of effective surface area [47]. Particularly for lipophilic interactions, there is a strong interdependency between accessible area and molecular size. Both polar and apolar enthalpic effects contribute to the size dependency of LE [48].

The FQ composite parameter ($FQ = LE/LE \text{ scale}$) compensates this effect empirically using a scaling function ($LE \text{ scale} = 0.0715 + 7.5328/(HA) + 25.7079/(HA^2) - 361.4722/(HA^3)$). Good hits are usually found at $FQ > 0.8$. The LLE value can be seen as a surrogate parameter to assess the potency contribution deriving from nonlipophilic interactions under the assumption that each increase in lipophilicity by one log unit increases the potency of a compound (in general) 10-fold. Decent hits for GPCR targets can often be found around an LLE of 2 and above ($pEC_{50} > 6$, $\log P < 4$). However, LLE values where a measured $\log D$ or calculated $\log P$ is low and potency is poor are overvalued (e.g., $pEC_{50} = 4.5$ and $\log D < 1$; $LLE > 32.5$). For example, a GPCR effect assay is designed to detect compounds typically in the range between 50 μM and 1 nM. Clusters containing low-potency compounds are particularly hard to evaluate since often it is not possible to establish SAR due to loss of potency. Also, counterscreens might not be designed to detect low-potency compounds. A good effect assay might typically show variations in potency (regarding IC_{50} or EC_{50} values) around a factor of 2–3. While it is easy to cope with potency variations between 3 μM and 1 μM , variations between 150 μM and 50 μM might lead to a compound appearing to be active one time and inactive the next time it is screened.

LLE_{AT} ($LLE_{AT} = 0.111 + 1.37(LLE/HA)$) adjusts the LLE value for the heavy atom count and it is scaled to the LE having the same target value of 0.3 to make comparison more easy. LLE_{AT} can be seen as a surrogate for the Gibbs free energy minus the nonspecific lipophilic potency contribution per heavy atom (HA). Figure 21.18 shows the LLE_{AT} , LLE, LE and FQ plots for cluster 4 coming from the GPR81 HTS screen. Most of the compounds were tested positive in the counterscreen (diamonds) with only two compounds within the cluster being confirmed hits (circles). LLE_{AT} and LLE are all below the threshold considered to be of interest. Variation in size did not have a significant impact on LLE_{AT} indicating no interdependency between LLE and size. The increase in

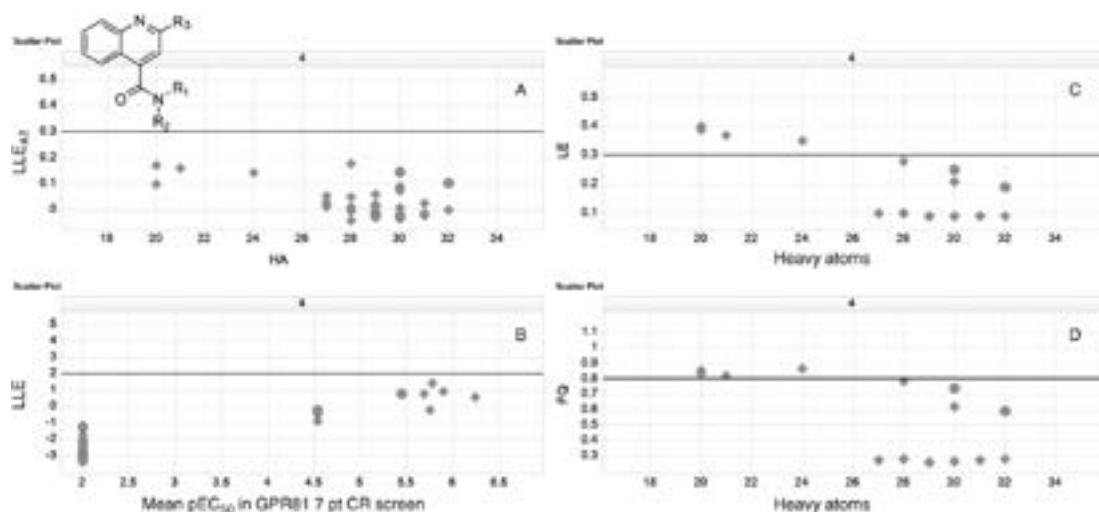


Figure 21.18 Cluster 4 lipophilicity and size performance. R_1 and R_2 indicate various amide substituents, and R_3 typically represents an aryl, heteroaryl, or benzyl substituent. The shape represents the difference in potencies between GPR81 and the counterscreen ($pEC_{50}[GPR81]-pEC_{50}[\text{counterscreen}]$). Diamonds indicate that there is no difference in potency and circles indicate that the compound did not show activity in the counterscreen or had a significantly lower activity. The black line represents the threshold values indicating good performance of a compound. (a) LLE_{AT} values indicate no size-dependent trend.

(b) No trend in LLE values indicate that the increase in potency is mainly achieved by increase in lipophilicity. (c) LE values show a typical size dependency, where the compounds with no activity in the counterscreen (circles) show a drop in LE . (d) FQ values show a similar trend as the LE values despite the compensation for the size of the compound. Taken all these results together, increasing the size of the compounds by introduction of polar groups leads to a drop in potency.

size was handled reasonably well in the cluster. However and more significantly, there is no real trend in the LLE data meaning the improvement in potency seems to be off-set by increase in lipophilicity (scatter plot panel B).

Figure 21.18c and d represent the data for LE and FQ respectively. Both plots show a clear size dependency of the hits and the impact on the efficiency values. While this is expected for LE, FQ is compensating for the size indicating a worse performance per atom by larger compounds. From a size and lipophilicity performance point of view, this cluster is less interesting to pursue. Figure 21.19 displays the size and lipophilicity performance of cluster 86 typically seen in a mediocre performing series of compounds from a lipophilicity perspective.

LLE_{AT} values show no size dependency. This shows that despite increase in size, the specific interactions between compound and receptor are still utilized effectively. The slight increase in LLE with increasing potency indicates that potency improvements are not brought about by the increase in clogP. In other words, there was no strong correlation between potency and lipophilicity increase (leading edge [49]). LE and FQ values confirm that potency contribution per atom remained constant with increase in size. Since most of the compounds showed no effect in the counterscreen, this cluster was considered for expansion.

Figure 21.20 represents the size and lipophilicity performance of cluster 200 that contains reference compound **1** and near neighbours. This cluster is an example of a series of compounds that performs well with respect to both size and lipophilicity.

All active compounds were inactive in the counterscreen. LLE_{AT}, LLE, LE, and FQ values are, for all active compounds, above the threshold. While R represents a lipophilic substituent, polarity within the central scaffold is well distributed. From a structural, size, and lipophilicity perspective, this cluster looks most attractive. All compounds, however, are partial agonists that can be detected only by examining the curves and is not captured within efficiency plots. Interestingly, there seems to be a trend toward higher efficacy by increasing size of the compounds (Figure 21.21).

This leads to the conclusion that increasing the size of the compounds might result in the discovery of full agonists.

21.6.4.2 Secondary Pharmacology Assessment

Cluster deconvolution also included an evaluation of the origin of the compounds and any secondary pharmacology associated with cluster members or of near neighbours. For this purpose, several internal and external databases were cross checked to identify possible off-target activities, metabolic weak spots, or general toxicity alerts of cluster representatives. A result of such a query is shown in Figure 21.22. For example, a cluster containing the aminopyrazine scaffold was submitted to a similarity-based query revealing that the compounds belong to a pan-kinase inhibitor family with known Ames-, cytotoxic, and DNA-damaging activity. The associated risk in developing the compounds to more selective GPR81 lead structures was judged as high.

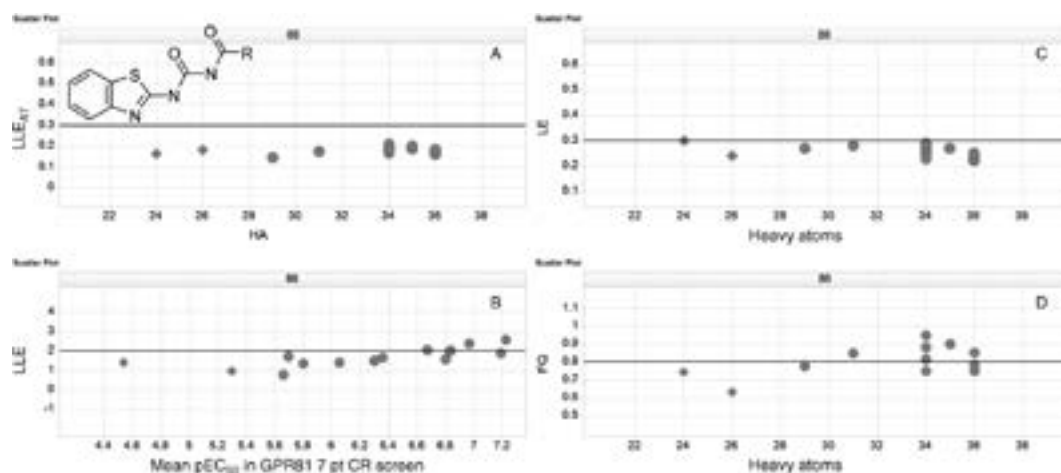


Figure 21.19 Cluster 86 lipophilicity and size performance. R typically represents an aryl-substituent. The shape represents the difference in potencies between GPR81 and the counterscreen. Diamonds indicate that there is no difference in potency and circles indicate that the compound did neither show activity in the counterscreen nor had a significantly lower activity. The black line represents the threshold values indicating a good performance of a compound. (a) LLE_{AT} values indicate no size-dependent trend, indicating an efficient

lipophilicity efficiency handling in larger compounds. This shows that compound variations can be performed effectively without sacrificing size performance. (b) Slight improvement in LLE values indicate that the increase in potency is achieved not only by increase in lipophilicity. (c) LE values show no size dependency. (d) FQ values show an improved performance with size. Most of the compounds show values above 0.8 indicating a good performance.

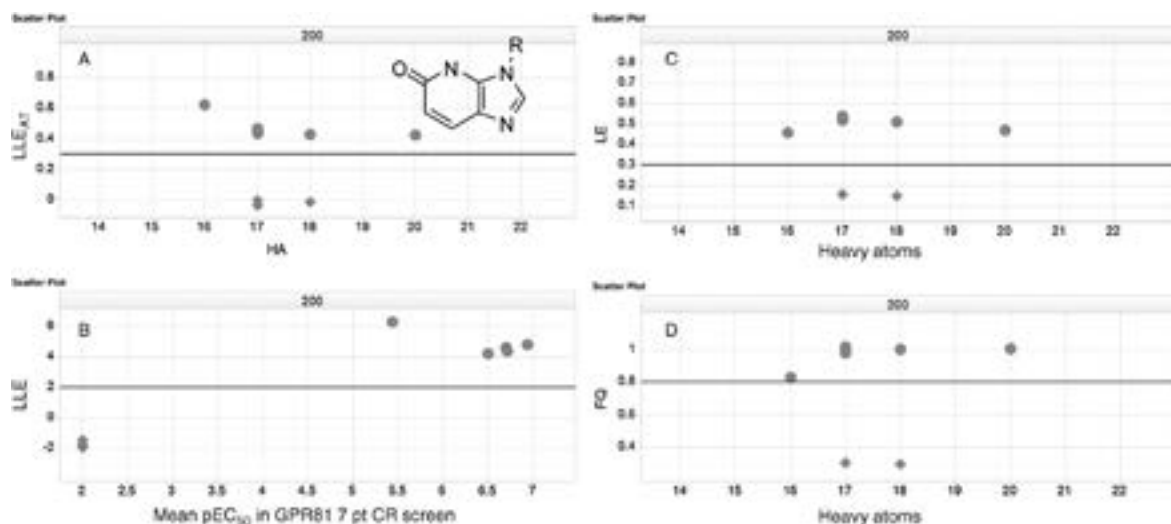


Figure 21.20 Cluster 200 lipophilicity and size performance. R typically represents a carbocycle. The shape represents the difference in potencies between GPR81 and the counterscreen. Diamonds indicate that there is no difference in potency and circles indicate that the compound did neither show activity in the counterscreen nor had a significantly lower activity. The black line represents

the threshold values indicating good performance of a compound. All active compounds display an excellent performance regarding size and lipophilicity. LLE values around 4–5 indicate typical lead to CD performance (b). FQ values in (d) are exceptional.

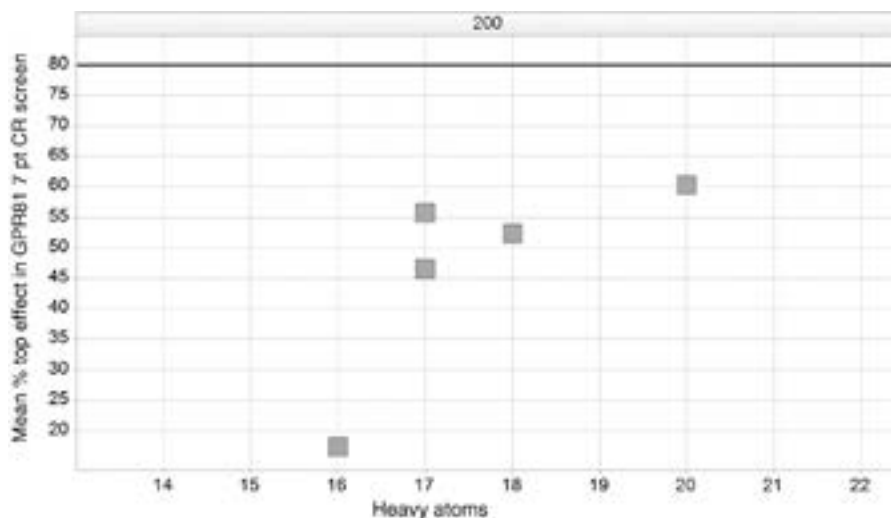


Figure 21.21 Cluster 200 size dependency of the top effect seen in the GPR81 screen. Eighty percent top effect (black line) was regarded as the threshold value for a full agonist.

As part of the secondary pharmacology assessment, we performed a frequent hitter analysis looking at the binomial survival function score (BSF) of each compound. Each compound was checked for how many times it was tested in an HTS and how many times it had been rated active or inactive. The BSF score of a compound is the log value of the chance that this compound is *not* a frequent hitter. So, a BSF score of -2 means there is a 1% (10^{-2}) chance that this compound is *no* frequent hitter.

Clusters with a high number of frequent hitters were flagged as high risk and were identified using the box plot statistics. The box plot in Figure 21.23 shows the distribution of the mean BSF scores across the clusters 3 to cluster 42. Two clusters, cluster 3 and 7, had a median BSF score below -4 (0.01% chance this is no frequent hitter) indicating a large number of compounds behave as frequent hitters.

There are many reviews dealing with the impact of physicochemical properties on off-target behavior, for example, toxicity of compounds due to structural and electronic makeup [5] as well as metabolic bioactivation [51]. With these reviews in hand, it is reasonable to assess the quality of a cluster based on peer literature. However, it is much better to assess the cluster quality using real data from compounds with high similarity to the compounds of the cluster.

Overall, four clusters and five singletons were prioritized at this stage of the evaluation due to their size, lipophilicity, potency, and efficacy performance as well as their behavior in the counterscreen.

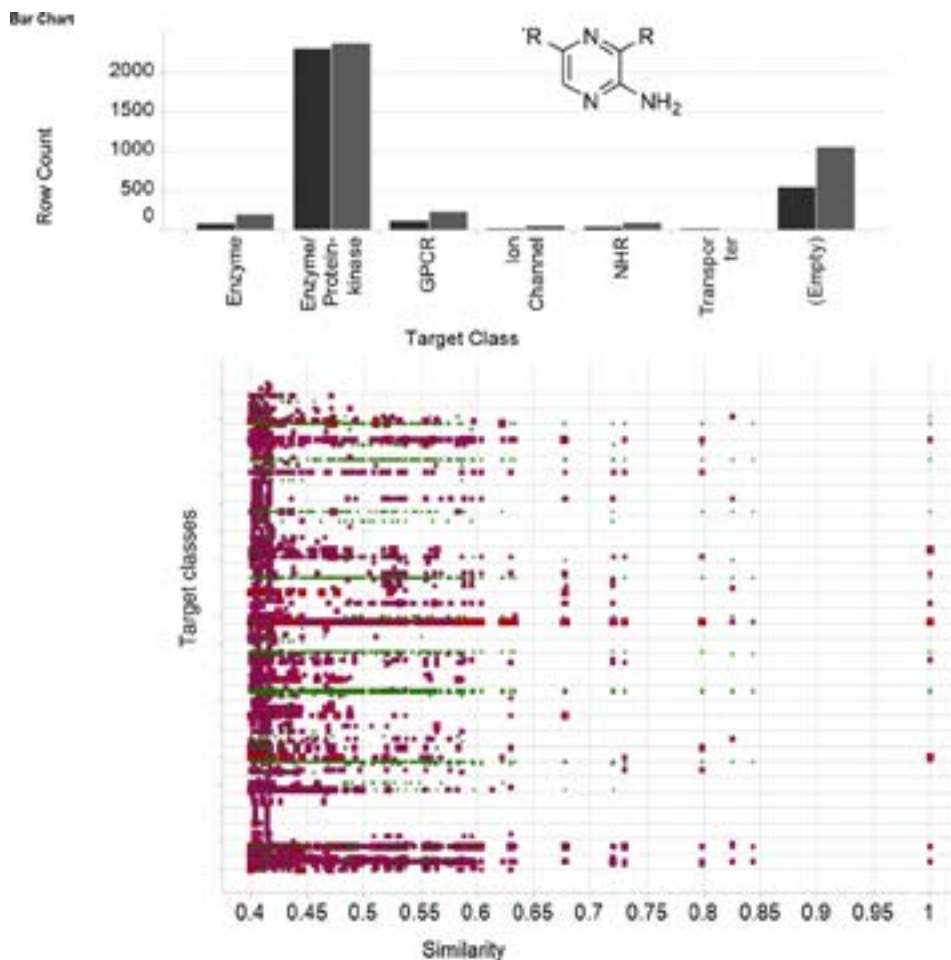


Figure 21.22 The bar chart shows how many times compounds sharing similarity with the aminopyrazine cluster compounds have been tested active (black) or inactive (gray) on various target classes. Compounds containing this substructural moiety show a clear pan-kinase inhibitor activity as seen in the scatter plot. Compounds with potencies on targets below AC_{50} value (activity) of 100 nM are shown red, between 1 μ M and 100 nM purple, and inactive green.

21.6.5

Secondary Screening Cascade and Hit Expansion

So far, all PD *in vitro* work focused around activity in the GPR81 cAMP assay. The nine remaining clusters and singletons were submitted to further hit confirmation and expansion. Key representatives of the clusters were resynthesized to confirm identity, purity, and activity. For further hit confirmation, the orthogonal radiometric GPR81 GTPyS binding assay was used to measure the agonistic

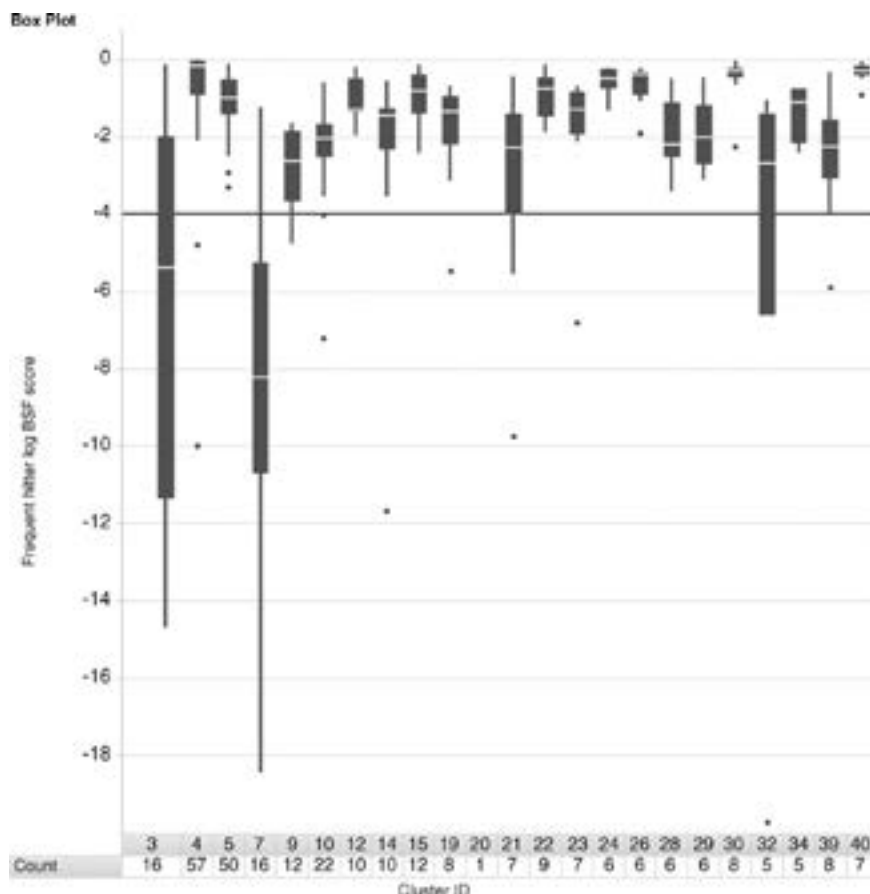
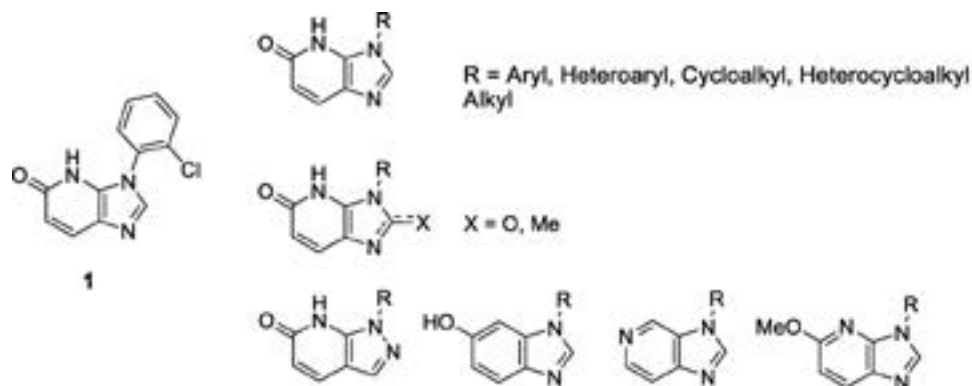


Figure 21.23 The y-axis shows the log BSF values (BSF score). The thin upper line in the box plot represents the upper adjacent value (UAV), the broad upper line in the box represent Q3, the median is marked in white, and the lower broad line in Q1 and the lower thin

line represent the lower adjacent value (LAV). Outliers are marked as spots. The cutoff value for a frequent hitter is -4 (black line). The table on the x-axis shows the median value and the number of compounds (count) with a log BSF value within the cluster.

activity and assess $G_{i/o}$ -mediated signaling [52]. The hit expansion strategy was cluster dependent. In case of singleton clusters, a nearest neighbour search was performed to identify similar or structurally related compounds from the compound collection. Most of the singletons could be expanded into larger clusters except one.

For cluster 200, containing the reference compound **1**, we synthesized a series of additional compounds and matched pairs [53] as shown in Scheme 21.1 to identify the principal SAR of the series.



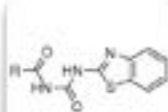
Scheme 21.1 Example of a design sets to evaluate SAR and key interactions around the reference compound 1. Other possible initial design sets included nitrogen walk, nitrogen, oxygen, and carbon switches, scaffold hopping [63], ring expansion, and contractions.

In case of cluster 86, a large number of compounds were already available in the compound collection (gray circles, Figure 21.24). Instead of expanding the cluster with nearest neighbours or close structural analogs, it was possible to approach hit expansion in a different way. For this purpose, a principal substructure search containing the acylaminothiazoleurea was performed. A frequency of group (FOG) analysis was performed on the scaffold. Hit expansion was performed starting from the initial hits and expanding the SAR information through changes to one substituent on the scaffold (core 86) at a time. This meant that hit expansion grew along the vertical and horizontal lines in a FOG plot (Figure 21.24). The advantage over a nearest neighbour search is that SAR can be developed more gradually and systematically.

The hu GPR81 GTP γ S assay confirmed all clusters and a good 1:1 correlation was demonstrated between the primary potency data and the secondary GTP γ S binding assay data. Outliers could all be explained due to irregular curve behavior in the primary screen as shown in Figure 21.25. However, during hit expansion, only cluster 86 and 200 showed any new additional hits with reasonable potency.

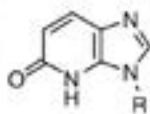
Representatives from all clusters were submitted to additional screens to assess the overall performance of the clusters. These screens included rat GPR81 cAMP agonism, human and rat antilipolytic effect in adipocytes, human liver microsomal stability (HLM), rat hepatocyte stability (Rat Hep Cl_{int}), reactive metabolites, Caco2 permeability, Caco2 efflux ratio, human plasma protein binding (PPB), bovine serum albumin (BSA) binding, Cyp inhibition, time-dependent inhibition of Cyp (TDI), phospholipidosis, mitochondrial toxicity, hERG inhibition, log*D*, solubility, and p*K*_a. With this data at hand and the profile from the secondary pharmacology assessment, cluster 86 and 200 were the frontrunners in the selection process.

Cluster 86



- Number of compounds: 105
 - clog P: 5.29 - 0.53
 - Solubility: 1 - 10 μ M
 - HLM CLint: 2 - 200 μ l/min/mg
 - reactive metabolites: No
 - Caco2 permeability: 2 - 77 1E-6cm/s
 - BSA fu%: 46% - 72%
 - Cyp 3A4 pIC₅₀: 4.5-6
 - Cyp 2C19 pIC₅₀: 4.5 - 5.5
 - Cyp 2D6 pIC₅₀: 4.5 -5.0
 - TDI 3A4: no
 - TDI 2C19: no
 - TDI 2D6: no
 - hERG: 5.5 - >100 μ M
 - Mitochondrial toxicity: no
 - hu GPR81 cAMP pEC₅₀: 4.5 - 7.2
 - hu GPR81 LLE: -0.6 - 4.5
 - hu GTPgS pEC₅₀: 4.5 -7.3
 - off-targets: Ghrelin
 - Mode of action: full agonist
- Number of actives: 53
 - log D: 4.3 - 1.3
 - pKa: 10.4 - 4.4
 - Rat Hep CLint: 2-180 μ l/min/1E6 cells
 - Caco2 efflux ratio: 1.8 - 0.1
 - PPB fu%: 0.01% - 31%
 - Cyp 2C9 pIC₅₀: 4.5 - 5.6
 - Cyp 1A2 pIC₅₀: 4.5 - 5.6
 - Cyp 2C8 pIC₅₀: 4.7 - 5.0
 - TDI 2C9: no
 - TDI 1A2: no
 - TDI 2C8: no
 - phospholipidosis: 15 - 30 μ M
 - hu GPR81 LE: 0.1 - 0.3

Cluster 200



- Number of compounds: 29
 - clog P: 4.3 - -1
 - Solubility: 1 - 774 μ M
 - HLM CLint: 5-12 μ l/min/mg
 - reactive metabolites: No
 - Caco2 permeability: 27 - 60 1E-6cm/s
 - BSA fu%: 10%
 - Cyp 3A4 pIC₅₀: 4.7 - 5.0
 - Cyp 2C19 pIC₅₀: 4.7
 - Cyp 2D6 pIC₅₀: 4.7 -4.9
 - TDI 3A4: yes
 - TDI 2C19: no
 - TDI 2D6: yes
 - hERG: 3.6 - >33 μ M
 - Mitochondrial toxicity: no
 - hu GPR81 cAMP pEC₅₀: 5.4 - 7.0
 - hu GPR81 LLE: 4.3 - 6.0
 - hu GTPgS pEC₅₀: 4.5 -7.1
 - off-targets: Unknown
 - Mode of action: partial agonists
- Number of actives: 5
 - log D: 3.9 - 0.0
 - pKa: -
 - Rat Hep CLint: 37 -47 μ l/min/1E6 cells
 - Caco2 efflux ratio: 0.3 - 0.5
 - PPB fu%: 5% - 20%
 - Cyp 2C9 pIC₅₀: 4.7
 - Cyp 1A2 pIC₅₀: 4.7
 - Cyp 2C8 pIC₅₀: 4.7
 - TDI 2C9: no
 - TDI 1A2: yes
 - TDI 2C8: yes
 - phospholipidosis: no
 - hu GPR81 LE: 0.4 - 0.5

Representative compounds from 10 clusters were tested in a rat GPR81 cAMP assay. Surprisingly, none of the cluster 200 compounds showed any activity in the rat assay, while cluster 86 showed a clear 1:1 correlation between human and rat data. As for the human receptor, most cluster 86 compounds behaved as full agonists on the rat GPR81 receptor.

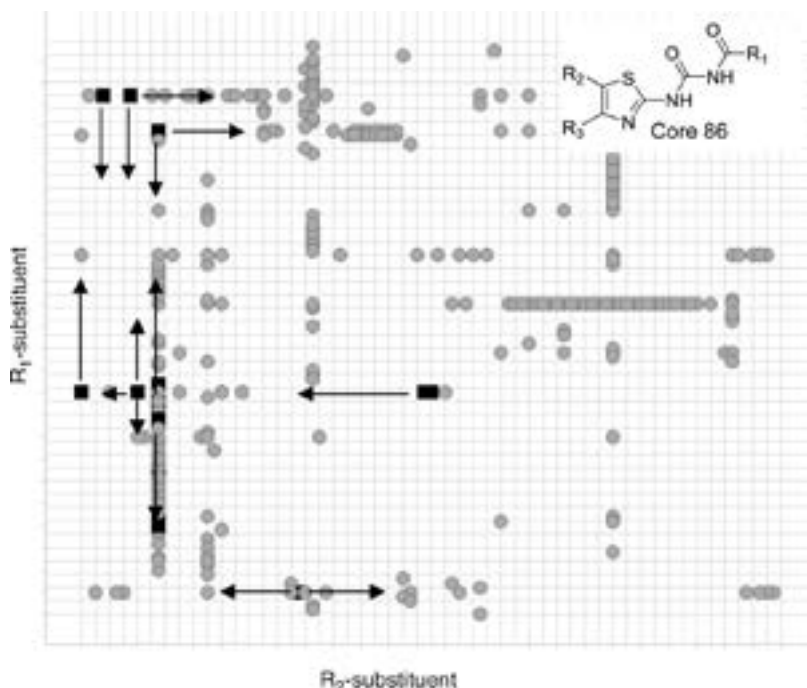


Figure 21.24 FOG analysis of cluster 86. Initial hits are marked in black squares. Circles represent available compounds from the collection. The y-axis represents changes of the R₁-substituent and the x-axis changes of the R₂-substituent. Hit expansion is performed

along rows and columns (black arrows) making a single change either at R₁ or at R₂ at a time. Selections along rows and columns of compounds are made in a way that new compounds should structurally not be too diverse from the initial starting point.

21.6.6

Biological Effect Assay

Compounds from all clusters were submitted to both human and rat antilipolytic assays in adipocytes. The assays were based on forskolin-induced lipolysis and glycerol release in the presence of GPR81 compounds. The release of glycerol was calculated with a standard curve. Compounds were tested in a 10-point concentration response using triplicate plates.

This was one of the most important steps in the HTS evaluation. The overarching working hypothesis to run an HTS was not simply to identify new chemical entities activating GPR81. The main objective was to demonstrate that activation of GPR81 leads to an antilipolytic effect on the most relevant cell line, the adipocyte. We knew from earlier studies that such an effect should translate into an *in vivo* antilipolytic effect with lowering of

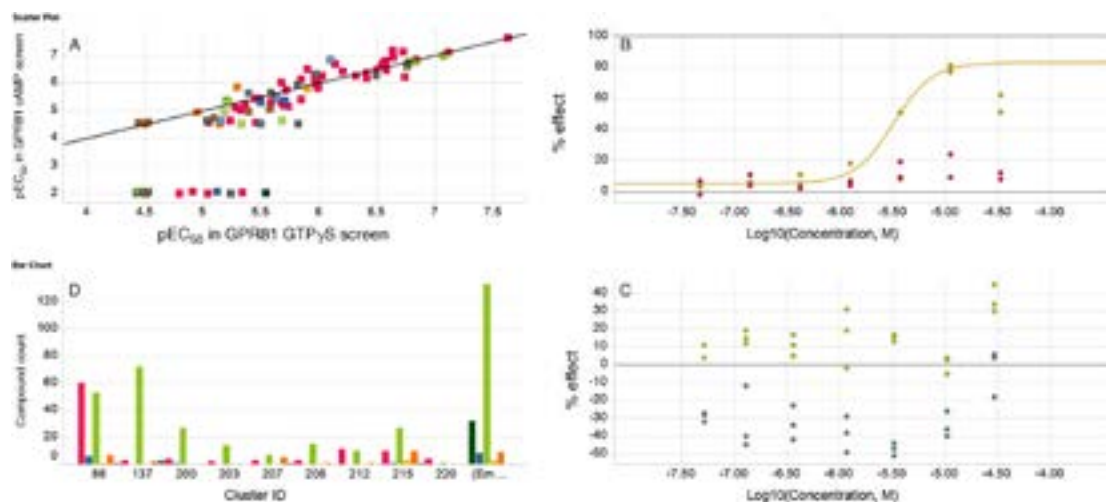


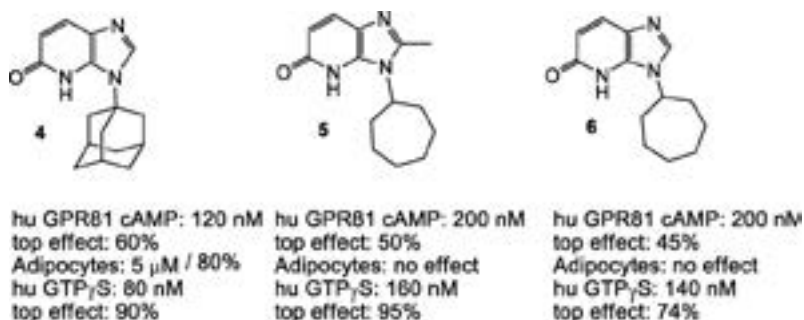
Figure 21.25 Scatter plot (a) shows the correlation between the hu GPR81 cAMP primary screen and the hu GPR81 GTPγS agonist screen. Clusters are colored. (b) GPR81 cAMP curve and (c) GPR81 GTPγS curve show examples of irregular concentration response behavior. In general, outliers showed highly irregular curves in the primary screen. The bar chart (d) shows the hit frequency

in the cluster after the first hit expansion selection. Cluster 86 had the highest number of confirmed hits (red). Inactive compounds count is colored green and irregular curve fits are colored orange and yellow, while compounds that have been active on one occasion and inactive on another occasion are colored blue.

free fatty acids and glycerol in the blood and an improvement in glucose tolerance. The assay also allows an estimation of how much GPR81 activation and unbound potency would be needed to achieve a sufficient antilipolytic effect. Would one of the series show sufficient potential to deliver starting points that could be developed into lead compounds with GPR81 as the key driver for antilipolytic potency and efficacy?

None of the cluster 200 compounds showed any activity in the rat antilipolysis assay. This was expected since no compound showed any agonistic activity on the rat GPR81 receptor in the rat cAMP assay. In human adipocytes, only the adamantyl-substituted compound **4** had an antilipolytic effect up to 80% with an EC_{50} around 5 μ M.

Compound **4**, EC_{50} =120 nM and a top effect of 60% in the cAMP assay, was the most potent and efficacious compound of the series. The compound showed bell-shaped behavior in the human cAMP assay at 30 μ M concentration. It was unclear if the partial antilipolytic effect of the compound seen in human adipocytes was due to its partial agonism in the GPR81 cAMP assay or due to low solubility (1 μ M) and/or toxicity at high concentrations. The next most promising compounds had EC_{50} values between 200 and 300 nM with a top efficacy at 45–50% and no drop-off in efficacy at high concentrations (Scheme 21.2).



Scheme 21.2 EC_{50} and efficacy values of cluster 200 compounds.

We interpreted the results in terms of partial agonism being a possible cause for the lack of antilipolytic efficacy in adipocytes. It is a well-described phenomenon in the literature that low-efficacy agonist need a high occupancy [54], particularly in the case of a low receptor reserve (RR) to deliver an effect *in vitro* and *in vivo*. In case of receptor overexpressing cell lines, the RR might be much higher compared to primary cells such as human adipocytes. If the RR is low and the efficacy of the agonist is also low, even a high occupancy might not be sufficient to result in the desired PD effect.

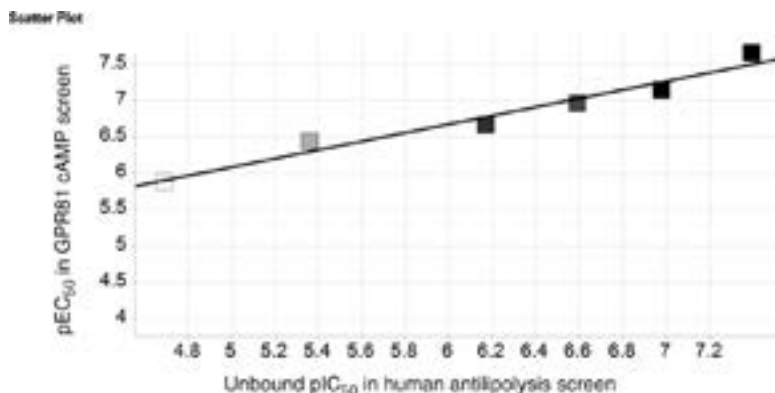


Figure 21.26 There is an excellent correlation between GPR81 and antilipolytic unbound potency with a $R^2 = 0.961$. The shades indicate the top effect in the GPR81 cAMP assay: black 100% and white 72%.

The results for cluster 86 were most intriguing. Five compounds with hu GPR81 cAMP potency in the pEC₅₀ range of 5.9–7.7, covering a 100-fold potency window, were tested in the antilipolysis assay. The unbound potencies of the compounds were calculated based on a 1:1 binding model with BSA. All compounds were full agonists against hu GPR81 with one exception. The results are plotted in Figure 21.26.

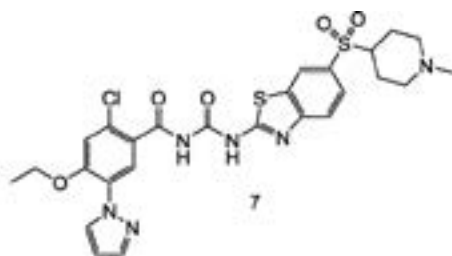
The *in vitro* PD profile of the most potent compound (7) from this cluster is shown in Scheme 21.3.

Since the compounds originated from a project targeting Ghrelin and had high affinity against this receptor, we were concerned that the antilipolytic effect was caused by Ghrelin binding. The first set of compounds from cluster 86 showed good correlation between Ghrelin activity and GPR81 activity. By comparing the SAR on the Ghrelin receptor and the initial SAR we obtained for the GPR81 receptor, we saw a chance to generate more selective compounds in the future and decided to proceed with the cluster.

21.7

Alternative Lead Generation Strategies

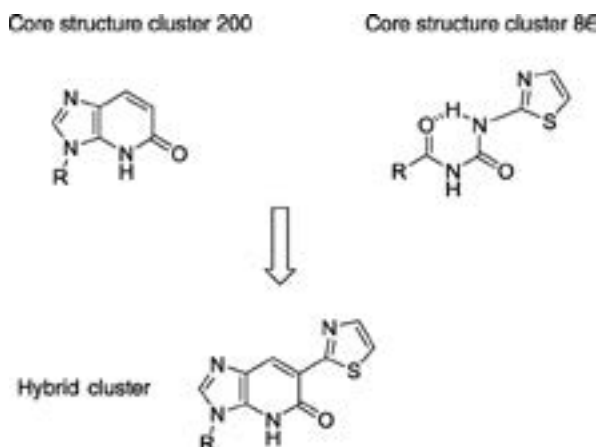
We initiated four additional lead generation strategies. The first was to expand cluster 200 into a full agonist by further exploring structurally related compounds and hybridizing the core scaffold with cluster 86 compounds. As mentioned above, there was a tendency seen that an increase in efficacy correlated with the size of the molecule. We hoped that larger molecules might stabilize the receptor in its agonistic state. To achieve this, we tried to establish an



Hu GPR81 cAMP pEC ₅₀ : 7.7	rat GPR81 cAMP pEC ₅₀ : 8.0
Top effect hu GPR81 cAMP: 108%	Top effect rat GPR81 cAMP: 100%
Hu GTPγS pEC ₅₀ : 7.6	Top effect GTPγS: 100%
Hu antilipolysis unbound pIC ₅₀ : 7.4	rat antilipolysis unbound pIC ₅₀ : 8.0
Activity in counter screen: No	
Hu Ghrelin binding pIC ₅₀ : 8.0 (inverse agonist)	

Scheme 21.3 PD profile of compound 7.

overlapping SAR between cluster 200 and 86. In the absence of a competitive binding assay, there was no information whether the compounds bind to a shared and/or orthosteric site of the receptor. In our hands, the GPR81 receptor model was not able to explain the SAR of either series 200 or series 86 in a reliable way, so we did not feel confident to use such a model to develop new hybrid series (Scheme 21.4).



Scheme 21.4 Hybrid structure between cluster 200 and 86. The acylurea is able to form an intramolecular hydrogen bond leading to a “pseudo”-cyclic conformation. This behavior of the acylurea-moiety could be observed in an X-ray structure.

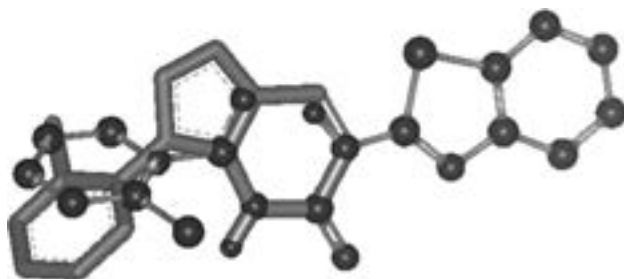


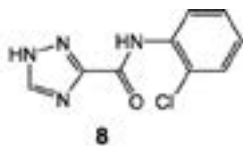
Figure 21.27 Alignment of two low-energy conformers. The cluster 200 scaffold is represented in sticks matching with the acyl urea moiety of cluster 86 (ball and sticks) under the assumption that the acyl urea forms an intramolecular hydrogen bond. The donor–acceptor pharmacophore of the imidazopyridine is matched with the donor–acceptor functionality of the acylurea.

One way to deal with such a situation is to overlay known structures with each other, either based on shape or based on their pharmacophore as shown in Figure 21.27. While one carbonyl group of the acylurea forms an intramolecular hydrogen bond with the amino-benzothiazole, the hypothesis is that the central carbonyl group of the acylurea represents the same donor–acceptor pharmacophore seen in cluster 200. Accepting that many assumptions are used in this argument, a set of hybrid structures was synthesized but showed no efficacy against GPR81. Other modifications did not result in improvements, either.

During the GPR81 campaign, several hydroxybenzoic acid analogs were identified as GPR81 agonists. Dvorak *et al.* [55] reported that they discovered this series of compounds based on a lactate binding model [56] applying a focused screen. We decided on a similar approach of exploring the SAR around 3-hydroxy benzoic acids with an aim to expand this series, but also through screening a set of short-chain acids and bioisosteres [57], possibly mimicking the lactate interaction. For this purpose, the human GPR81 cAMP assay was adapted to be run up to a concentration of 90 μM . As a counterscreen, a human GPR109a cAMP TRF agonist screen was employed. This screen used the same assay technology as the human GPR81 cAMP TRF agonists screen measuring the decrease in cAMP concentration in the cell. This was done to ensure identification of GPR81 selective compounds avoiding activity on the nicotinic acid receptor [58].

The subset screen of lactate bioisosteres and GPCR target class chemical libraries identified the singleton compound **8**. The compound had a reproducible top effect of 70% and an EC_{50} of 1.6 μM . No activity against the nicotinic acid receptor (hu GPR109a) was detected (Scheme 21.5).

We expanded this hit with an additional 140 compounds that either contained the triazole amide moiety or were close analogs and matched pairs of compound **8**. All compounds were inactive in our screen. LCMS purity of **8** indicated a low

**8**Hu GPR81 cAMP EC_{50} : 1.6 μ M**Scheme 21.5** Hu GPR109a cAMP EC_{50} : no activity (measured up to 100 μ M).

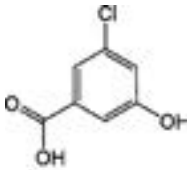
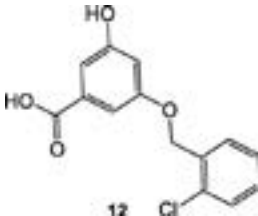
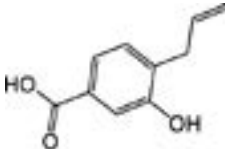
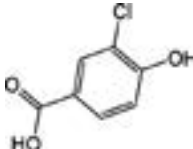
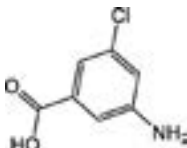
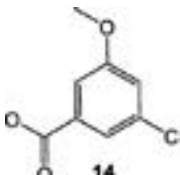
purity, so we resynthesized the compound and confirmed its identity by NMR. The second batch showed no activity against GPR81. This underlines the importance of resynthesis and purity check while interpreting data. Attempts to identify the active ingredient of the first batch failed. We suspected that activation of GPR81 might be mediated by an activated ester contamination that could possibly covalently bind to GPR81. However, the clear plateau of the compound(s) at 70% above a concentration of 10 μ M and a high apparent solubility (precipitation could limit the free concentration of the compound in the assay leading to partial agonistic behavior due to incomplete binding to all available receptors) made this unlikely.

Expansion of the benzoic acid compound class confirmed the SAR reported in the literature [56] with the 3-hydroxy-5-chloro-benzoic acid **9** being the most active compound of the series. In our hands, the compound had a full agonistic effect at about 6 μ M in the human GPR81 cAMP assay. The activity on the human nicotinic acid receptor was determined at EC_{50} = 1.3 mM showing a more than 200-fold selectivity between the two GPCRs. We identified only a handful of additional compounds in this series. Minor changes lead to complete loss of activity indicating that hit expansion would be very difficult (Table 21.4).

It is worth mentioning that we identified one-additional series of compounds with agonistic activity on GPR81 and no activity on GPR109a. We decided to progress this series since activity on GPR81 transfected cell line and no activity on the GPR109 transfected cell line seemed to indicate that this was an on-target activity. However, checking the logBSF score of the compounds revealed a high likelihood for frequent hitter activity. While the cellular background in the GPR81 assay was a CHO cell line and in the GPR109a assay a HEK cell line, we decided to rerun the compounds in the GPR81 counterscreen based on the CHO cell line. The compounds were equally active in the “empty”, untransfected cells as they were in the GPR81 transfected cell line. The activity of this series was, despite being specific for different cellular backgrounds, artifactual in cells coming from the same background. It is a classical mistake to assume that cells coming from various backgrounds produce similar signals with the same compound using the same assay technology.

Late in the GPR81 campaign, two GPR81 agonists **15** and **16** were published showing human/mice GPR81 agonistic activity (Table 21.5) and an antilypolytic

Table 21.4 Benzoic acid analogs and their activity against GPR81.

Compound structure	Human GPR 81 cAMP EC ₅₀	Compound structure	Human GPR 81 cAMP EC ₅₀
	6 μ M		8 μ M
	30 μ M		—
	>30 μ M		—

No compound showed activity against GPR109a at 100 μ M concentration.

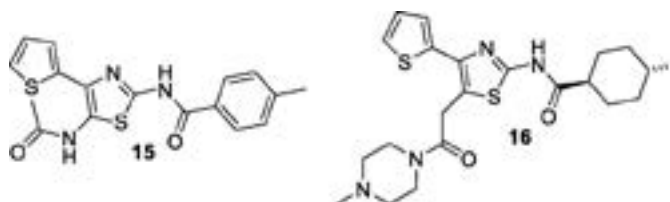
effect on mice and differentiated murine 3T3-L1 cells [59]. Both compounds were full agonist in CHO cells overexpressing human GPR81.

Compound **16** had excellent selectivity against the nicotinic acid receptor with no activity observed at a concentration up to 30 μ M. Most surprisingly, compound **16** did not show any agonistic activity in our *in-house* hu and rat GPR81 cAMP HTRF assay. Furthermore, the compound in our hands was not active in primary human or rat adipocytes either.

21.7.1

Pepducins and Other Modified Peptides

From HTS, one interesting agonist cluster against GPR81 remained after completion and evaluation of the screening cascade. We were interested in additional

Table 21.5 *In vitro* potencies of aminothiazoles against GPR81 and GPR109a.

Compound	h GPR81 EC ₅₀	h GPR109a EC ₅₀	m GPR81 EC ₅₀
15	810 nM		
16	58 nM	>30 μ M	50 nM

starting points to increase the chance of successful project delivery. The expansion of literature hits and cross hybridization failed in our hands, and a subset screen of fatty acid GPCR libraries did not reveal any additional compounds fitting the desired PD profile either.

Pepducins have been proposed in the literature as another rational approach to identify agonists and antagonists against GPCRs [60]. Pepducins are N-terminally palmitylated peptides (Figure 21.28).

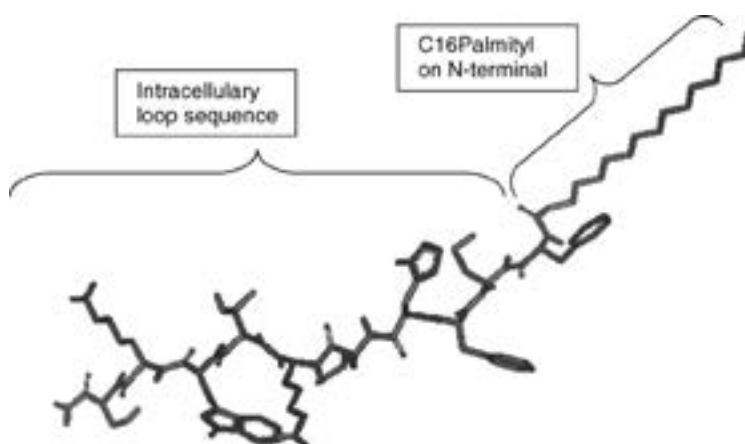


Figure 21.28 Structure of a pepducin. The palmitoyl residue is the long carbon chain to the right at the N-terminal of the peptide sequence. The C-terminal to the left is in most

cases a primary amide to avoid a carboxylic acid negative charge, since this amino acid is in the GPCR adjacent to one of the seven α -helical transmembrane domains.

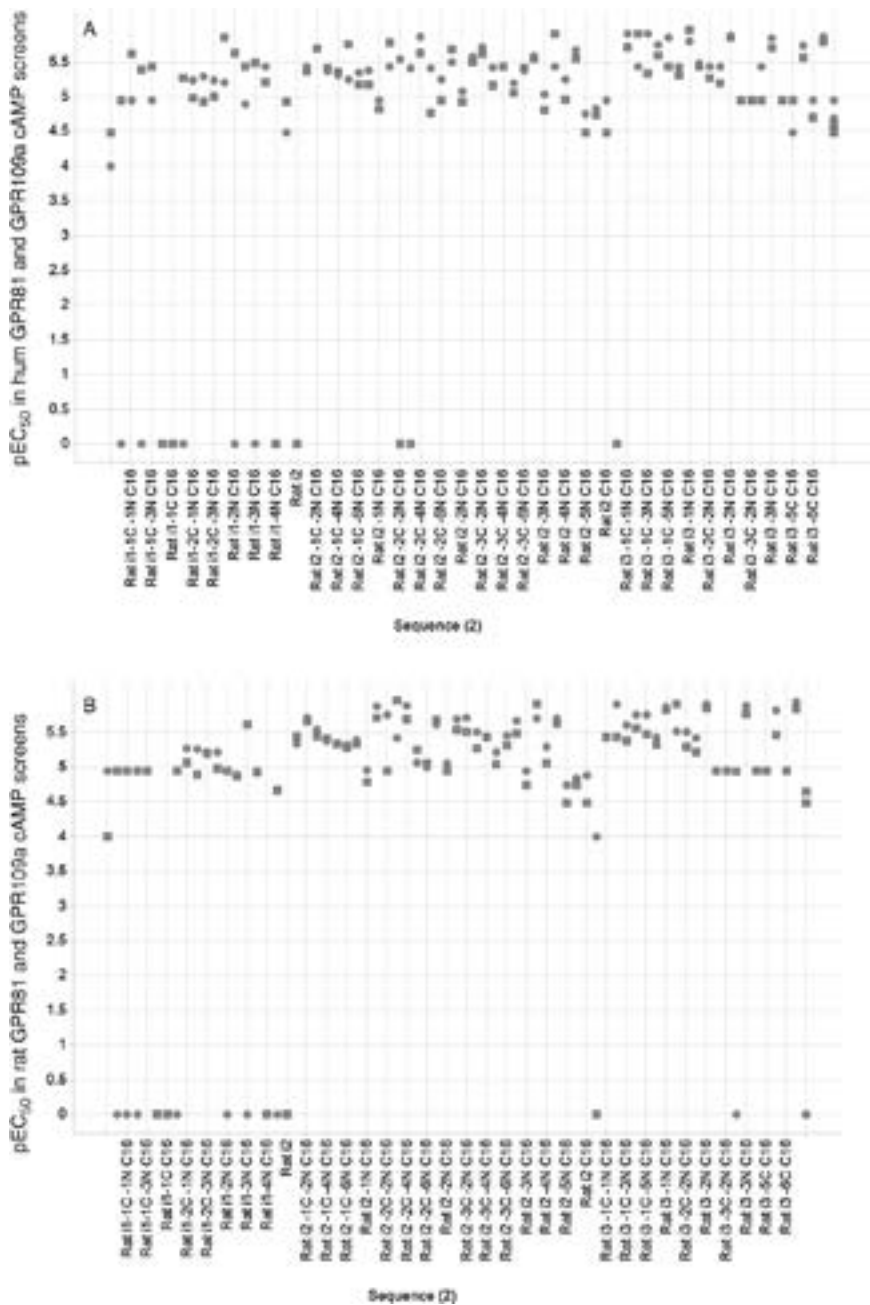


Figure 21.29 The scatter plot A shows the agonistic potency of pepducins on human GPR81 (squares) and GPR109a (circles) receptor. The x-axis shows the sequence the pepducin was based on. For example, Rat i1-1C-2N C16 indicates a peptide sequence based on

the intracellular rat loop sequence i1, where one amino acid at the C-terminal and 2 amino acids at the N-terminal are deleted. The peptide is C16-palmitoylated at the N-terminal. The scatter plot B shows the same data on the rat receptors.

The peptide sequence is derived from one of the three intracellular loop regions (i1, i2, and i3) of the GPCRs. It is believed that they mimic the interaction between the loop region of the receptor and the G-protein thereby acting as allosteric modulators. This is achieved by anchoring the peptide chain via the palmitoyl residue in the cell membrane and the pepducins will act, at least in part, as cell penetrating peptides [61]. The sequence of the intracellular loop determines the selectivity over other receptors, particularly other GPCRs.

We decided to screen a library of intracellular loop mimetics (i1, i2, and i3 based on the rat sequence) in our human and rat GPR81 cAMP screen. As counterscreen, we used the human and rat GPR109a cAMP screen. Sequences between rat and human GPR81 and GPR109a are rather different, so there was hope that some of the compounds might show selectivity. As shown in Figure 21.29, almost all peptides showed agonistic activity on rat GPR81 with a pEC_{50} up to 6. Unfortunately, the compounds were also active on all the other receptors tested and this was an indication of a bulk property effect rather than a specific interaction.

Most of the curves showed steep curve behavior with a top effect up to 120% that indicates complete inhibition of cAMP production and might be caused by cell toxicity. Other compounds had bell-shaped curves.

The compounds were also tested in the human GTP γ S GPR81 binding assay. Again, most of the compounds tested were active in the assay with sometimes extreme top efficacies, up to 2000%. Random sequence compounds and sequences originating from a third GPCR unrelated to the hydroxycarboxylic acid receptor family [62] showed the same type of behavior. Finally, the compounds were submitted to a dynamic mass redistribution response screen and ran in agonist and in antagonist mode on an unrelated GPCR receptor. In the agonist screen, most of the compounds were returned as actives, while the antagonist screen yielded only a few hits. There was a good correlation between potency data independent of the receptor type overexpressed in the cells. All potency data of rat versus human GPR81 and/or GPR109a showed good correlations. Correlations based on the straight line fits are given in Table 21.6.

Table 21.6 R^2 -values resulting from the straight line fit between the various GPCR cAMP assays.

GPCR receptors	Human 81	Rat 81	Human 109a
Rat 109a	0.73	0.73	0.76
Human 109a	0.62	0.73	—
Rat 81	0.73	—	0.73

The data is based on the pEC_{50} values of the active compounds in the respective cAMP TRF screen.

All of this data supported a conclusion that we were looking at physico-chemical compound property behavior or an unspecific assay interference property rather than specific interactions with a given receptor. It was surprising that all three assay technologies against various GPCRs showed a clear response to the compounds with exception of the antagonist screen. The conclusion was that in our hands the pepducin approach would not provide a clear rational approach to identify true hits.

21.8

Conclusions

For a given target, HTS is perhaps the most important tool for lead generation. It is often combined with other strategies, for example, subset screening based on target families and known ligands, fragment-based lead generation, fast follower programs, known literature hit-, lead-, and endogenous ligand expansion. All these strategies need a well-defined screening cascade to ensure the compounds have the right PD profile. It has been suggested that many HTS campaigns in the past have been potency driven resulting in highly lipophilic compounds that make lead optimization and clinical success less likely. Addressing this, the medicinal chemistry community has generated a wealth of literature describing how to monitor lipophilicity and how to define clear ligand lipophilicity and size efficiency parameters as well as elucidating how such properties drive wanted and unwanted drug effects. Many articles imply that composite parameters might offer better drivers for hit evaluation, lead generation, and lead optimization campaigns. We propose a more holistic approach. Campaigns should be efficacy driven in the first place. Independent of whether an HTS is measuring signaling, affinity, or competitive binding, identified hits need to demonstrate efficacy in either a cell free or cellular system before progression. Off-target effects, efficacy in relevant species assays, and counterscreen effects should capture and filter compounds with the right PD profile. Once a basic PD and selectivity profile is established, translation into a more relevant system should be monitored. The effect in such systems, that is, phenotypic screens or biological effect assays, should be predictive for an *in vivo* PD effect. The way a binder achieves efficacy is also important. Biased signaling, receptor internalization, orthosteric versus allosteric, full-, partial-, and inverse agonism or other mode of action, receptor occupancy, kinetics, and curve behavior are just some of the factors that may play an important role in understanding the efficacy of a compound. Compound potency and SAR remain a major driver in that respect. No potency no drug. Purity needs to be checked! Toxicity assessment, metabolism, permeability, efflux, PGP substrates, protein binding, and Cyp, TDI, hERG, and PK profiling should follow. Lipophilicity, size, number of hydrogen donors and acceptors, rotatable bonds, pK_a , sp^3 content, number of aromatic ring systems are all easy to compute and to analyze from a statistical perspective. While this

is still a reasonable exercise, it should not be the primary or even secondary filter criterion in any campaign. To judge the attractiveness of a series, all these parameters and effects should be weighed against each other before making a decision on how to progress. Drug discovery remains an exciting challenge to be mastered.

References

- 1 Ahmed, K., Tunaru, S., and Offermanns, S. (2009) *Trends in Pharmacological Sciences*, **30** (11), 557–562.
- 2 Ge, H., Weiszmann, J., Reagan, J.D., Gupte, J., Baribault, H., Gyuris, T., Chen, J.-L., Tian, H., and Li, Y. (2008) *Journal of Lipid Research*, **49**, 797–803.
- 3 Cai, T.Q., Ren, N., Jin, L., Cheng, K., Kash, S., Chen, R., Wright, S.D., Taggart, A.K., and Waters, M.G. (2008) *Biochemical and Biophysical Research Communications*, **377** (3), 987–991; Xu, H.-J. (2009) *The Journal of Biological Chemistry*, **284**, 2811–2822.
- 4 Taggart, A.K., Kero, J., Gan, X., Cai, T.Q., Cheng, K., Ippolito, M., Ren, N., Kaplan, R., Wu, K., Wu, T.J., Jin, L., Liaw, C., Chen, R., Richman, J., Connolly, D., Offermanns, S., Wright, S.D., and Waters, M.G. (2005) *Journal of Biological Chemistry*, **280**, 26649–26652.
- 5 Akinaga, J., Lima, V., Kiguti, L.R., Hebelers-Barbosa, F., Alcántara-Hernández, R., García-Sáinz, J.A., and Pupo, A.S. (2013) *Molecular Pharmacology*, **83** (4), 870–878.
- 6 Whalen, E.J., Rajagopal, S., and Lefkowitz, R.J. (2011) *Trends in Molecular Medicine*, **17** (3), 126–139.
- 7 Wermuth, C.G. (2006) *Drug Discovery Today*, **11** (3–4), 160–164.
- 8 Klabunde, T. (2007) *British Journal of Pharmacology*, **152**, 5–7.
- 9 (a) Hughes, J.D., Blagg, J., Price, D.A., Bailey, S., DeCrescenzo, G.A., Devraj, R. V., Ellsworth, E., Fobian, Y.M., Gibbs, M. E., Gilles, R.W., Greene, N., Huang, E., Krieger-Burke, T., Loesel, J., Wager, T., Whiteley, L., and Zhang, Y. (2008) *Bioorganic and Medicinal Chemistry Letters*, **18**, 4872–4875; (b) Leeson, P.D. and Empfield, J.R. (2010) *Annual Reports in Medicinal Chemistry*, **45**, 393–407; (c) Bickerton, G.R., Paolini, G. V., Besnard, J., and Muresan, S., and Hopkins, A.L. (2012) *Nature Chemistry*, **4** 90–98.
- 10 Johnson, T.W., Dress, K.R., and Edwards, M. (2009) *Bioorganic and Medicinal Chemistry Letters*, **19**, 5560–5564.
- 11 Warring, M.J. (2009) *Bioorganic and Medicinal Chemistry Letters*, **19**, 2844–2851.
- 12 Hann, M.M. (2011) *Medicinal Chemistry Communications*, **2**, 349–355.
- 13 Albert, J.S., Blomberg, N., Breeze, A.L., Brown, A.J., Burrows, J.N., Edwards, P.D., Folmer, R.H., Geschwindner, S., Griffen, E. J., Kenny, P.W., Nowak, T., Olsson, L.L., Sanganeer, H., and Shapiro, A.B. (2007) *Current Topics in Medicinal Chemistry*, **7** (16), 1600–1629.
- 14 Cai, T.-Q., Ren, N., Jin, L., Cheng, K., Kash, S., Chen, R., Wright, S.D., Taggart, A.K.P., and Waters, M.G. (2008) *Biochemical and Biophysical Research Communications*, **377**, 987–991.
- 15 Boatman, P.D., Johnson, B.R., Jung, J.-K., Kasem, M., Schrader, T.O., Skinner, P.J., and Colletti, S.L. WO2010030360 A1; published 2010; Application number PCT/US2009/005083; Applicant Arena Pharmaceuticals, Inc.; Merck & Co., Inc.
- 16 Finkel, R., Clark, M.A., Cubeddu, L.X. (2009) *Lippincott Williams & Wilkins, Lippincott's Illustrated Reviews: Pharmacology*, Lippincott Williams & Wilkins, 4th edn, p. 32; 351 West Camden Street Baltimore, PA 19106.
- 17 (a) Varin, T., Gubler, H., Parker, C.N., Zhang, J.H., Raman, P., Ertl, P., and Schuffenhauer, A. (2010) *Journal of Chemical Information and Modeling*, **50**

- (12), 2067–2078; (b) Varin, T., Schuffenhauer, A., Ertl, P., and Renner, S. (2012) *Journal of Medicinal Chemistry*, **55**, 1161–1170.
- 18 Bemis, G.W. and Murcko, M.A. (1996) *Journal of Medicinal Chemistry*, **39**, 2887–2893.
- 19 Cao, Y., Jiang, T., and Girke, T. (2008) *Bioinformatics*, **24**, i366–i374.
- 20 Varin, T., Schuffenhauer, A., Ertl, P., and Renner, S. (2011) *Journal of Chemical Information and Modeling*, **51**, 1528–1538.
- 21 Abad-Zapatero, C. and Metz, J.T. (2005) *Drug Discovery Today*, **10** (7), 464–469.
- 22 Hopkins, A.L., Keserü, G.M., Leeson, P.D., Rees, D.C., and Reynolds, C.H. (2014) *Nature Reviews Drug Discovery*, **13**, 105–121.
- 23 Wermuth, C.G., Ganellin, C.R., Lindberg, P., and Mitscher, L.A. (1998) *Pure and Applied Chemistry*, **70** (5), 1129–1143.
- 24 Cambridge MedChem Consulting© 2012, Dr Chris Swain BA MA (Cantab) PhD CChem FRSC. Bioisosteric Replacements, <http://www.cambridgemedchemconsulting.com/resources/bioisosteres/last> (accessed 2 April 2014).
- 25 Nicholls, A., McGaughey, G.B., Sheridan, R.P., Good, A.C., Warren, G., Mathieu, M., Muchmore, S.W., Brown, S.P., Grant, J.A., Haigh, J.A., Nevins, N., Jain, A.N., and Kelley, B. (2010) *Journal of Medicinal Chemistry*, **53** (10), 3862–3886.
- 26 Ishikawa, M. and Hashimoto, Y. (2011) *Journal of Medicinal Chemistry*, **54**, 1539–1554.
- 27 (a) Chan, L.L., Lidstone, E.A., Finch, K.E., Heeres, J.T., Hergenrother, P.J., and Cunningham, B.T. (2009) *Journal of Laboratory Automation*, **14**, 348–359. (b) Coan, K.E.D., Maltby, D.A., Burlingame, A.L., and Shoichet, B.K. (2009) *Journal of Medicinal Chemistry*, **52** (7), 2067–2075.
- 28 Shoichet, B.K. (2006) *Journal of Medicinal Chemistry*, **49** (25), 7274–7277.
- 29 Strauss, O. and Goldstein, W.D.A. (1943) *Journal of General Physiology*, **26** (6), 559–585.
- 30 (a) Keighley, W. (2011) *Drug Discovery World Summer*, **13** (26), 39–45, Kinetics_layout 1, 23/06/2011; (b) Zhang, R. and Monsma, F. (2010) *Expert Opinion in Drug Discovery*, **5** (11), 1023–1029; (c) Copeland, R.A., Pompliano, D.L. and Meek, T.D. (2006) *Nature Reviews Drug Discovery*, **5** (9), 730–739; (d) Nunez, S., Venhorst, J. and Kruse, C.G. (2012) *Drug Discovery Today*, **17**, 10–22; (e) Lu, H. and Tonge, P.J. (2010) *Current Opinion in Chemical Biology*, **14**, 467–474.
- 31 Zhang, R. and Monsma, R.F. (2009) *Current Opinion in Drug Discovery and Development*, **12** (4), 488–496.
- 32 Rishton, G.M. (1997) *Drug Discovery Today*, **2** (9), 382–384.
- 33 Baell, J.B. and Holloway, G.A. (2010) *Journal of Medicinal Chemistry*, **53**, 2719–2740.
- 34 Metz, J.T., Huth, J.R., and Hajduk, P.J. (2007) *Journal of Computer-Aided Molecular Design*, **21**, 139–144.
- 35 (a) Hann, M.M. and Keserü, G.M. (2012) *Nature Reviews Drug Discovery*, **11** (5), 355–365; (b) Leeson, P.D. and Springthorpe, B. (2007) *Nature Reviews Drug Discovery*, **6** (11), 881–889; (c) Waring, M. (2010) *Expert Opinion on Drug Discovery*, **5** (3), 235–248; (d) Hann, M.M. (2011) *Medicinal Chemistry Communications*, **2**, 349–355.
- 36 Ritchie, T.J., Macdonald, S.J.F., Young, R.J., and Pickett, S.D. (2011) *Drug Discovery Today*, **16** (3–4), 164–171.
- 37 Núñez, S., Venhorst, J., and Kruse, C.G. (2012) *Drug Discovery Today*, **17** (1/2), 10–22.
- 38 (a) Peters, J.-U., Schnider, P., Mattei, P., and Kansy, M. (2009) *ChemMedChem*, **4**, 680–686; (b) Pelletier, D.J., Gehlhaar, D., Tilloy-Ellul, A., Johnson, T.O., and Greene, N. (2007) *Journal of Chemical Information and Modeling*, **47**, 1196–1205.
- 39 (a) Lovering, F. (2013) *Medicinal Chemistry Communications*, **4**, 515–519; (b) Lovering, F., Bikker, J., and Humblet, C. (2009) *Journal of Medicinal Chemistry*, **52** (21), 6752–6756.
- 40 (a) Whitty, A. (2011) *Future Medicinal Chemistry*, **3** (7), 797–801; (b) Baell, J.B.

- and Holloway, G.A. (2010) *Journal of Medicinal Chemistry*, **53**, 2719–2740.
- 41 Johnston, P.A. (2011) *Current Opinion in Chemical Biology*, **15**, 174–182.
 - 42 Lipinski, C.A., Lombardo, F., Dominy, B. W., and Feeney, P.J. (1997) *Advanced Drug Delivery Reviews*, **23**, 3–25.
 - 43 Reynolds, C.H., Tounge, B.A., and Bembenek, S.D. (2008) *Journal of Medicinal Chemistry*, **51**, 2432–2438.
 - 44 Kuntz, I. D., Chen, K., Sharp, K.A., and Kollman, P.A. (1999) *Proceedings of the National Academy of Sciences of the United States of America*, **96**, 9997–10002.
 - 45 (a) Shultz, M.D. (2013) *Bioorganic and Medicinal Chemistry Letters*, **23**, 5980–5991; (b) Shultz, M.D. (2013) *Bioorganic and Medicinal Chemistry Letters*, **23**, 5992–6000.
 - 46 Mortenson, P.N. and Murray, C.W. (2011) *Journal of Computer-Aided Molecular Design*, **25** (7), 663–667.
 - 47 Reynolds, C.H., Tounge, B.A., and Bembenek, S.D. (2008) *Journal of Medicinal Chemistry*, **51** (8), 2432–2438.
 - 48 Nissink, J.W.M. (2009) *Journal of Chemical Information and Modeling*, **49** (6), 1617–1622.
 - 49 Drug Design Strategies: Quantitative Approaches. Edited by David J. Livingstone and Andrew M. Davis.; Matter, H. (2012), Drug Design Strategies: Quantitative Approaches. Edited by David J. Livingstone and Andrew M. Davis.; Royal Society of Chemistry 2012, Thomas Graham House, science Park, Milton Road, Cambridge CB4 = WF, UK; Chapter 2, p. 52.
 - 50 (a) Price, D.A., Blagg, J., Jones, L., Greene, N., and Wager, T. (2009) *Expert Opinion on Drug Metabolism and Toxicology*, **5** (8), 921–993. (b) Testa, B. and Krämer, S.D. (2009) *Chemistry and Biodiversity*, **6** (5), 591–684.
 - 51 Kalgutkar, A.S., Gardner, I., Obach, R.S., Shaffer, C.L., Callegari, E., Henne, K.R., Mutlib, A.E., Dalvie, D.K., Lee, J.S., Nakai, Y., O'Donnell, J.P., Boer, J., and Harriman, S.P. (2005) *Current Drug Metabolism*, **6**, 161–225.
 - 52 Hudson, B.D., Due-Hansen, M.E., Christiansen, E., Hansen, A.M., Mackenzie, A.E., Murdoch, H., Pandey, S.K., Ward, R.J., Marquez, R., Tikhonova, I.G., and Ulven, T. (2013) *Journal of Biological Chemistry*, **288**, 17296–17312.
 - 53 (a) See at web page http://physchem.org.uk/symp03/symp03_al.pdf (accessed 15 May 2014); (b) Hu, Y., de la Vega de León, A., Zhang, B., and Bajorath, J. (2014) *F1000Research*, **3** (36), 1–12.
 - 54 (a) Zhao, H. and Akritopoulou-Zanze, I. (2010) *Expert Opinion on Drug Discovery*, **5** (2), 123–134; (b) Ritchie, T.J., Macdonald, S.J.F., Peace, S., Pickett, S.D., and Luscombe, C.N. (2012) *Medicinal Chemistry Communications*, **3**, 1062–1069.
 - 55 Grimwood, S. and Hartig, P.R. (2009) *Pharmacology and Therapeutics*, **122**, 281–301.
 - 56 Dvorak, C.A., Liu, C., Shelton, J., Kuei, C., Sutton, S.W., Lovenberg, T.W., and Carruthers, N.I. (2012) *Medicinal Chemistry Letters*, **3** (8), 637–639.
 - 57 Kuei, C., Yu, J., Zhu, J., Wu, J., Zhang, L., Shih, A., Mirzadegan, T., Lovenberg, T., and Liu, C. (2011) *Molecular Pharmacology*, **80** (5), 848–858.
 - 58 (a) Taylor, J.B. and Trigg, D.J. (2007) *Comprehensive Medicinal Chemistry II*, Elsevier, Elsevier Ltd PO Box 800, Oxford OX5 1DX UK, pp. 649–671; (b) Wassermann, A.M. and Bajorath, J. (2011) *Medicinal Chemistry Communications*, **2**, 601–606.
 - 59 Liu, C., Kuei, C., Zhu, J., Yu, J., Zhang, L., Shih, A., Mirzadegan, T., Shelton, J., Sutton, S., Connelly, M.A., Lee, G., Carruthers, N., Wu, J., and Lovenberg, T. W. (2012) *Journal of Pharmacology and Experimental Therapeutics*, **341**, 794–880.
 - 60 Sakurai, T., Davenport, R., Stafford, S., Grosse, J., Ogawa, K., Cameron, J., Parton, L., Sykes, A., Mack, S., Bousba, S., Parmar, A., Harrison, D., Dickson, L., Leveridge, M., Matsui, J., and Barnes, M. (2014) *European Journal of Pharmacology*, **727**, 1–7.
 - 61 (a) Carlson, K.E., McMurry, T.J., and Hunt, S.W. III (2012) *Drug Discovery*

- Today: Technologies*, **9** (1), e33–e39. (b) Dimond, P., Carlson, K., Bouvier, M., Gerard, C., Xu, L., Covic, L., Agarwal, A., Ernst, O.P., Janz, J.M., Schwartz, T.W., Gardella, T.J., Milligan, G., Kuliopulos, A., Sakmar, T.P., and Hunt, S.W. III (2011) *Annals of the New York Academy of Sciences*, **1226**, 34–49; (c) Kuliopulos, A. and Covic, L. (2003) *Life Sciences*, **74**, 255–262.
- 62** Milletti, F. (2012) *Drug Discovery Today*, **17** (15/16), 850–860.
- 63** Offermanns, S., Colletti, S.L., Lovenberg, T.W., Semple, G., Wise, A., and IJzerman, A.P. (2011) *Pharmacological Reviews*, **63** (2), 269–290.

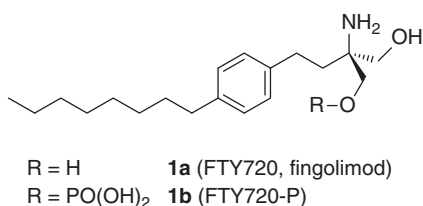


Figure 22.1 Structure of fingolimod (FTY-720) and FTY-720 phosphate.

multiple sclerosis and in 2010 was the first S1P₁ receptor agonist to have gained FDA approval. Fingolimod is a prodrug that undergoes enantiospecific phosphorylation to **1b** (Figure 22.1) *in vivo* to exert its activity. It is also a lipophilic drug able to penetrate the brain, and while this may contribute to efficacy in the CNS [9], central penetration was considered undesirable for treatment of peripheral indications such as psoriasis and IBD. The pharmacokinetics (PK) of fingolimod are characterized by a prolonged oral absorption phase and long elimination half-life (100–200 h), driven by a large volume of distribution [10, 11], which in turn drives a sustained pharmacodynamic (PD) effect of lymphocyte reduction in humans and also rodents [12]. Transient bradycardia was noted in patients and in rodent studies after the first dose with the effect in rodents attributed to agonism of the S1P₃ receptor. Other adverse events (including macular edema, modest hypertension, and some pulmonary effects) were observed in early clinical studies and thought to be mediated via the nonselective action of FTY-720 phosphate on S1P_{3–5} receptors [9].

Due to the positive efficacy data with fingolimod in the clinic, there was urgency to discover molecules with an improved profile.

22.1.2 Overview of the Strategy and Screening Cascade

The aim of the lead optimization campaign was to discover non-prodrug, potent, and selective S1P₁ agonists in “drug-like” space [13–15] and with an improved profile over fingolimod. The promising anti-inflammatory activity was suitable for central and peripheral disease indications, and medicinal chemistry starting points were considered tractable. The desired product profile included a direct, non-prodrug molecule to theoretically drive a greater consistency in target site exposure due to the absence of the *in vivo* phosphorylation step required with fingolimod. Potency, coupled with a PK profile capable of delivering once daily administration, was essential to drive a low human dose to reduce attrition risk in safety and clinical studies through a low body burden. A shorter PK half-life than fingolimod was also considered desirable to drive a more controlled lymphocyte reduction profile and mitigate any potential risk associated with compromised immunity. Receptor selectivity for S1P₁, particularly against S1P₃, was essential to minimize the potential for bradycardia in the clinic.

The screening strategy initially employed by the program is shown in Figure 22.2. It is depicted “upside down” compared with traditional illustrations to emphasize the focus on the patient and the desired clinical profile, which in turn dictated the preclinical requirements and molecule profile. All animal studies were ethically reviewed and carried out in accordance with Animals

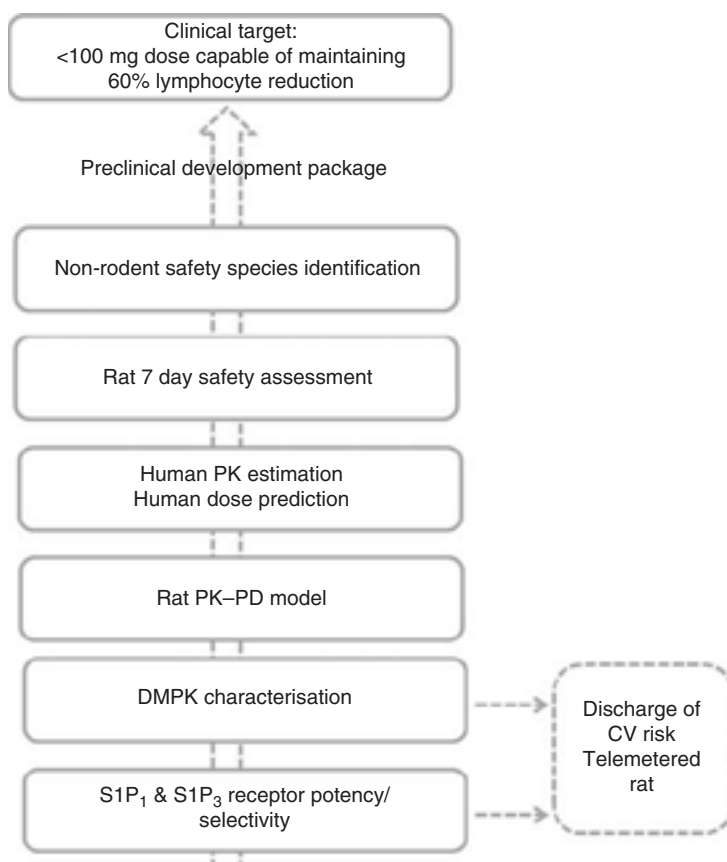


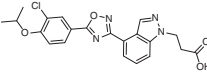
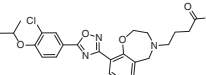
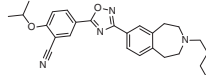
Figure 22.2 Core elements of the screening cascade for the design and selection of S1P₁ agonists.

(Scientific Procedures) Act 1986 and the GSK Policy on the Care, Welfare, and Treatment of Animals.

22.2 Early Attention to Preclinical Safety

Intensive medicinal chemistry and the implementation of the screening strategy resulted in the successful delivery of numerous molecules suitable for evaluation in preliminary rodent safety studies. Examples of compounds progressed into such studies were compounds 2–4 [16, 17], with the key parameters summarized in Table 22.1. These compounds were in physicochemical drug-like space and had a high potency and receptor selectivity, a preclinical PK profile suitable for oral administration, no drug–drug interaction (DDI) liability, and a low human dose prediction. These molecules were progressed to rodent safety studies to assess the general toxicology profile and the potential for further development and provide an early estimation of the therapeutic index. Several molecules were progressed

Table 22.1 The overall profile of exemplar molecules entering early safety studies.

Compound	2	3	4
Structure			
MW, Log $D_{7.8}$, PSA	427, 2.3, 103	472, 2.4, 98	460, 1.8, 112
SIP ₇ /SIP ₂ EC ₅₀ (μM)	0.020/>31 (>1500-fold)	0.040/>31 (800-fold)	0.008/8 (1000-fold)
Human hepatocyte CL ₁ (μl min ⁻¹ 10 ⁶ cells ⁻¹)	<7.1	11	<7.1
CYP450 inhibition (IC ₅₀ μM)	2C9 : 7 Others >25	>27	>40
PK rat ^a			
CL _b (ml min ⁻¹ kg ⁻¹)	2.0	7.0	7.0
V _{ss} (l kg ⁻¹)	1.0	1.2	1.5
T _{1/2} (h)	7.5	3.0	2.6
F _{po} (%)	96	83	62
PK dog ^b			
CL _b (ml min ⁻¹ kg ⁻¹)	4.0	26	3.0
V _{ss} (l kg ⁻¹)	1.0	1.0	1.6
T _{1/2} (h)	3.9	0.4	8.0
F _{po} (%)	94	57	69
Estimated human oral dose	≤50 mg twice daily	≤100 mg once daily	<50 mg once daily

CL_i: intrinsic clearance; PK: pharmacokinetics; CYP450: cytochrome P450 enzymes CYP1A2, 2C9, 2C19, 2D6, 3A4; CL_b: blood clearance; V_{ss}: volume of distribution at steady state; F_{po}: oral bioavailability.

a) Rat PK: IV 1 mg kg⁻¹, oral 3 mg kg⁻¹.

b) Dog PK IV 1 mg kg⁻¹, oral 2 mg kg⁻¹.

c) Source: From Skidmore et al. 2014 [17]. Reproduced with permission of American Chemical Society.

in parallel as this chemical template was previously uncharacterized. Compounds were administered orally, once daily, to rats at three different dose levels for 7 days. Dose levels were selected to provide multiples of the estimated human systemic exposure to ensure an appropriate therapeutic index was investigated.

22.2.1 Use of Toxicogenomics in Early Rodent Safety Studies

In addition to collecting tissue pathology and histopathology endpoints from these safety studies, toxicogenomic data were also generated. Such data provide an opportunity to identify pathways and processes affected by the test article that may be predictive of adverse findings following longer-term drug exposure (see Chapter 21 for an additional case study on the use of toxicogenomics). Data may suggest mechanisms of toxicity and “off-target” activity and are considered supplemental to clinical pathology and histopathology measurements. Transcript changes in the liver, for example, offer a means of predicting hepatotoxicity or safety events associated with dysregulation of hepatic function. Panels of genes have been identified through comparison with known hepatotoxins that, if affected, are representative of modes of hepatotoxicity (hepatotox). These panels include genes that code for increased expression of drug-metabolizing enzymes including the pregnane X receptor (PXR), the constitutive androstane receptor (CAR), and the aryl hydrocarbon receptor (AhR), which are involved in the regulation of cytochrome P450 enzymes 3A, 2C, and 1A, respectively [18].

22.3 Aryl Hydrocarbon Receptor Activation Observed in Rat

The toxicokinetic data collected on the first and last days of the studies indicated that the exposure of the compounds increased in line with dose and no change in exposure was observed on repeat administration. However, analysis of the toxicogenomic data revealed an unexpected finding. Compounds 2–4 all caused marked increases in CYP1A1, CYP1A2, NAD(P)H quinone oxidoreductase (NQO1), and epoxide hydrolase (Ephx) genes, a gene panel indicating AhR activation (Figure 22.3). A positive response for this gene panel occurs when the upregulation of each gene exceeds its own threshold value, which was threefold for CYP1A2, twofold for CYP1A1 and NQO1, and 1.5-fold for Ephx.

The level of CYP1A1 mRNA increase in particular was very high, up to 10 000-fold the control value, and at the time of this finding was the highest in the data set at GlaxoSmithKline. Other genes in the panel (CYP1A2, NQO1, and Ephx) were all also upregulated, confirming an interaction with the AhR. It should be noted that the level of gene upregulation was comparable with that of the prototypical CYP1A inducers β -naphthoflavone (BNF) and 3-methylcholanthrene (3MC) exemplifying the magnitude of this finding. Similar observations with these structurally related compounds suggested a common mechanism. When focusing on CYP1A1 mRNA, it was clear that the magnitude of increase was related to systemic exposure (and dose), but an interesting observation at this

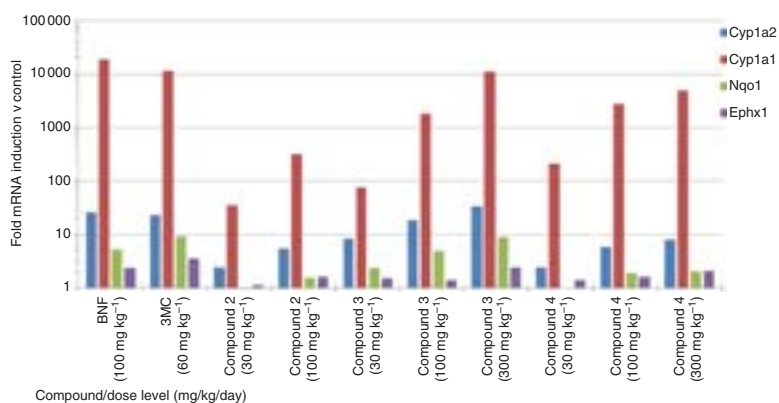


Figure 22.3 Upregulation of genes associated with the AhR gene panel for 2, 3, and 4 following 7-day oral administration to rats. The response to prototypical AhR agonists β -naphthoflavone (BNF) and 3-methylcholanthrene (3MC) after 4-day administration is included for reference. Cyp: cytochrome P450. NQO1: NAD(P)H quinone oxidoreductase. Ephx1: epoxide hydrolase. *Source:* From Taylor et al. 2015 [16]. Reprinted with permission American Chemical Society.

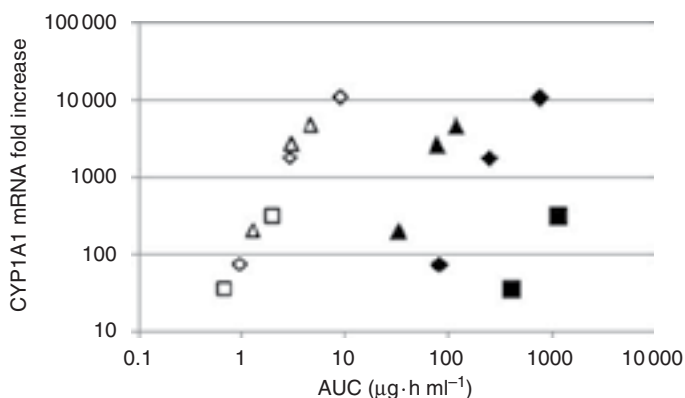


Figure 22.4 The relationship between systemic exposure (AUC) and hepatic CYP1A1 mRNA induction for compounds **2** (squares), **3** (diamonds), and **4** (triangles) following 7-day oral administration to the rat. Daily doses were 30 and 100 mg kg⁻¹ for **2** and 30 and 100 and 300 mg kg⁻¹ for **3** and **4**, respectively. The figure illustrates the alignment of a relationship when the AUC is adjusted to represent the unbound exposure (open shapes) compared with the total exposure (closed shapes). *Source:* From Taylor et al. 2015 [16]. Reprinted with permission American Chemical Society.

early stage was that a strong relationship was observed across all compounds when plotted against unbound rather than total systemic exposure as in Figure 22.4. This observation was explored and used in the design of future safety studies.

22.4 CYP1A (Auto) Induction Observed in Non-rodent Species

Further progression of **2** required the definition of a non-rodent species for use in safety assessment evaluation. Repeated oral administration to dogs resulted in a lack of tolerability and body weight loss, and so an alternate species was sought. A repeat-dose oral study (30 mg kg⁻¹) using cynomolgus monkeys was conducted over 7 days with the objective of evaluating if appropriate systemic exposure could be achieved in this species to allow further safety evaluation. Analysis of the toxicokinetic data revealed substantial reduction in systemic exposure over the study duration. Figure 22.5 illustrates the reduction in both C_{\max} and AUC on repeat administration. Similar to the findings in rat, gene expression analysis from liver samples confirmed a substantial increase of CYP1A1 and CYP1A2 mRNA up to ninefold the control value (Figure 22.6). The reduction in exposure coupled with the upregulation of CYP1A1 and 1A2 mRNA was suggestive of auto-induction, a phenomenon where the molecule induces its own metabolism. This was confirmed through experiments designed to evaluate the intrinsic clearance rate of **2** in the induced liver versus control liver using microsomes prepared from the livers of animals on the study. In control microsomes **2** was metabolically stable with no measurable disappearance of

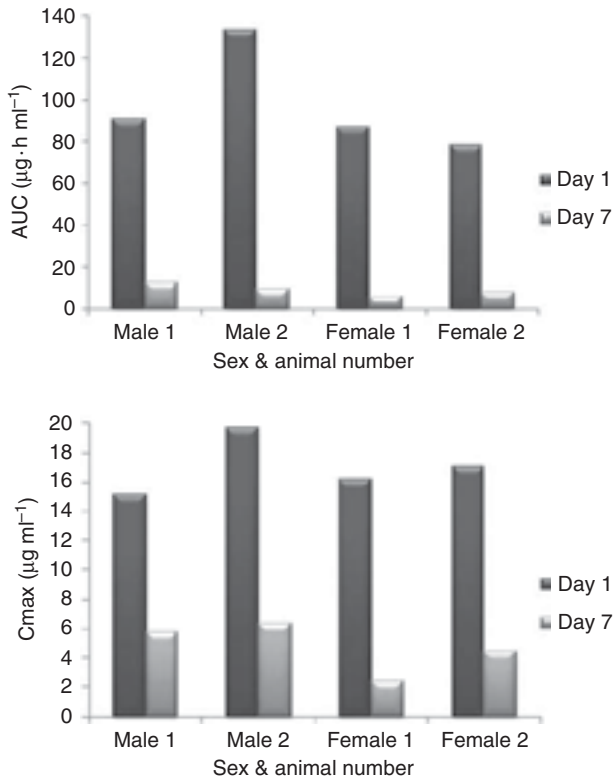


Figure 22.5 Compound **2** is an auto-inducer in cynomolgus monkeys. Toxicokinetic data (exposure, as area under the curve and Cmax) for **2** on days 1 and 7 following oral dosing at 30 mg kg⁻¹ day⁻¹ to monkeys. *Source:* From Taylor et al. 2015 [16]. Reprinted with permission American Chemical Society.

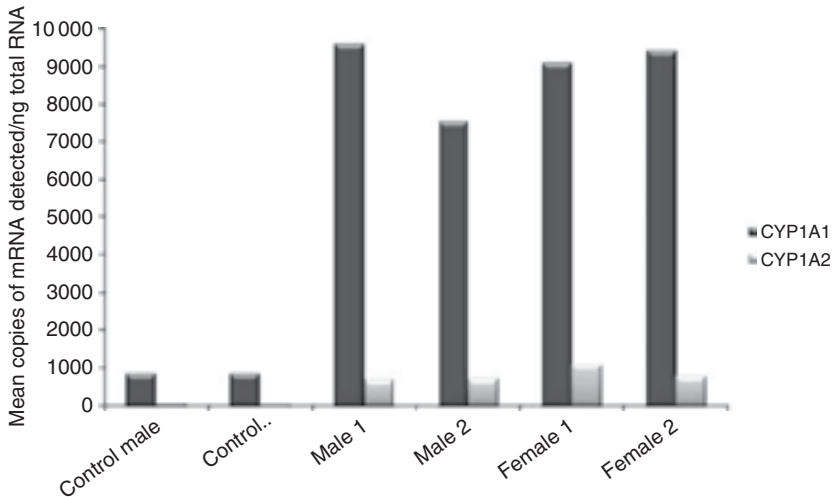


Figure 22.6 Upregulation of hepatic CYP1A1 and CYP1A2 mRNA in cynomolgus monkeys by **2** following 7-day oral dosing at 30 mg kg⁻¹. *Source:* From Taylor et al. 2015 [16]. Reprinted with permission American Chemical Society.

compound during the incubation period, whereas a high intrinsic clearance was observed in microsomes prepared from treated animals ($11 \text{ ml min}^{-1} \text{ g}^{-1}$ liver). The auto-induction effect ultimately prevented **2** from progressing to further safety studies in cynomolgus monkey as adequate exposure to provide a therapeutic index suitable for development could not be achieved on chronic administration.

The extent of CYP1A1 mRNA upregulation in the rat (up to 10 000-fold the control value), a finding at this level unprecedented at GSK, and a similar finding in the cynomolgus monkey prompted a review into the implications of progressing compounds that were agonists of the AhR into further development.

22.5 Introduction to the Biology and Function of the Aryl Hydrocarbon Receptor

In order to fully appreciate the strategy and approach taken in this case study, a brief introduction to the biology and function of the AhR is provided, and the impact of this information in the context of this drug development program as interpreted within GlaxoSmithKline at the time the S1P₁ program was active is described. More detailed information on AhR biology, function, and impact can be obtained from several review articles [19–25].

22.5.1 CYP1A Induction via the AhR

The AhR is a ligand-dependent transcription factor responsible for the regulation of gene expression in a wide range of tissues and species [19]. AhR is activated by a diverse range of endogenous and exogenous substrates and mediates numerous biological and toxicological responses [26]. Following ligand binding to the cytosolic AhR, the multi-protein complex translocates to the nucleus where the AhR ligand complex dimerizes with a related protein (ARNT). This high affinity complex then binds to specific DNA recognition sites stimulating gene transcription including those of CYP1A and other AhR responsive genes including those described earlier.

The consequences of AhR activation have been extensively characterized using high affinity ligands found as environmental contaminants. These include the potent and high affinity halogenated aromatic hydrocarbons (HAHs) such as 2,3,7,8-tetrachlorodibenzo-*p*-dioxin (TCDD) (dioxin) and the lower affinity polycyclic aromatic hydrocarbons (PAHs) such as 3MC and benzo(a)pyrene. PAHs are also present as components of exhaust fumes, cigarette smoke, and charbroiled food. Natural ligands also exist. Structure–activity relationships (SAR) from these compound classes suggest the binding pocket favors planar hydrophobic ligands though more diverse structures are also reported. Exposure to dioxin causes an array of species and tissue-specific biological and toxic events including tumor promotion, teratogenicity, modulation of cell growth, differentiation, proliferation, wasting and immune, and hepatotoxicity and dermal toxicities. The latter toxicities generally take several weeks to manifest

and can only be observed with intact animal systems, suggesting a continuous and modified gene expression profile in responsive cells [19].

22.5.2 CYP1A Enzyme Family

The upregulation of CYP1A enzymes is an AhR-dependent response that has been consistently observed across species and is considered one of the most sensitive AhR activation endpoints [19, 27].

The CYP1A enzyme subfamily comprises CYP1A1 and 1A2, both having high amino acid sequence conservation across rats, mice, dogs, monkeys, and human species although variation is seen in the constitutive and inducible nature of these enzymes across species and tissues. This profile impacts the location and magnitude of responses to AhR agonists, the opportunities for measurement of upregulation, and also the consequences of the findings across species in the context of drug development.

CYP1A1 basal expression is negligible yet variable. Only very low levels are expressed in the liver with CYP1A1, predominantly an extrahepatic enzyme inducible in virtually all body tissues most notably in the small intestine and lung. Higher levels are found in smokers and those having ingested chargrilled meats though other dietary factors are also involved.

In contrast CYP1A2 is predominantly a hepatic enzyme being absent or only weakly expressed in extrahepatic tissues. In humans it represents approximately 13% of total hepatic cytochrome P450 content [28] and is involved in the metabolism of up to 20% of marketed drugs plus many environmental aromatic amines [22]. The function of this enzyme and also the consequences for any change in the level of expression or activity should therefore be considered as part of a drug development program. It is inducible in tissues such as the lung and intestine with large (>60-fold) interindividual variability in CYP1A2 expression reported [29] attributable to genetic, epigenetic, and environmental factors such as smoking.

Induction of CYP1A1/1A2 via AhR-mediated pathways is generally considered to be a feedback mechanism in the maintenance of cellular homeostasis with many enzyme substrates also ligands for the AhR as is the case for the PAHs 3MC and benzo(a)pyrene. As cellular exposure to these enzyme substrates increases, enzyme induction follows to enhance the capability to detoxify the substance. As the substrate is removed, the extent of induction declines.

In vitro studies have shown that substrates of CYP1A enzymes such as benzo(a)pyrene form reactive intermediates as part of their metabolism, which are the ultimate carcinogen capable of DNA adduct formation. *In vitro* enzymology studies indicate a role for CYP1A as a perpetrator in driving these toxicities. Paradoxically, an overall protective role of CYP1A induction from oral chemical-induced carcinogenesis is observed *in vivo* [24]. As explained by Uno et al. [30], it is the balance of these processes that ultimately determines the effect. The interplay is clearly complex.

In addition to the environmental contaminants mentioned above, examples of drugs that are inducers of CYP1A2 most notably include the widely prescribed antiulcer drug omeprazole. Omeprazole, an inducer of hepatic CYP1A2 in

humans, but not rodents, is an example of a species-specific inducer. It has been used safely for more than 25 years. Minimizing exposure to cigarette smoke and dietary sources of PAHs was at one time recommended for patients on long-term omeprazole therapy, but a connection between omeprazole use and cancer incidence has yet to be described. More detail on this sequence of events is described in an article by Ma and Lu [24].

22.6 Considerations of AhR Binding and CYP1A Induction on Compound Progression

The consequences of continuing to develop molecules that are AhR agonists in the context of this drug discovery program were considered. Judgments in drug discovery are frequently problematic. The impact of termination decisions are rarely known, but an overconservative approach prevents therapeutically useful molecules from reaching patients. However, factors such as the patient population, indication, and competitive landscape should always be considered as progressing a molecule with a known risk resulting in later attrition is costly. In the case of this particular program, the molecules did not represent a first-in-class mechanism, and a “clean” profile at this early stage was preferred so as not to introduce additional risks over fingolimod.

The discussions associated with AhR activation and CYP1A induction were broadly categorized as follows: (i) increased risk of carcinogenicity in certain individuals and specific tissues, (ii) functional consequences of increased CYP1A enzyme activity, and (iii) impact of strong AhR agonism given the other emerging biological roles of the AhR.

The evidence for the role of CYP1A as a causal agent and/or detoxifier in PAH-induced carcinogenicity in mice was complex although suggestive of an overall protective effect *in vivo*. The absence of a connection between the CYP1A2 inducer omeprazole and carcinogenicity was also acknowledged though the mechanism of omeprazole induction is not fully understood and may not involve AhR binding [31]. However, the extent of CYP1A1 mRNA upregulation by the S1P₁ compounds was concerning, and, if translatable in human, the risk of potentiating carcinogenicity in directly exposed tissues such as the lung in smokers was considered to remain, as discussed by Nebert et al. [29] The possibility of mitigating these risks via preclinical experiments was also considered low with a clear result unlikely. The worst-case scenario was considered to be the emergence of a finding in humans in late-stage trials or postmarketing. Furthermore, the large interindividual variability in CYP1A2 expression across the population may put some individuals at greater risk, with the risk being largely unpredictable.

Induction and inhibition of cytochrome P450 enzymes have been shown to be responsible for numerous DDI in the clinic. Such interactions can limit the clinical and commercial viability of drugs, and therefore the potential is best addressed early in lead optimization [32]. P450 induction by a drug may increase the clearance of itself (auto-induction) or of co-administered drugs.

Auto-induction has the potential to result in a reduction or loss of efficacy of therapeutic agents and/or the generation of an altered metabolite profile. Focus is normally placed on CYP3A due to its importance in the metabolism of many therapeutic drugs [20] but with CYP1A2 contributing to the metabolism of around 20% of therapeutic drugs [22] there are several known DDI as a consequence of altered CYP1A metabolism [23]. Changes to the levels of this enzyme therefore require consideration in clinical practice.

Several examples of the potential for CYP1A induction to perpetrate a DDI with co-administered drugs in the clinic have been reported. Exposure to PAHs in cigarette smoke has been shown to induce CYP1A2 and increase the clearance and therefore reduce plasma concentrations of drugs including caffeine, theophylline, melatonin, clozapine, lidocaine, verapamil, erlotinib, and fluvoxamine [22, 33, 34]. Caffeine itself has also been shown to induce CYP1A2 in certain population groups [35]. A carbamazepine interaction has been reported with schizophrenic patients taking clozapine [36]. These interactions cited above for CYP1A2, while important, are usually managed in the clinic through dosage adjustment, therapeutic monitoring, and control of co-medications. In the case of smoking, this is particularly important as CYP1A2 levels can be altered abruptly via changes in smoking habits. The risk of the S1P₁ compounds perpetrating a DDI was acknowledged but ultimately considered a manageable issue in a clinical context. Moreover the expected clinical dose was low, reducing the likelihood of clinically significant DDI [37]. It was decided that, if necessary, a definitive DDI study could form part of the early clinical development program and, even if positive, while undesirable, this was considered manageable.

Evidence from the cynomolgus monkey study indicated the potential for these S1P₁ agonists to be CYP1A auto-inducers in the clinic. The potential impact of auto-induction on clinical efficacy, previously described, could ultimately result in termination. This finding would not emerge until the multiple ascending dose part of a phase I study after significant investment in preclinical development. Therefore, selecting only compounds without this property in discovery was considered essential.

In addition to enzyme regulation, numerous other physiological functions mediated by the AhR were emerging during the lifecycle of this S1P₁ agonist program. These included a role for the receptor in development, regulating cell differentiation and cycling, hormonal and nutritional homeostasis, coordination of cell stress responses (including inflammation and apoptosis), immune responses, aging, and cancer promotion [38]. While other literature at the time was suggesting the therapeutic potential of AhR agonism [39], the consequences of a strong AhR agonist on the emerging biological functions were not yet well defined. As attrition in late-stage drug development is unwanted and certainly costly, the uncharacterized effect of this agonist profile on longer-term administration in chronic toxicity studies and the clinic was also considered a high risk.

We contextualized these considerations for our drug discovery program relative to the desired product profile. Decisions were taken to continue progression of **3** toward 28-day safety studies but in parallel modify the screening strategy with the objective of identifying compounds with an improved profile devoid of any potential induction risk.

This decision was pragmatic as the properties of a molecule can only be modified during lead optimization. However, the decision may also be considered cautious. This was acknowledged by the team but was felt justified particularly as the compound was not a first-in-class mechanism, and in a highly competitive field, a successful molecule would likely require a “clean” profile.

22.7 Reacting to Data: Strategy Modification in Lead Optimization

The observation of AhR gene panel activation in rats and substantial CYP1A enzyme induction in cynomolgus monkey represented a body of evidence indicating this series of S1P₁ agonists were also agonists of the AhR in these species. However it is the effect in human systems that are of ultimate importance. The strategy to address this is now described along with the modifications to the screening cascade to bring forward compounds without the induction liability. In order to achieve this, an understanding of the structural features driving AhR agonism was required to influence the medicinal chemistry approach.

22.7.1 Evaluating CYP1A Induction in Human Systems

A human AhR binding assay was not available within GlaxoSmithKline at the time. We therefore turned to human hepatocytes as a well-characterized experimental system for studying enzyme induction *in vitro*. However, the low level of hepatic CYP1A1 expression in a human liver (recall that CYP1A1 is largely an extrahepatic enzyme in humans) meant the primary endpoint would be upregulation of CYP1A2. Due to the extensive CYP1A1 mRNA induction observed in rat liver, it was recognized that the true induction potential of these compounds may be underrepresented in human hepatocytes. Methods to study upregulation in extrahepatic tissues, where CYP1A1 is highly inducible, are less straightforward and poorly characterized due to, as an example, the complexities of obtaining metabolically competent cells from lung tissue. On balance a decision was taken to incorporate the available human hepatocyte assay into the S1P₁ program immediately and assume any observed CYP1A2 induction was also an indicator of CYP1A1 induction potential in other tissues. A strategic decision was also taken to introduce an AhR binding assay for future utility with this and other programs.

22.7.2 Evaluating Induction in Human Hepatocytes

Briefly, this experiment involved incubating test compounds over a concentration range with thawed cryopreserved hepatocytes for 48 h. Induction potential was assessed using dual methods of CYP1A2 mRNA levels and also catalytic enzyme activity. Catalytic enzyme activity was measured by using the rate of CYP1A-mediated deethylation of the fluorescent probe substrate 7-ethoxyresorufin where induction was represented by an increase in deethylation versus a control.

Table 22.2 Comparison of the CYP1A1, CYP1A2 (rat), or CYP1A2 (human) induction observed across various *in vivo* and *in vitro* assay formats.

Compound	^{a)} Rat <i>in vitro</i>		^{b)} Rat <i>in vivo</i>		^{c)} Human <i>in vitro</i>	
	CYP1A1 mRNA	CYP1A2 mRNA	CYP1A1 mRNA	CYP1A2 mRNA	CYP1A2 mRNA	Catalytic activity (EROD)
2	<1	<1	35	2	45	7.7
3	5	3	75	8	0.6	1.1
4	3	2	210	2	–	–
5	<1	<1	3	1	0.2	1.1
6	43	19	2	2	–	–
7	32	8	1	1	–	–

All data expressed as fold change versus control to enable comparison.

a) Rat *in vitro* assays conducted at 10 μ M.

b) Compounds 2–5: 7-day dosing 30 mg kg^{−1}. Compounds 6–7: 4-day dosing 20 mg kg^{−1}.

c) Human mRNA assay at 10 μ M, EROD assay at 5 μ M. EROD: 7-ethoxyresorufin *O*-deethylase activity.

Source: From Taylor et al. 2015 [16]. Reprinted with permission of American Chemical Society.

Compounds **2** and **3** were profiled in human hepatocytes. Although both compounds were considered AhR activators in rat, only **2** showed CYP1A2 upregulation in human hepatocytes, resulting in a 45-fold increase in CYP1A2 mRNA and an associated increase (eightfold) in catalytic enzyme activity (Table 22.2). While these data highlighted a potential species difference for **3** in hepatocytes, the inducing potential in other tissues was not fully discharged.

The development of **2** was terminated for reasons associated with the AhR induction potential, the primary reasons being the auto-induction in cynomolgus monkey previously described and the magnitude of exposure reduction preventing achievement of a sufficient therapeutic index. Alternative non-rodent species were also deemed inappropriate following preliminary safety studies. The development of **3** and **4** was also eventually terminated due to a variety of developability issues but not because of the AhR agonism finding alone.

Further medicinal chemistry efforts resulted in the rapid identification of **5** [40]. Based on its improved developability properties including preclinical PK and predicted human dose (Table 22.3), the compound was advanced rapidly into the human hepatocyte induction assay in addition to a rat 7-day safety assessment study. Despite the structural similarity to the predecessor compounds, the human hepatocytes assay showed no induction potential of CYP1A2 (Table 22.2), and toxicogenomic data from the rat safety study showed that over the same range of unbound AUC, no activation of the AhR gene panel occurred (Figure 22.7). These data positioned **5** as the most promising molecule for further development.

After much investment in a target, it is a common strategy to ensure that multiple candidate quality molecules are available. The search for additional molecules suitable for preclinical development continued in order to mitigate risk against a potential termination of **5** at a later stage. For example, the zwitterionic compounds presented so far (**2**–**5**) were restricted in distribution,

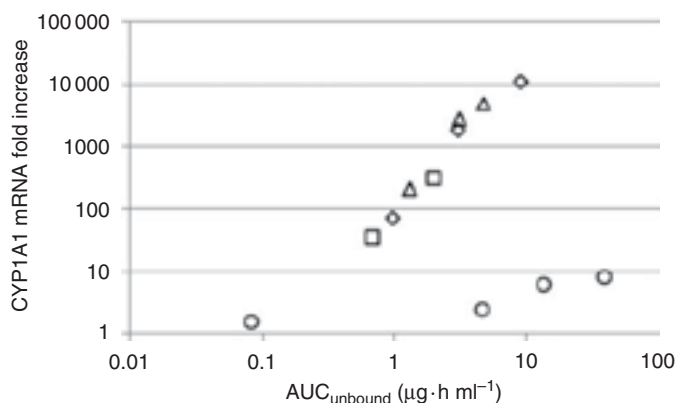


Figure 22.7 The relationship between unbound systemic exposure (AUC) and hepatic CYP1A1 mRNA for the inducers **2** (squares), **3** (diamonds), **4** (triangles) and the non-inducer **5** (circles) following 7-day administration to the rat. Daily oral doses were 1, 30, 100, and 300 mg kg⁻¹ for **5** and as previously stated for **2–4**. Source: From Taylor et al. 2015 [16]. Reprinted with permission American Chemical Society.

human though operating 7-day rat studies using three dose levels during lead optimization for iterative screening and design purposes was unfeasible. An *in vitro* rat hepatocyte induction assay, analogous to the human assay previously described, was therefore implemented as a tool intended for the iterative screening and design of compounds in lead optimization.

The effectiveness of the rat hepatocytes assay was first tested by evaluating several compounds previously studied *in vivo* and comparing the results. The data in Table 22.2 shows that unfortunately the extent of induction observed in the rat *in vivo* was not reflected in the hepatocyte *in vitro* assay. The discrepancies were not consistently explained by comparison of systemic versus *in vitro* concentration, and despite numerous assay refinements and attempting alternative data analysis methods, an adequate explanation was not found.

22.7.4 Development of a Rat *In Vivo* Induction Protocol

As the rat hepatocyte assay was unable to reproduce the *in vivo* data, a repeat-dose *in vivo* protocol in the rat, fit for use in a drug discovery screening environment, was introduced. Considerations in the protocol design included the duration and magnitude of dosing. Previous characterization of induction in the rat [44] had demonstrated that hepatic CYP1A induction by BNF occurred after three daily administrations. We therefore designed a protocol using four daily administrations to $n = 3$ rats to ensure the maximal effect was captured. A nominal oral dose level of 30 mg kg⁻¹ was selected to be representative of a dose used in future safety studies. Based on the experiences with previous compounds, this was considered sufficiently high enough to observe an induction effect yet balanced against the feasibility of compound provision in drug discovery (~150 mg for this study). In reality, due to the insufficient availability of some compounds, dose levels ranged from 15 to 30 mg kg⁻¹. Blood samples

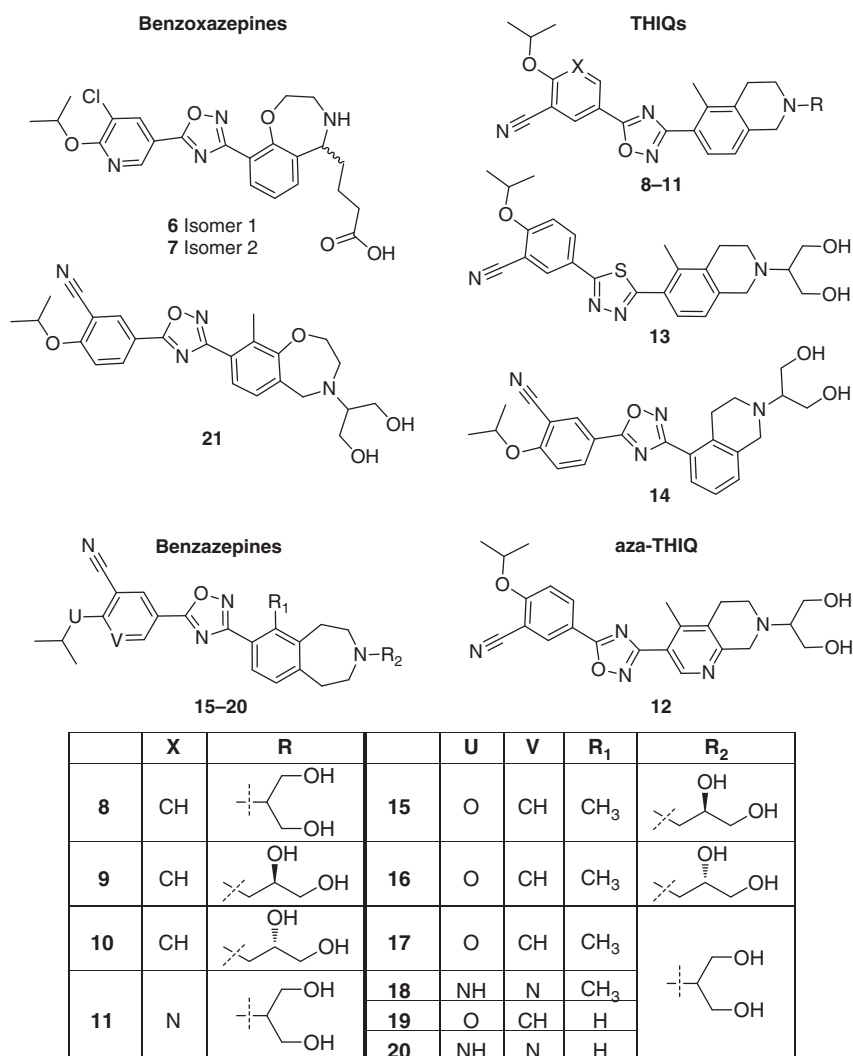


Figure 22.8 Structures of compounds 6–21 progressed to the 4-day rat *in vivo* induction assay. THIQ: Tetrahydroisoquinoline.

were collected after the first and fourth doses to determine the PK profile and systemic exposure. Twenty-four hours after the final dose, the animals were culled, the livers harvested, and sections prepared for mRNA/hepatotaq analysis.

22.8 Iterative Experimentation Identifies Molecules for Progression

The short 4-day induction protocol in rat was successfully implemented and used to profile several compounds across multiple subseries, as illustrated in

Figure 22.8. Due to the resource-intensive nature of this assay, compounds were first triaged using several criteria, and only those with suitable physicochemical properties, *in vitro* pharmacology, PK, efficacy, and human dose prediction were profiled. Those satisfying all these criteria and identified as non-inducers in both the rat 4-day *in vivo* study and the human hepatocyte *in vitro* assay were then considered as candidates for preclinical development.

As previously described CYP1A1 is more highly inducible than CYP1A2, and this is reflected in the magnitude of induction observed. Given the numbers of compounds profiled, we applied a criterion where a non-inducer was classified when CYP1A1 mRNA increased <20-fold and CYP1A2 mRNA increased <5-fold. A summary of the data from the 4-day study is provided in Figure 22.9, illustrating the extent of induction using CYP1A1 and 1A2 mRNA upregulation.

Systemic exposure (determined using C_{\max} and AUC) was generally consistent across the 4-day dosing period, providing no evidence of auto-induction in the rat (Figure 22.10), which was in keeping with the observations drawn from the original compounds (2–4).

The remit of discovering non-inducer compounds resulted in substantial effort to interrogate SAR to drive iterative compound design. A literature survey

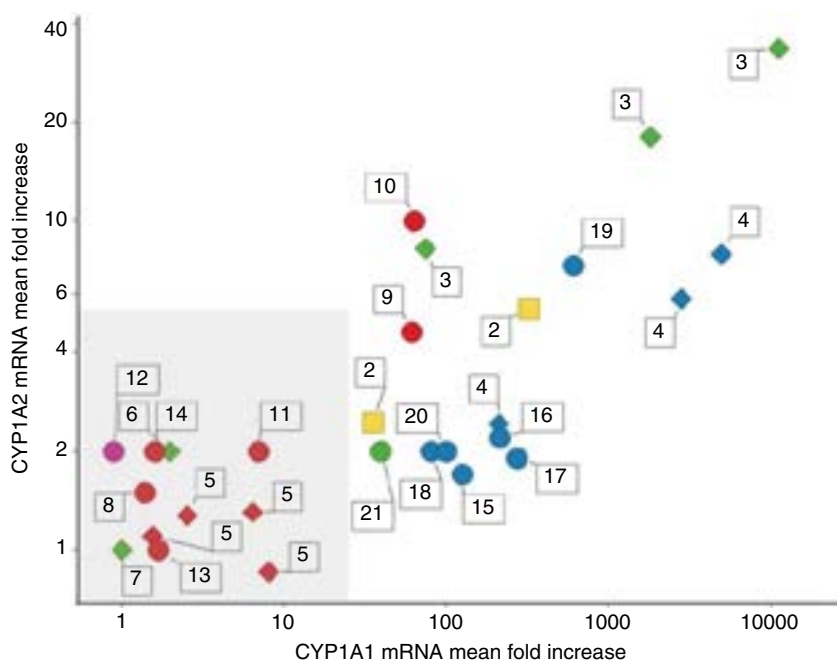


Figure 22.9 Summary of the upregulation of CYP1A1 and CYP1A2 mRNA following 4–7-daily oral administrations of various S1P₁ agonists to the rat. The shaded area represents the boundaries of compounds considered non-inducers at a given dose. The compounds are colored by template: THIQ (red), aza-THIQ (pink), indazoles (yellow), benzazepines (blue), and benzoxazepines (green), and shaped by class: acid (square), amine (circle), and zwitterions (diamond). *Source:* From Taylor et al. 2015 [16]. Reproduced with permission of American Chemical Society.

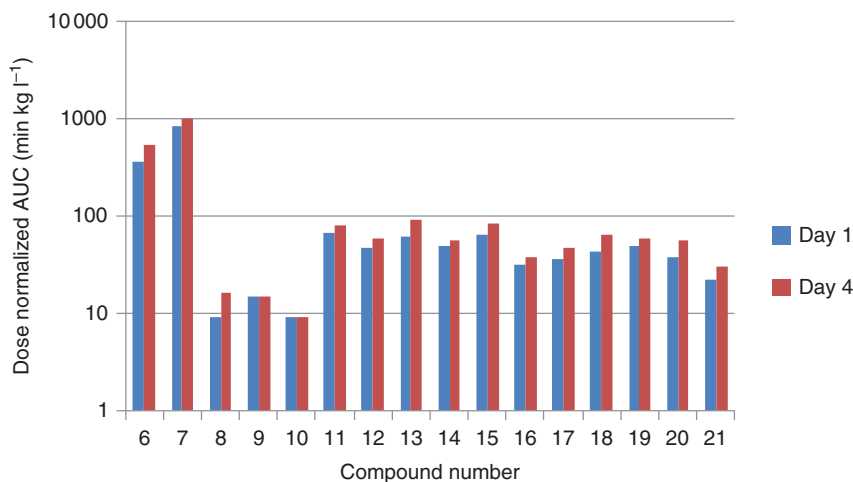


Figure 22.10 Consistent exposure (as shown by dose-normalized AUC) was observed with all compounds throughout the 4-day rat induction study, indicating the absence of auto-induction in the rat.

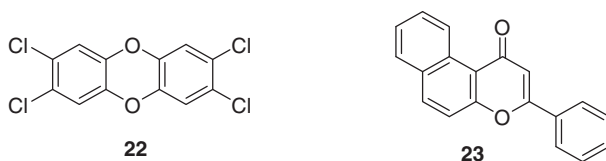


Figure 22.11 Examples of reported AhR agonists of a planar hydrophobic nature. TCDD, **22**, and BNF, **23**.

indicated that the majority of classical AhR ligands were planar with a high degree of hydrophobicity. Examples, shown in Figure 22.11, include the PAHs including **22** (TCDD) and **23** (BNF) though detailed SAR analysis of the PAHs showed that absolute planarity was not a requirement for binding [45].

Crystallography data for **3** and **5** highlighted that one of the aromatic rings in **5** (non-inducer) was out of plane when compared with **3** (inducer). The dihedral angles between the oxadiazole ring and the phenyl closest to the basic nitrogen were 18° and 5°, respectively, as illustrated in Figure 22.12. A working hypothesis followed by the team was that this “twist” in **5** was sufficient to introduce a lack of planarity and avoid AhR binding. This was also reinforced by other compounds (such as non-inducers **6** and **7**) having a carboxylic acid chain, which was also projected out of main aromatic moiety plane. Unfortunately this hypothesis did not hold uniformly as subsequent compounds (such as **9**) showed a high level of induction despite having an identical core structure to **5**. The relationship to physicochemical properties such as pK_a was also investigated, and while trends were apparent, for example, greater induction occurred with the more basic benzazepines compared with the less basic tetrahydroisoquinolines (THIQs); compounds such as the benzoxazepine **21** were not compliant to the rule.

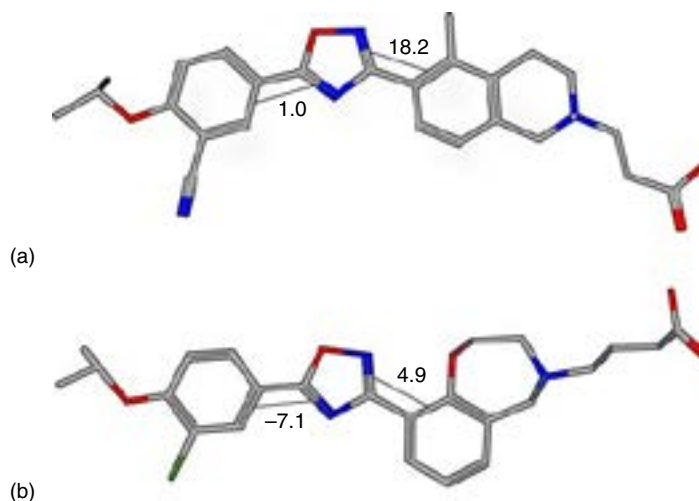


Figure 22.12 Crystallographic data for **5** (a) and **3** (b) illustrating the dihedral angles. *Source:* From Taylor et al. 2015 [16]. Reproduced with permission of American Chemical Society.

A comprehensive analysis of SAR was also conducted across many compound pairs within and across series, as reported in the literature [16]. It became apparent that the SAR was complex; for example, **9** and **10** were considered inducers, whereas the structurally similar **8** was a non-inducer, in contrast with more radical-shaped changes as in **14** that retained the profile of a non-inducer. The SAR was also extremely subtle; for example, **17** and **21** differ from **8** by only a single carbon or oxygen, respectively, and showed induction. In summary, only conclusions at the level of the “template” were defined with the benzazepines and benzoxazepines generally showing greater induction than the THIQs.

This example illustrates the type of assessments and analysis attempted to determine medicinal chemistry SAR with iterative cycles of hypothesis generation and testing. Firm relationships are always preferred, but in lead optimization, ambiguity often exists, requiring the scientist to exercise judgment. In this case links between compound structure and AhR gene panel upregulation were complex, subtle, multifactorial, and appeared to extend beyond properties such as planarity, lipophilicity, and basicity [16].

22.9 Delivery of Human AhR Agonist Assay

Unfortunately, due to the time required for development and validation, this assay did not deliver in time to be impactful for this S1P₁ agonist program. However, a selection of compounds were retrospectively profiled. This assay, developed using intestinal human colon adenocarcinoma cells (LS180), utilized a β -lactamase reporter gene downstream of the CYP1A1 promoter. 3MC was used as a positive control with novel compounds considered potential activators of AhR if the maximum response was >40% of the control.

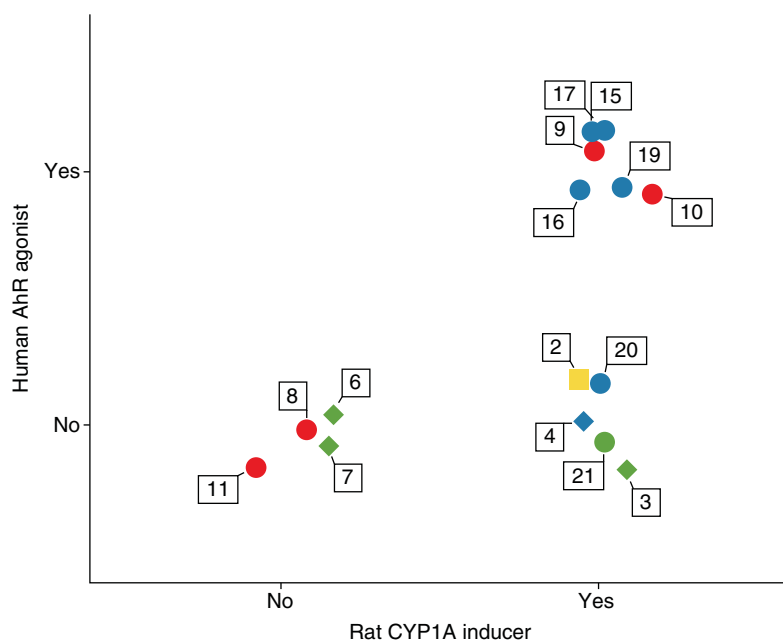


Figure 22.13 Data comparison for 15 S1P₁ agonists comparing agonist activity in the human AhR reporter gene assay and the rat *in vivo*. The compounds are colored by template and symbols separated for clarity: THIQ (red), indazoles (yellow), benzazepines (blue), and benzoxazepines (green), and shaped by class: acid (square), amine (circle), and zwitterions (diamond).

The potential for human AhR agonism was compared with the CYP1A inducing potential from the rat *in vivo* study. In the rat-only compounds having both <20-fold CYP1A1 and <5-fold, CYP1A2 were considered non-inducers. This limited data set shown in Figure 22.13 indicates some agreement between the assays though the rat appears to be a more sensitive indicator of induction potential using these criteria. Pleasingly, all compounds that were classified as non-inducers in the rat were also non-inducers in the human assay. These data justified our conservative strategy to design out induction across all species and assay formats.

22.10 Minimizing Cardiovascular Safety Risk Through S1P Receptor Selectivity

The potential for an improved clinical safety profile over fingolimod was an essential aspect of the program. To ensure the series of compounds under optimization did not carry a similar risk of bradycardia, telemetered rat studies were conducted early in lead optimization. This safety pharmacology model requires the surgical implantation of a telemetry device capable of remote monitoring of hemodynamic parameters. We confirmed that a series of compounds based on a promising THIQ template had the potential for >1000-fold human S1P₁ versus human S1P₃ receptor selectivity based on *in vitro* assay systems of receptor

binding [40]. This was in sharp contrast to fingolimod (see Table 22.4), which displayed equal potency at S1P₁ and S1P₃. Confirmation that the lack of potency at S1P₃ would drive an appropriate hemodynamic profile *in vivo* was tested with our lead compounds using the telemetered rat model. The profile for **5** is shown in Figure 22.14 from a single ascending dose experiment. In keeping with the

Table 22.4 S1P Receptor selectivity comparing fingolimod with **5**, a novel compound from lead optimization.

Compound	5	1b (FTY720 phosphate)
S1P ₁ EC ₅₀ (nM)	32	4
S1P ₃ EC ₅₀ (nM)	>40 000	5
Selectivity	>1250-fold	No selectivity

Source: Adapted from Demont 2011 [40].

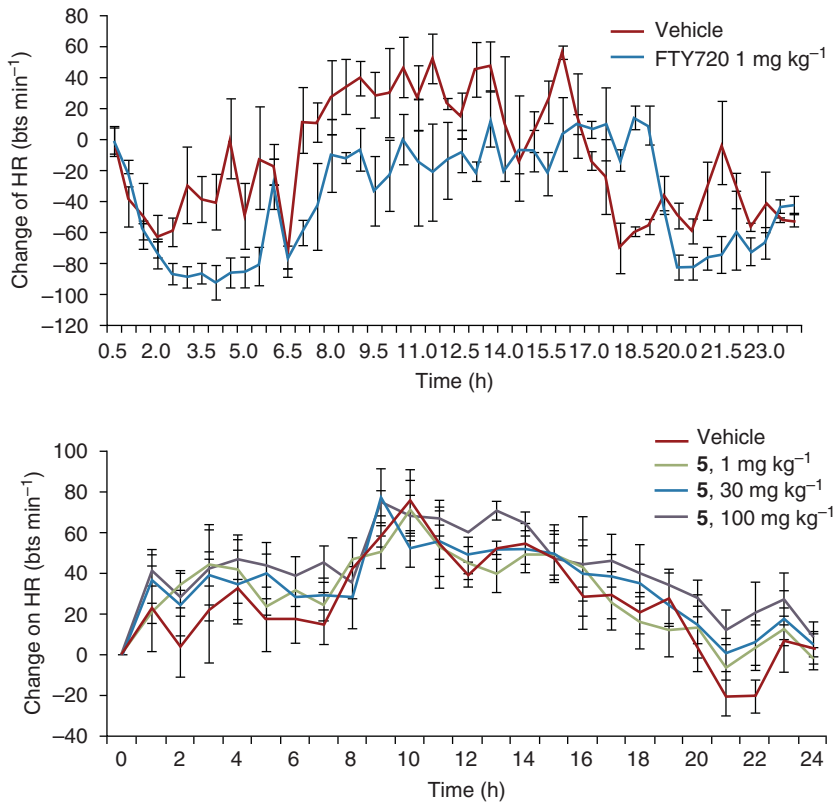


Figure 22.14 The absence of bradycardia in telemetered rats with **5** at 1, 30, or 100 mg kg⁻¹ compared with **1a** (FTY720). Source: From Demont et al. 2011 [40]. Reproduced with permission of American Chemical Society.

in vitro receptor selectivity profile and in contrast with **1b** (FTY720 phosphate), no change in heart rate was observed [40].

22.11 Positioning Dose as the Focus of Lead Optimization

Compound failure in late-stage development is costly to the pharmaceutical industry. Analysis has been performed looking at the reasons for later stage clinical attrition with safety and efficacy remaining key factors [46, 47].

With respect to safety events, cardiovascular safety and hepatotoxicity remain a leading cause of attrition. In the case of the cardiovascular findings, the mechanistic link between QTc prolongation and blockage of the hERG channel has enabled effective screens to be established in discovery to ensure compounds with a risk are deselected early [48]. Other safety events, such as hepatotoxicity, can be idiosyncratic [49] sometimes only emerging in large-scale phase III trials or postmarketing with serious consequences for the patient and loss of return on investment for the developer. One key factor that has emerged as being linked to such events is the dose. The higher the dose, the higher the body burden, and research indicates correlations between higher doses and an increased risk of adverse findings such as hepatotoxicity [50] and DDI [37].

With respect to efficacy, understanding the relationships between concentration and response or pharmacokinetics–pharmacodynamics (PKPD) is fundamental to the prediction of drug behavior in the clinic and so should be placed at the center of drug design and selection. The development and deployment of PKPD models early in lead optimization allows for an estimation of the likely human exposures and dose. These are essential parameters in the overall integrated assessment of safety risks when contextualized with other indicators of hepatotoxicity and enzyme inhibition for example [32, 50].

For the S1P₁ program the PD response of interest was lymphocyte reduction, and the PKPD evaluation was positioned centrally in the lead optimization strategy [41]. A preclinical PKPD model of lymphocyte reduction in the rat was used to derive *in vivo* compound potency, which was subsequently used in conjunction with predicted human PK in a human PKPD model to estimate dose. The estimated human dose was a key factor in compound selection with the program aim to target a daily dose of ideally <100 mg. Through incorporation of PKPD in the screening cascade, several of the molecules identified had predicted doses within the desired range (Tables 22.1 and 22.4), providing confidence of minimizing other adverse events such as hepatotoxicity.

22.12 Delivery of Multiple Candidates for Development

While numerous compounds were ultimately identified as satisfying the product profile, exemplified in Table 22.3, **5** was considered the most promising, having physicochemical properties within drug-like space, >1000-fold selectivity for

S1P₁ over S1P₃, and no bradycardia observed in the telemetered rat. It displayed a favorable PK profile in two preclinical species and when coupled with nanomolar potency at the target had a low predicted human dose (<10 mg once daily), which was deemed appropriate for minimizing body burden and thus the risk of off-target findings. No evidence of CYP1A induction was observed in the rat *in vivo* nor in the human *in vitro* hepatocyte assay.

22.13 Conclusions

This case study highlights a typical lead optimization campaign where several molecule properties required investigation and iterative approaches were needed to deliver the desired target product profile. Substantial investment was made against this target with emphasis placed on early safety assessment of molecules. Toxicological consequences were identified and associated with related receptors and required optimization. Bradycardia was a known potential issue at the outset, and evaluation in telemetered rat studies was conducted early in the program cycle with lead molecules to confirm that receptor selectivity, in this case S1P₁ over S1P₃, mitigated the risk in these preclinical experiments.

A low dose reduces the overall body burden and, in turn, the risk of adverse findings such as DDI and hepatotoxicity. Human PK prediction, coupled with a translatable PKPD model, was used to provide an early estimate of the likely efficacious dose with only compounds having the potential for low dose (<100 mg) considered for further development.

An unusual finding of substantial CYP1A induction, consistent with AhR activation, was observed during early rodent safety studies. The SAR within the template was subtle with the exemplified non-inducer candidate molecule, **5**, having remarkable structural similarity to the molecules where the finding was initially observed. This highlights the detailed, iterative, and tenacious nature required in a lead optimization campaign to deliver the optimal molecule profile. This example also reveals how small structural changes can lead to a marked change and the need for continuous profiling across assays of importance. After careful consideration of the potential impact of AhR activation during late-stage development and in the clinic, the first compounds with this finding continued to progress, while the lead optimization strategy was revised to ensure that subsequent candidate molecules were devoid of this effect. This approach could be considered cautious, and others may decide on alternative courses of action. Our decision was taken with regard to minimizing late-stage attrition but also in light of the emerging positive clinical data with fingolimod and working with the assumption that another molecule entering the market with this mechanism would require a clean off-target profile. It should not be concluded from this article that AhR agonism will always be a significant cause for concern. The literature reports a complex picture with its function as a drug-metabolizing enzyme regulator. Moreover, it is clear that the functions of this receptor are far more broad reaching and the AhR may yet emerge as a therapeutic drug target [39].

For this set of compounds, *in vitro* assays were unsuccessful in predicting the extent of CYP1A induction *in vivo* in rat, so a short-term 4-day *in vivo* protocol

coupled with an aggressive pre-triage approach was used to discover compounds without induction potential. Modification of screening strategies resulted in the successful identification of several small molecule S1P₁ agonists that were progressed to preclinical development.

The issues arising in this case study extend across numerous areas of expertise and line functions within a drug discovery organization. For example, the assessment of bradycardia required early engagement with safety assessment and the development of combined strategies with biology from a scientific, operational, and strategic perspective. The design and operation of the 4-day *in vivo* rat protocol required expertise across DMPK and safety assessment plus medicinal chemistry scale-up and collective thinking around the SAR evaluation of induction. *In vitro* hepatocyte induction assays required DMPK resource as did the PKPD modeling and simulation. This case study exemplifies the importance of effective collaboration to rapidly identify and deliver promising new drugs for patients.

Acknowledgments

This work could not have been conducted without the expertise and dedication of the S1P₁ program team plus many colleagues working in the Immuno-Inflammation Therapy Area and other business partners within GlaxoSmithKline. The author is particularly grateful to Emmanuel Demont, Jason Witherington, and Mike Kelly who were key contributors to the strategy and leadership of this program. In addition to Emmanuel, the author gratefully acknowledges Dr Peter Eddershaw for critical review of this chapter.

References

- 1 Buzard, D.J., Thatte, J., Lerner, M. et al. (2008). Recent progress in the development of selective S1P1 receptor agonists for the treatment of inflammatory and autoimmune disorders. *Expert Opin. Ther. Pat.* **18**: 1141–1159.
- 2 Bolli, M.H., Lescop, C., and Nayler, O. (2011). Synthetic sphingosine 1-phosphate receptor modulators--opportunities and potential pitfalls. *Curr. Top. Med. Chem.* **11**: 726–757.
- 3 Roberts, E., Guerrero, M., Urbano, M., and Rosen, H. (2013). Sphingosine 1-phosphate receptor agonists: a patent review (2010–2012). *Expert Opin. Ther. Pat.* **23**: 817–841.
- 4 Marsolais, D. and Rosen, H. (2009). Chemical modulators of sphingosine-1-phosphate receptors as barrier-oriented therapeutic molecules. *Nat. Rev. Drug Discov.* **8**: 297–307.
- 5 Gonzalez-Cabrera, P.J., Brown, S., Studer, S.M., and Rosen, H. (2014). S1P signaling: new therapies and opportunities. *F1000Prime Rep.* **6** (109).
- 6 Forrest, M., Sun, S.Y., Hajdu, R. et al. (2004). Immune cell regulation and cardiovascular effects of sphingosine 1-phosphate receptor agonists in rodents are mediated via distinct receptor subtypes. *J. Pharmacol. Exp. Ther.* **309**: 758–768.

- 7 Sanna, M.G., Liao, J., Jo, E. et al. (2004). Sphingosine 1-phosphate (S1P) receptor subtypes S1P1 and S1P3, respectively, regulate lymphocyte recirculation and heart rate. *J. Biol. Chem.* **279**: 13839–13848.
- 8 Salomone, S., Potts, E.M., Tyndall, S. et al. (2008). Analysis of sphingosine 1-phosphate receptors involved in constriction of isolated cerebral arteries with receptor null mice and pharmacological tools. *Br. J. Pharmacol.* **153**: 140–147.
- 9 Cohen, J.A. and Chun, J. (2011). Mechanisms of fingolimod's efficacy and adverse effects in multiple sclerosis. *Ann. Neurol.* **69**: 759–777.
- 10 Budde, K., Schutz, M., Glander, P. et al. (2006). FTY720 (fingolimod) in renal transplantation. *Clin. Transpl.* **20** (Suppl. 17): 17–24.
- 11 Skerjanec, A., Tedesco, H., Neumayer, H.H. et al. (2005). FTY720, a novel immunomodulator in de novo kidney transplant patients: pharmacokinetics and exposure-response relationship. *J. Clin. Pharmacol.* **45**: 1268–1278.
- 12 Meno-Tetang, G.M. and Lowe, P.J. (2005). On the prediction of the human response: a recycled mechanistic pharmacokinetic/pharmacodynamic approach. *Basic Clin. Pharmacol. Toxicol.* **96**: 182–192.
- 13 Hann, M.M. and Keseru, G.M. (2012). Finding the sweet spot: the role of nature and nurture in medicinal chemistry. *Nat. Rev. Drug Discovery* **11**: 355–365.
- 14 Bayliss, M.K., Butler, J., Feldman, P.L. et al. (2016). Quality guidelines for oral drug candidates: dose, solubility and lipophilicity. *Drug Discovery Today* **21**: 1719–1727.
- 15 Lipinski, C.A. (2004). Lead- and drug-like compounds: the rule-of-five revolution. *Drug Discovery Today Technol.* **1**: 337–341.
- 16 Taylor, S.J., Demont, E.H., Gray, J. et al. (2015). Navigating CYP1A induction and arylhydrocarbon receptor agonism in drug discovery. A case history with S1P1 agonists. *J. Med. Chem.* **58**: 8236–8256.
- 17 Skidmore, J., Heer, J., Johnson, C.N. et al. (2014). Optimization of sphingosine-1-phosphate-1 receptor agonists: effects of acidic, basic, and zwitterionic chemotypes on pharmacokinetic and pharmacodynamic profiles. *J. Med. Chem.* **57**: 10424–10442.
- 18 Weir, P. Integrating liver toxicogenomics with clinical pathology, histopathology and drug metabolism data in preclinical studies <http://www.fda.gov/drugs/scienceresearch/researchareas/ucm079222.htm> (accessed 1 August 2016).
- 19 Denison, M.S. and Nagy, S.R. (2003). Activation of the aryl hydrocarbon receptor by structurally diverse exogenous and endogenous chemicals. *Annu. Rev. Pharmacol. Toxicol.* **43**: 309–334.
- 20 Martignoni, M., Groothuis, G.M., and de, K.R. (2006). Species differences between mouse, rat, dog, monkey and human CYP-mediated drug metabolism, inhibition and induction. *Expert Opin. Drug Metab. Toxicol.* **2**: 875–894.
- 21 Nebert, D.W., Dalton, T.P., Okey, A.B., and Gonzalez, F.J. (2004). Role of aryl hydrocarbon receptor-mediated induction of the CYP1 enzymes in environmental toxicity and cancer. *J. Biol. Chem.* **279**: 23847–23850.

- 22 Wang, B. and Zhou, S.F. (2009). Synthetic and natural compounds that interact with human cytochrome P450 1A2 and implications in drug development. *Curr. Med. Chem.* **16**: 4066–4218.
- 23 Zhou, S.F., Wang, B., Yang, L.P., and Liu, J.P. (2010). Structure, function, regulation and polymorphism and the clinical significance of human cytochrome P450 1A2. *Drug Metab. Rev.* **42**: 268–354.
- 24 Ma, Q. and Lu, A.Y. (2007). CYP1A induction and human risk assessment: an evolving tale of in vitro and in vivo studies. *Drug Metab. Dispos.* **35**: 1009–1016.
- 25 Kawajiri, K. and Fujii-Kuriyama, Y. (2007). Cytochrome P450 gene regulation and physiological functions mediated by the aryl hydrocarbon receptor. *Arch. Biochem. Biophys.* **464**: 207–212.
- 26 Denison, M.S., Soshilov, A.A., He, G. et al. (2011). Exactly the same but different: promiscuity and diversity in the molecular mechanisms of action of the aryl hydrocarbon (dioxin) receptor. *Toxicol. Sci.* **124**: 1–22.
- 27 Budinsky, R.A., LeCluyse, E.L., Ferguson, S.S. et al. (2010). Human and rat primary hepatocyte CYP1A1 and 1A2 induction with 2,3,7,8-tetrachlorodibenzo-p-dioxin, 2,3,7,8-tetrachlorodibenzofuran, and 2,3,4,7,8-pentachlorodibenzofuran. *Toxicol. Sci.* **118**: 224–235.
- 28 Michaels, S. and Wang, M.Z. (2014). The revised human liver cytochrome P450 “pie”: absolute protein quantification of CYP4F and CYP3A enzymes using targeted quantitative proteomics. *Drug Metab. Dispos.* **42**: 1241–1251.
- 29 Nebert, D.W., McKinnon, R.A., and Puga, A. (1996). Human drug-metabolizing enzyme polymorphisms: effects on risk of toxicity and cancer. *DNA Cell Biol.* **15**: 273–280.
- 30 Uno, S., Dalton, T.P., Derkenne, S. et al. (2004). Oral exposure to benzo[a]pyrene in the mouse: detoxication by inducible cytochrome P450 is more important than metabolic activation. *Mol. Pharmacol.* **65**: 1225–1237.
- 31 Zhu, B.T. (2010). On the general mechanism of selective induction of cytochrome P450 enzymes by chemicals: some theoretical considerations. *Expert Opin. Drug Metab. Toxicol.* **6**: 483–494.
- 32 Shardlow, C.E., Generaux, G.T., MacLauchlin, C.C. et al. (2011). Utilizing drug-drug interaction prediction tools during drug development: enhanced decision making based on clinical risk. *Drug Metab. Dispos.* **39**: 2076–2084.
- 33 Kroon, L.A. (2007). Drug interactions with smoking. *Am. J. Health Syst. Pharm.* **64**: 1917–1921.
- 34 Zevin, S. and Benowitz, N.L. (1999). Drug interactions with tobacco smoking an update. *Clin. Pharmacokinet.* **36**: 425–438.
- 35 Djordjevic, N., Ghotbi, R., Bertilsson, L. et al. (2008). Induction of CYP1A2 by heavy coffee consumption in serbs and swedes. *Eur. J. Clin. Pharmacol.* **64**: 381–385.
- 36 Jerling, M., Lindstrom, L., Bondesson, U., and Bertilsson, L. (1994). Fluvoxamine inhibition and carbamazepine induction of the metabolism of clozapine: evidence from a therapeutic drug monitoring service. *Ther Drug Monit* **16**: 368–374.
- 37 Levy, R.H., Hachad, H., Yao, C., and Ragueneau-Majlessi, I. (2003). Relationship between extent of inhibition and inhibitor dose: literature evaluation

- based on the metabolism and transport drug interaction database. *Curr. Drug Metab.* **4**: 371–380.
- 38 Matsumura, F., Puga, A., and Tohyama, C. (2009). Biological functions of the arylhydrocarbon receptor: beyond induction of cytochrome P450s. *Biochem. Pharmacol.* **77**: 473–760.
- 39 Guyot, E., Chevallier, A., Barouki, R., and Coumoul, X. (2013). The AhR twist: ligand-dependent AhR signaling and pharmaco-toxicological implications. *Drug Discovery Today* **18**: 479–486.
- 40 Demont, E.H., Andrews, B.I., Bit, R.A. et al. (2011). Discovery of a selective S1P1 receptor agonist efficacious at low oral dose and devoid of effects on heart rate. *ACS Med. Chem. Lett.* **2**: 444–449.
- 41 Taylor, S., Gray, J.R., Willis, R. et al. (2012). The utility of pharmacokinetic-pharmacodynamic modeling in the discovery and optimization of selective S1P(1) agonists. *Xenobiotica* **42**: 671–686.
- 42 Brinkmann, V. (2009). FTY720 (fingolimod) in multiple sclerosis: therapeutic effects in the immune and the central nervous system. *Br. J. Pharmacol.* **158**: 1173–1182.
- 43 Noguchi, K. and Chun, J. (2011). Roles for lysophospholipid S1P receptors in multiple sclerosis. *Crit. Rev. Biochem. Mol. Biol.* **46**: 2–10.
- 44 Baldwin, S.J., Bramhall, J.L., Ashby, C.A. et al. (2006). Cytochrome P450 gene induction in rats ex vivo assessed by quantitative real-time reverse transcriptase-polymerase chain reaction (TaqMan). *Drug Metab. Dispos.* **34**: 1063–1069.
- 45 Nguyen, L.P. and Bradfield, C.A. (2008). The search for endogenous activators of the aryl hydrocarbon receptor. *Chem. Res. Toxicol.* **21**: 102–116.
- 46 Kola, I. and Landis, J. (2004). Can the pharmaceutical industry reduce attrition rates? *Nat. Rev. Drug Discov.* **3**: 711–715.
- 47 Arrowsmith, J. and Miller, P. (2013). Trial watch: phase II and phase III attrition rates 2011–2012. *Nat. Rev. Drug Discov.* **12**: 569.
- 48 Redfern, W.S., Carlsson, L., Davis, A.S. et al. (2003). Relationships between preclinical cardiac electrophysiology, clinical QT interval prolongation and torsade de pointes for a broad range of drugs: evidence for a provisional safety margin in drug development. *Cardiovasc. Res.* **58**: 32–45.
- 49 Uetrecht, J. (2008). Idiosyncratic drug reactions: past, present, and future. *Chem. Res. Toxicol.* **21**: 84–92.
- 50 Sakatis, M.Z., Reese, M.J., Harrell, A.W. et al. (2012). Preclinical strategy to reduce clinical hepatotoxicity using in vitro bioactivation data for >200 compounds. *Chem. Res. Toxicol.* **25**: 2067–2082.

22

The Integrated Optimization of Safety and DMPK Properties Enabling Preclinical Development: A Case History with S1P₁ Agonists

Simon Taylor

Immuno-Inflammation Therapy Area, Quantitative Pharmacology, GlaxoSmithKline, Gunnels Wood Road, Stevenage SG1 2NY, UK

22.1 Introduction to the S1P₁ Agonist Lead Optimization Program

22.1.1 Objectives and Challenges

The latter part of the twentieth and first decade of the twenty-first centuries saw a high level of research activity into sphingosine-1-phosphate (S1P) receptor biology with numerous pharmaceutical companies looking to exploit this understanding in the development of new drugs [1–3]. S1P is the endogenous ligand and potent modulator of the activity of a family of five S1P G-protein-coupled receptors, S1P_{1–5}. These receptors are known to regulate a range of biological processes including cell survival, adhesion, migration, and endocytosis, leading to physiological responses such as endothelial barrier enhancement, modulation of vascular tone, heart rate, and lymphocyte trafficking [4]. The latter two responses were of particular interest to the drug discovery program described in this case history.

Lymphocytes continuously circulate throughout the body, acting as surveillance for invading pathogens and return home to secondary lymphoid organs. To leave these secondary organs, the lymphocytes sense the S1P gradient that exists between lymph and blood. The S1P₁ receptor is present on the surface of lymphocytes, and agonism of this receptor results in receptor internalization and removes the ability of the lymphocyte to sense the gradient causing sequestration of these cells in the secondary lymphoid tissue. Interfering with lymphocyte trafficking via S1P₁, agonism represented an attractive mechanism to target autoimmune diseases such as relapsing–remitting multiple sclerosis, inflammatory bowel disease (IBD), lupus, and psoriasis [5]. However agonism of S1P₃ was considered undesirable due to relationships observed in animal studies with broncho- and vasoconstriction and modulation of heart rate [6–8].

At the time of this lead optimization program, the nonselective S1P receptor agonist FTY-720, fingolimod, now marketed as Gilenya® (Compound **1a**, Figure 22.1), had shown clinical efficacy as a new oral drug in relapsing–remitting

14

BACE Inhibitors

Daniel F. Wyss, Jared N. Cumming, Corey O. Strickland, and Andrew W. Stamford

14.1

Introduction

β -Secretase, widely known as β -site amyloid precursor protein cleaving enzyme 1 (BACE1), initiates production of the toxic amyloid- β (A β) peptides that are believed to play a crucial early part in Alzheimer's disease (AD) pathogenesis. AD is a devastating neurodegenerative disease characterized by the accumulation of two hallmark structures in the brain – amyloid plaques and neurofibrillary tangles. Amyloid plaques are extracellular deposits of insoluble fibrils of A β peptides that are primarily 40 and 42 residues in length. Neurofibrillary tangles are intracellular aggregates of aberrantly hyperphosphorylated forms of tau, a microtubule-associated protein. The amyloid hypothesis postulates that accumulation of A β plaques and soluble neurotoxic A β oligomers in the brain is a critical, required early step that leads to formation of neurofibrillary tangles, neuroinflammation, synaptic loss, neuronal cell death, and ultimately dementia [1–3]. If this hypothesis is correct, then preventing accumulation of A β in the brain, either through reduced production (e.g., BACE1 inhibition) or through increased clearance (e.g., A β -antibodies [4,5]), should be an effective approach to slow or halt progression of AD when given early enough in the disease process [3,6].

A β peptides are formed as minor products (5–10%) of the metabolism of amyloid precursor protein (APP) via two consecutive cleavages – first by BACE1, in competition with the major pathway (90–95%) of nonamyloidogenic processing of APP by α -secretase, followed by γ -secretase (see Figure 14.1 in [6]). The active site of BACE1 is within the acidic environment of the endosomes, with a pH optimum correspondingly in the 4.5–5.5 range, and is relatively shallow and hydrophilic. BACE1 is mainly expressed in the central nervous system (CNS). A closely related enzyme, BACE2, is predominantly expressed in the periphery and does not function as a β -secretase

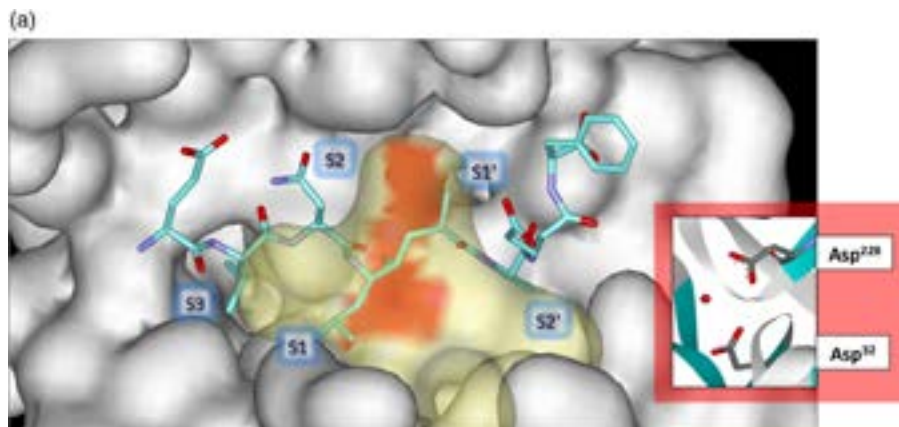


Figure 14.1 (a) BACE1 structural characteristics and binding mode of an early-generation peptidomimetic BACE1 inhibitor (OM99-2) showing its relatively large size and the extended BACE1 active site (PDB code 1FKN) [17]. The overall folding of BACE1 is typical for an aspartic acid protease, consisting of N- and C-terminal lobes with the substrate binding site located in a crevice between the

two lobes. A flexible hairpin loop, called the flap (yellow transparent surface), partially covers the active site of BACE1 and can adopt many different conformations as a result of inhibitor binding. In the center of the active site are the two aspartic acid residues Asp32 and Asp228 (orange and inset with a bound water molecule at the catalytic center) that are involved in the enzymatic reaction.

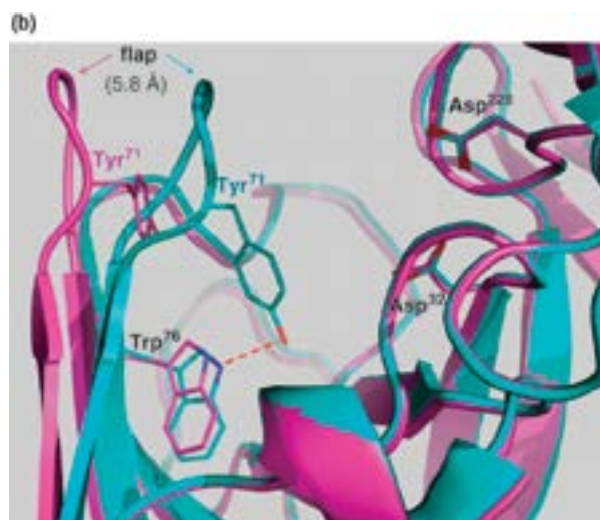


Figure 14.1 (b) Close-up view of the active site of superimposed crystal structures of flap-open (PDB code 2OHU, magenta) [28] and flap-closed (PDB code 1W51, cyan) [29] BACE1. Ligands have been omitted for clarity. Due to the conformation of Tyr71 in the flap-open 2OHU structure (magenta), the hydrogen

bond with Trp76 is broken and Tyr71 no longer occupies the position between the S1 and S2' subsites. The changing position of the flap relative to the catalytic dyad provides a means for the substrate and the ligands to diffuse into and out of the active site.

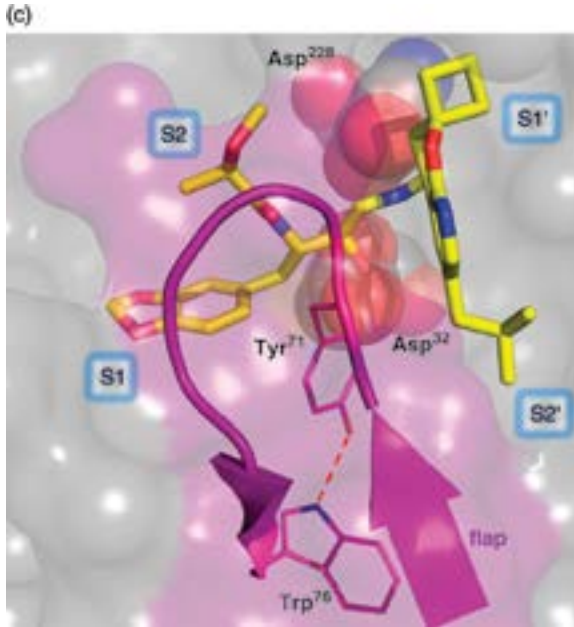


Figure 14.1 (c) Bound conformation of an evolved hydroxyethylamine containing peptidomimetic inhibitor (yellow) bound with BACE1 (PDB code 4DH6). This compound demonstrated robust reduction of central β -amyloid in a preclinical rat animal model [27]. BACE1 is in the flap-closed

conformation (purple surface) where the Tyr71 side chain hydroxyl is hydrogen-bonded to the NH of the Trp76 side chain that physically separates the S1 and S2' subsites. The catalytic aspartyl dyad is shown as spheres and the proximal subsites are labeled.

in vivo [3,6]. BACE1 belongs to the pepsin family under the aspartyl protease superfamily and has sequence identity not only with BACE2 (52%) but also with cathepsin D (29%), cathepsin E (27%), pepsin (27%), and renin (24%) [7].

The amyloid hypothesis is supported by a large body of genetic, biochemical, and histopathological evidence (see [3,6] for recent reviews). Since its discovery in 1999 [8–12], inhibition of BACE1 has been viewed as the best small molecule approach to test this hypothesis, underscored by initial observations that BACE1 knockout (KO) mice do not produce A β and show a relatively benign overt phenotype [13]. Furthermore, the well-studied Swedish mutation of APP causes early onset familial AD by specifically enhancing BACE1-dependent cleavage by as much as 100-fold [14,15]. More recently, identification of a naturally occurring variant of APP (the “Icelandic mutation”) with a reduced propensity to proteolysis by BACE1 and association with a decreased risk of dementia further solidified the role of this enzyme in the etiology of AD [16]. Although BACE1

has emerged as a prime therapeutic target for AD, the recent identification of multiple new substrates and reports of its involvement in a much wider range of physiological processes within and outside the CNS have raised concerns about potential mechanism-based side effects of drugs targeting this enzyme [3,6]. While the science around BACE1 continues to evolve, the bulk of the data, including both heterozygous KO and chronic small molecule treatment across multiple species, suggests that long-term dosing with a sufficient therapeutic window should be possible with a potent, selective, brain-penetrant small molecule inhibitor.

Localization of BACE1 in the CNS, however, has posed a significant challenge in identifying low molecular weight (MW) compounds with the aforementioned profile. Initial drug design efforts focused on noncleavable peptide-based transition state analogs in which the residues of APP around the site of BACE1 cleavage served as a template [10,17,18]. The first wave of published BACE1 crystal structures featured molecules that interacted with the catalytic dyad using classical aspartyl protease transition state mimics, for example, hydroxyethylene (HE) [17,18] and hydroxyethylamine (HEA) isosteres [19,20] (see [21] for a recent review). These peptidomimetic structures bound to the flap-closed form of the enzyme and filled most of the pockets that the substrate occupies around the active site (Figure 14.1). While potent *in vitro*, these molecules had poor ligand efficiencies (LE) [22] and high polar surface areas (PSA) due to their high MW and peptidic nature. These properties contributed to deficient profiles common to many peptidomimetics, including poor oral bioavailability and low blood–brain barrier penetration driven by susceptibility to permeability glycoprotein (P-gp) efflux. In fact, only a handful of literature examples in this class of inhibitors exhibited brain permeability and measurable central pharmacodynamic (PD) effects *in vivo* (e.g., see examples in [23–27]).

Beyond the peptidomimetics, it has proven challenging to develop nonpeptidic “second-generation” BACE1 inhibitors that exhibit brain A β lowering with a dose and safety profile suitable for clinical progression. Fragment-based approaches have provided novel and structurally diverse chemotypes that, together with extensive SAR exploration using *in vitro* and *in vivo* model systems, have afforded a wealth of structure- and property-based knowledge over the past decade, significantly advancing our understanding of what makes a “good” BACE inhibitor [30,31]. This chapter will discuss the major role FBDD played in the development of such chemotypes, including the nonplanar cyclic amidines, a chemotype that ultimately enabled researchers to develop selective BACE inhibitors that are more drug-like in terms of MW, ClogP, and PSA, that have lower susceptibility to P-gp efflux, and most importantly that penetrate the CNS and effectively reduce A β levels, some of which progressed into clinical development [32–41].

14.2

FBDD Efforts on BACE1

14.2.1

Fragment Hit Identification, Validation, and Expansion

Diverse approaches to FBDD have been employed across many groups in the discovery of novel nonpeptidic low MW BACE1 inhibitors (Table 14.1). These efforts ranged from extensive fragment screening campaigns that tested hundreds to thousands of compounds from diverse libraries to more knowledge-based (e.g., structure- and property-based) campaigns that tested focused libraries of tens to hundreds of fragments. As can be seen from the left two columns in Table 14.1, a combination of both biophysical/biochemical screening and confirmation methods were used in early efforts to discover diverse pharmacophores that bind to the BACE1 active site. In the majority of cases, an X-ray crystal structure of BACE1 with a fragment or fragment-derived analog was ultimately obtained to validate those hits and subsequently to serve as a basis to guide challenging and diverse hit expansion campaigns. While some of these efforts were successful, many others failed to produce legitimate leads against this challenging drug target. Nevertheless, the wealth of new chemical matter that was discovered and the associated structural information that was generated through fragment-based approaches turned out to be invaluable for BACE1 drug discovery. Among the nonpeptidic scaffolds identified through this process, a number of amidine- or guanidine-containing structures, both cyclic and acyclic, were discovered early on and, through X-ray crystallography, were shown to form complex and highly productive hydrogen-bonding networks with the catalytic aspartic acid dyad of BACE1 (Table 14.1).


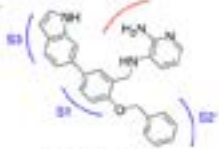
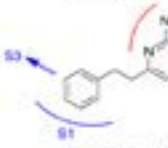
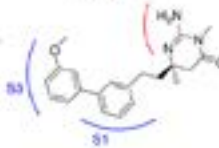
As can be seen from the middle column in Table 14.1, multiple approaches were taken for initial elaboration of the fragment hits, generally using either “SAR by catalog” and/or parallel synthesis. These efforts were aimed both at SAR development for occupancy of neighboring subsites to increase affinity in a ligand-efficient manner and at improvement of PK and other properties. This process was complex for BACE1 given the many challenges for drug discovery that were mentioned in the introduction. A combination of biophysical and biochemical screening methods were used, supported steadily with X-ray crystal structures, to measure progress with the weakly binding low MW compounds (Table 14.1, right-hand columns). The amidine- and guanidine-based hits ultimately provided, after significant design and exploration, an excellent platform for optimization by providing what would later prove to be favorable substitution vectors that led to a series of potent BACE1 inhibitors with high ligand efficiency.

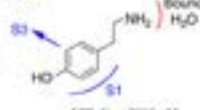
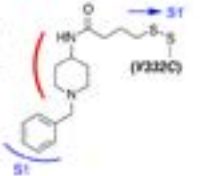

14.2.2

Fragment Optimization

The fragment-derived hits in Table 14.1 were optimized using a combination of structure-based design and biochemical functional assays to develop SAR and

Table 14.1 Summary of BACE1 inhibitors derived from various FBO approaches.


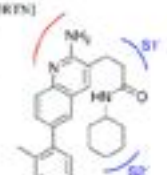
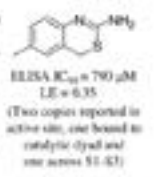

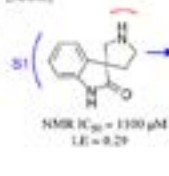
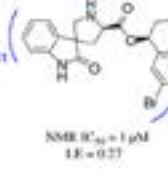
Ref.	Fragment based approach	Representative validated fragment hit	Fragment hit to lead expansion strategy	Representative evolved hit/lead class	Evolved hit/lead binding mode characteristics
[2642]	<ul style="list-style-type: none"> • 347 drug fragments and 45 virtual screening (VS) hits selected for X-ray docking • Access to S1 and S2 from S2 based on binding mode of 2,3-dihydroxyphenylalanine 	 <p>BACE1: IC_{50} = 710 μM LE = 0.32</p>	<ul style="list-style-type: none"> • Rapid substitution to better occupy S2–S3 hydrophobic pocket • Extension at ortho-position of S1 phenyl explore hydrophobic S2' while under the flap • Enzyme assay and X-ray for hit validation 	 <p>BACE1: IC_{50} = 0.60 μM LE = 0.26</p>	<ul style="list-style-type: none"> • 2,3-Dihydroxyphenylalanine 18-bonds to catalytic aspartates and 3-bonded occupies S3 • Phenyl methyl group sits in S1–S3 and interacts at ortho-position extends toward S2'
[6146]	<ul style="list-style-type: none"> • Competitive water-LDCK/1 NMR screen of 2000 fragment library • Competitive SPR and NMR to test analogs followed by molecular docking 3 way hit validation • Inexpensive scaffold hopping and fragment growing toward S1–S3 	 <p>ISA SPR: K_D = 600 μM LE = 0.27</p>	<ul style="list-style-type: none"> • 3-Substituted isoxantoin and dihydroisoxantoin analogs to optimize molecular power of 10:1:1 addition • Enzyme assay and LDCK/1 3 way hit validation 	 <p>BACE1: IC_{50} = 0.09 μM LE = 0.37</p>	<ul style="list-style-type: none"> • Dihydroisoxantoin core filled toward prime side while maintaining key interactions with catalytic aspartates • Less favorable pyridine acid conformation stabilized by quaternary cation on cation • Diphenyl deeper in S1–S3 with 3-methyl 11-bond to hydroxyl group of Ser200 displacing water molecule deep in S3

- [40]
- VS and SPB to select 40 fragments for X-ray soaking
 - Binding mode of tyrosine fragment for as starting point for design of low MW inhibitors
- [188A]
- 
- SPB $K_d = 2000 \mu\text{M}$
L.E. = 0.37
- [46]
- Tethering technology to screen 15,000 morphomers
 - X-ray for validation of aminobenzyl-piperidines (ABP) and 3-carbamoyl-benzylpiperidines (CBP)
 - Conformation of tethered ligands to noncovalent BACE1 solution
- [223H]
- 
- (V232C)
- BACE1 $K_i = 74 \mu\text{M}$
L.E. = 0.16
- [223N]
- 
- BACE1 $K_i = 74 \mu\text{M}$
L.E. = 0.16
- [223N]
- Fragment growing toward S3 through substructure searches of Bocchi compound collection
 - SPB and X-ray soaking for analog hit validation
- [223N]
- SAGE and structural studies of affinity-improved tethered analogs to S2/S1 substrate
 - Follow-up by replacing thiol-containing linker with substituents that pack against S1 substrate
 - FL substrate cleavage assay and X-ray for hit validation
- [223N]
- Aminobenzylpiperidine core 10 binds to catalytic aspartates
 - Design binds to hydrophobic S1 substrate
 - 3-Sulfonamide phenyl substituents directed toward the S2 substrate causing BACE1 conformational change

(continued)



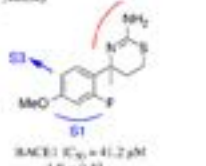
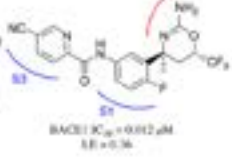
Table 14.1 (Continued)

Ref.	Fragment-based approach	Representative validated fragment hit	Fragment hit to lead expansion strategy	Representative evolved hit/lead class	Evolved hit/lead binding mode characteristics
[4746]	<ul style="list-style-type: none"> • ROC of 26 000 fragment library in enzyme primary assay and hit triaging by counterassay • Hit confirmation with a secondary BACE1 assay and competition SPB to select hits for 5-ray validation • Structure-based growing of 2-aminobenzimidazole into S1 and S2 	<p>[3MSU]</p> <p>BACE1 $K_{i,50}$ = 770 μM LE = 0.28</p>	<ul style="list-style-type: none"> • Structure profiling with related 2-amino-3,4-dihydroquinazoline [54] suggested a branched analog to grow toward S2 and prime side, respectively • Enzyme assay and 5-ray for hit validation • Series discontinued due to NQX off-target activity 	<p>[5MSL]</p> <p>BACE1 $K_{i,50}$ = 7 μM LE = 0.28</p>	<ul style="list-style-type: none"> • 2-Aminobenzimidazole and hydroxyl H-bond to catalytic aspartates • Aryl unit forms face-to-edge π-interaction with flap-Tyr78 • 5-Chloro sits in a pocket between Tyr71 and Tyr76 • A branched ethyl occupies prime side and cyclohexylmethyl reaches S2 subsite
[4936]	<ul style="list-style-type: none"> • Target-derived NMR to screen 10 000 fragment library and heterocyclic sulfonamide isomers yielding several 5-ray structures • Novel cyclic acyl-guanidine core designs as starting points for structure- and property-based fragment growing to explore S1-S2 and S2 	<p>[36MX]</p> <p>NMR K_D = 15 μM LE = 0.39</p>	<ul style="list-style-type: none"> • Structure-guided design of heterocyclic sulfonamide isomers led to discovery of 2-amino-pyridones, imino-hydantoin and iminoguanidines • Structure- and property-based SAR exploration of S1-S2 and S2 • Target-derived NMR, enzyme assay and 5-ray for hit validation 	<p>[4DRU]</p> <p>BACE1 K_i = 4 μM LE = 0.37</p>	<ul style="list-style-type: none"> • Non-planar cyclic acyl-guanidine motif in the imino-hydantoin head group H-bonds to catalytic aspartates • One of the phenyl groups is placed into S1 • Other phenyl group is placed into S2' near S2 which is occupied by Tyr71 in the "closed" flap conformation

- [34] • SFF screen of 6000 fragment library
• 70% NMR functional assay for hit validation
• 4-substituted 2-aminopyridines yield 3-ray fragment structures
• Structure- and property-based fragment growing to explore S1 and S1'-S2
- [38TH]

SPR $K_D = 6.1 \mu\text{M}$
LE = 0.31
- Structure- and property-based SAR exploration of S1' and S2 using 4,6-substituted 2-aminopyridines provided more ligand efficient potency than toward S1
• Fragment assay and X-ray for hit validation
- [38FN]

BACE1 $IC_{50} = 0.074 \mu\text{M}$
LE = 0.34
- 4,6-Substituted 2-aminopyridines uses 11 bonds to catalytic separation
• 4-Tolyl group changes flap conformation and makes face-edge interaction with Flap308
• 3-methyl chain oriented toward S1 side and N-cyclohexyl occupies S2
- [36] • FCS of 6000 fragment library in enzyme assay identified 3-aminobenzothiazole and 3-aminobenzothiazole hits
• X-ray structure (not discussed) guided exploration of S1-S3
- [38SA]

ELISA $IC_{50} = 790 \mu\text{M}$
LE = 0.35
(Two copies reported in active site, one bound to catalytic dyad and one across S1-S3)
- Depositionation of rigid bicyclic scaffold for optimal fragment growth (see S1-S3) followed by property-based optimization
• Fragment assay and X-ray for hit validation
- [38TS]

BACE1 $IC_{50} = 0.24 \mu\text{M}$
LE = 0.41
- 3-Amino-dihydrothiazole uses 11 bonds to catalytic separation
• Difluorophenyl group (see S1)
• Pyrimidine extended into S3
- [36] • 240 member diverse subset of proprietary fragment library for X-ray soaking
• Fragment growing toward S1/S2 based on unique binding mode of spiroproline
- [38UR]

NMR $IC_{50} = 1100 \mu\text{M}$
LE = 0.29
- 20R assessment by co-crystals NMR and had been (inter)assay, and functional NMR activity assay
• Structure- and property-based SAR exploration of S1' and S2
- [38UR]

NMR $IC_{50} = 1 \mu\text{M}$
LE = 0.27
- Spirocyclic proline uses 11 bonds to catalytic separation and rotates CO of Asp208 by $\sim 90^\circ$
• Oxadiazole site in S1 with its N1/N3 bonding to the flap and no contacts to extend toward S3
• Several spirocyclic proline extensions (see pp 337-32)

(Continued)

Table 14.1 (Continued)

Ref	Fragment-based approach	Representative validated fragment hit	Fragment hit to lead expansion strategy	Representative evolved hit/lead class	Evolved hit/lead binding mode characteristics
[30]	<ul style="list-style-type: none"> VS, NMR and HCS validated to discover if an arylidic acid derivative hit for theory synthesis SAR exploration X-ray structure-guided exploration of S1/S2 	 <p>BACE1 $K_i = 0.67 \mu\text{M}$ LE = 0.29</p>	<ul style="list-style-type: none"> Structure centered theory explores to explore optimal acylonyl into S1/S2 Enzyme assay and X-ray for hit validation 	 <p>BACE1 $K_i = 0.04 \mu\text{M}$ LE = 0.34</p>	<ul style="list-style-type: none"> Proximal amide of arylidic acylonyl/methyl H-bonds to aspartate Nitrobenzylidene extends into S2 3,3-Dichlorobenzyl occupies S1 and 4-amine group H-bonds to backbone carbonyl of Phe18 Chp Gly71 side chain H-bonds to imide carbonyl oxygen
[34,35]	<ul style="list-style-type: none"> OTC enzyme assay and X-ray co-crystallization of intermediate state Fragment 3.3 Property-based lead group replacement and structure-based fragment growing into S1 Med. chem. optimization 	 <p>BACE1 $K_{50} = 41.2 \mu\text{M}$ LE = 0.37</p>	<ul style="list-style-type: none"> Final group was to improve PK and extending toward S2 Extensive fluorine scan of L3-positions to improve PK profile Enzyme assay and X-ray for hit validation 	 <p>BACE1 $K_{50} = 0.012 \mu\text{M}$ LE = 0.36</p>	<ul style="list-style-type: none"> Naphthyl cyclic amide methyl is fluorinated to final group H-bond to catalytic aspartate and glucose (phenyl) into S1 Amino S1/H1 bonds to C12 of Gly71 and pyrrolidine p-Cyano projects deep into S1-displacing bound water

For each structure (as applicable), the interaction with the catalytic dyad (as bound, water where specified) is shown by the red arc; sulfate interactions (as potential interactions) are shown in blue, and the Protein Data Bank (PDB) ID for the X-ray structure with BACE1 is indicated in brackets.

generate bona fide leads. These efforts eventually led several groups to discover nonplanar cyclic amidines that can all be described with general structure **1** (Figure 14.2a), which would later be regarded as a key minimal pharmacophore [57] and ultimately yield a large variety of novel, potent BACE1 inhibitors that possess drug-like properties. In addition to forming a complex hydrogen-bonding network with the catalytic aspartyl dyad of BACE1, this framework provided opportunities to explore SAR in both S1 and S2' subsites through direct substitution of the core (Figure 14.2b). Furthermore, extensions at the *meta*-position of the S1 phenyl group provided a favorable trajectory to access the

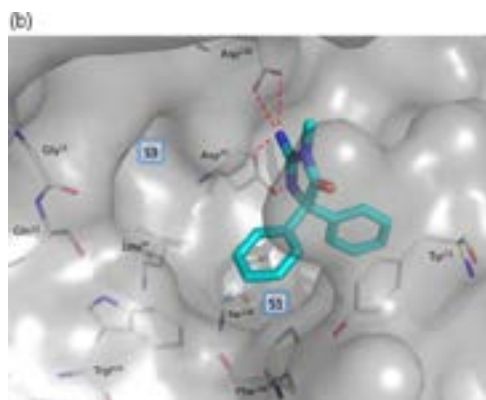
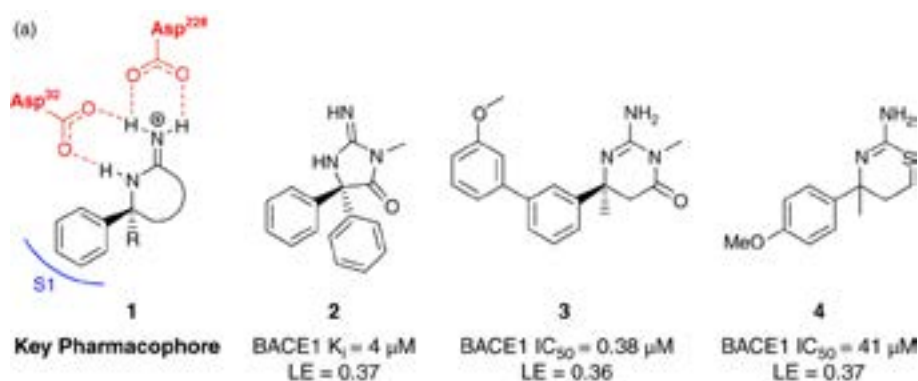


Figure 14.2 (a) Nonplanar cyclic amidine key pharmacophore **1** and derived BACE1 inhibitor leads discovered by diverse FBDD approaches. (b) Crystal structure of **2** bound to BACE1 (PDB code 4DJU) [58]. (c) Crystal structure of **3** bound to BACE1 (PDB code 2VA6) [44]. The amidine portion of the key pharmacophore **1**

present in hits **2–4** hydrogen bonds (dashed red lines) to the catalytic dyad, Asp32 and Asp228, while the nonplanar sp^3 carbon displays the pendant phenyl moiety into the hydrophobic S1 pocket to enable extensions toward S3 and allowing additional access to the prime side.

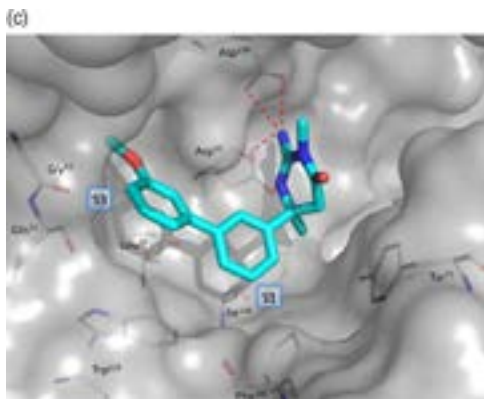


Figure 14.2 (Continued)

adjacent S3 pocket (Figures 14.2c), offering the potential for ligand-efficient inhibitors for this challenging drug target.

Relative to cores that share minimal pharmacophore **1**, the other structures in Table 14.1 offered less direct access to the subpockets around the catalytic dyad, generally leading to less efficient ligand designs. For example, vectors from the planar cyclic amidines [28,42,47,48,51], the acyclic acylguanidines [53], and the 4-aminobenzylpiperidine [46] were perpendicular to the S1 subsite due to the binding pose required to achieve a productive binding to the catalytic aspartic acids. With no direct access to S1, many optimization strategies have used less ligand efficient access to S1 and/or have required occupation of alternate subsites including S1', S2, and S2' to gain affinity. The spiropyrrolidine fragment core has been plagued by similar limitations since the phenyl group that occupies S1 does so with a suboptimal trajectory into S3 [52]. These cores have all faced similar challenges linked to inferior PK properties, P-gp issues, poor brain penetration, or unacceptable off-target activities that have been difficult to mitigate during fragment optimization.

14.2.3

From a Key Pharmacophore to Clinical Candidates

The first iminoheterocycles exemplifying pharmacophore **1**, for example, imino-hydantoin **2** and iminopyrimidinone **3**, were reported in the patent literature in 2005 [59]. These and related structures were independently discovered using FBDD by scientists at Schering-Plough (**2**, **3**) [50,58,60–62] and AstraZeneca (**3**) [44] as well as through traditional high-throughput screening (HTS) methods by the Wyeth group (**2**) [63,64]. Beginning in 2007 [65–67], a number of groups disclosed dihydrothiazine-based structures (e.g., **4**). Both Lilly [38] and Roche [54] identified low MW dihydrothiazine fragments through high-

concentration biochemical screening, whereas Shionogi [65] and Eisai [66] arrived at their structures through undisclosed methods. X-ray crystal structures of a number of initial isothiourea leads with BACE1 have recently been published, including compound **4** from Roche [54].

Researchers at Schering-Plough discovered iminoheterocycles **2** and **3** via a design effort based on isothiourea fragment hit **5** (Figure 14.3a and Table 14.1), which they had identified through screening by NMR and validated with X-ray crystallography [49,50]. The array of hydrogen bond donor–acceptor interactions formed between the amidine portion of **5** and the catalytic dyad of BACE1 was at the time unprecedented for aspartyl protease inhibitors. Recognizing the potential liabilities of an isothiourea – susceptibility to oxidative degradation, chemical reactivity, and toxicity – they designed cyclic acylguanidine scaffolds **6**

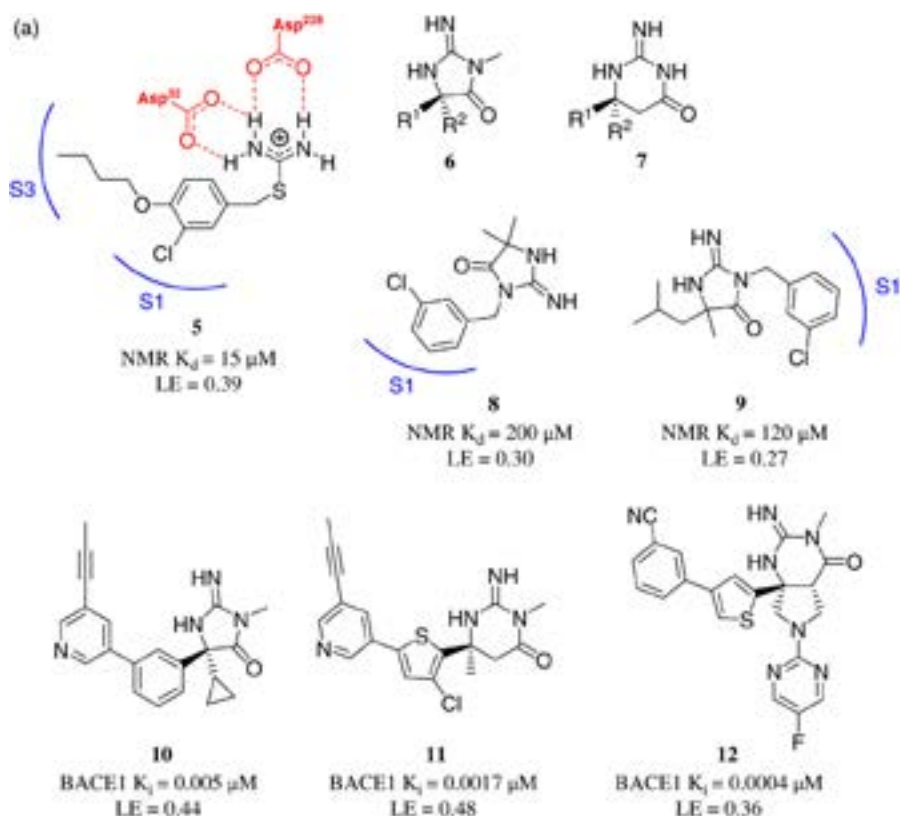


Figure 14.3 (a) Optimization of NMR isothiourea fragment hit **5** from Schering-Plough [49,50,58,60–62]. Merck has progressed the most advanced lead from this effort into two phase 3 clinical trials. (b) Optimization of NMR pyrimidinone fragment hit **13** to an early clinical compound from AstraZeneca [34,37,43,44,68]. (c) Optimization of HTS dihydrothiazine fragment hit **21** to first two clinical candidates from Eli Lilly [38,39].

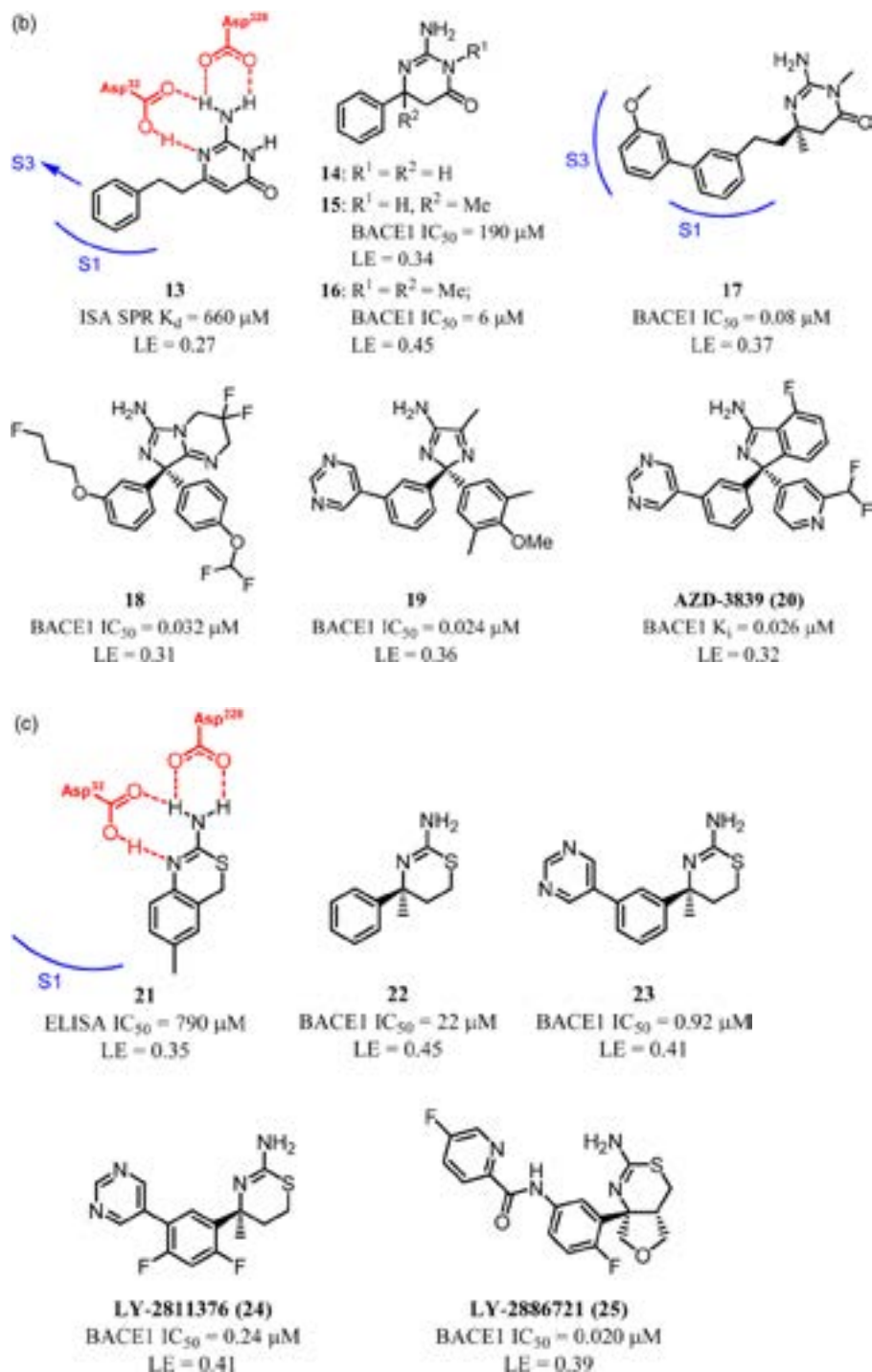


Figure 14.3 (Continued)

and **7** using the detailed structural information provided by the X-ray cocrystal structure of isothioureia **5** in conjunction with *in silico* modeling. The concept of these chemotypes was to preserve the key interactions with the catalytic aspartates using a minimal number of hydrogen bond donors while tuning basicity and having fewer rotatable bonds. In addition to these characteristics, which were intended to favor CNS penetration, the group also incorporated an sp^3 center on the cores to enable ligand-efficient access to both the prime and the nonprime sides of the active site.

Initially, both N3-substituted (e.g., **6**) and regioisomeric N1-substituted imino-hydantoin were examined, but only the N3-substituted analogs showed binding to BACE1 by NMR, likely due to the nonbasic nature of the N1-substituted analogs (calculated pK_a values for N3- and N1-substitution are ~ 7 and ~ 4 , respectively). As SAR developed within the N3-substituted series, minor differences in the substitution pattern, for example, C5-gem-dimethyl analog **8** versus C5-methyl-isobutyl compound **9**, unexpectedly caused the core binding mode to flip by 180° , projecting the benzyl group into either S1' or S1 as evidenced by X-ray crystallography [50,60]. Taken together, these early findings emphasized both the importance of the protonation state of the core in maintaining the productive hydrogen bonding interactions with the catalytic dyad and the key role that X-ray crystallography played in understanding emerging, often complex SAR.

Through continued structure-enabled optimization and a focus on drug-like properties, both iminohydantoin **2** and iminopyrimidinone **3** were eventually identified as ligand-efficient leads that demonstrated a minimal shift in potency in the cellular assay and reasonable rat PK [50,60,61]. It should be noted that the ring size of the cyclic acylguanidine core (i.e., five-membered iminohydantoin **2**, **6**, and **10** versus six-membered iminopyrimidinones **3**, **7**, and **11**) had a profound impact on both the physicochemical properties and the binding conformation of these structures, which therefore required very different strategies for optimization [61]. This highlights the fact that, even starting with a minimal pharmacophore like **1**, a significant degree of optimization is required to find advanced leads. A major driver in subsequent development of both series was the use of an *in vivo* rat pharmacodynamic assay early in the design cycle, which allowed differentiation of compounds based on their ability to lower both brain and cerebrospinal fluid (CSF) A β levels. This integrated approach ultimately resulted in the discovery of orally bioavailable, brain-penetrant inhibitors **10–12** that afforded reductions of central A β 40 levels in rats following single oral doses [58,61,62]. Additional extensive SAR development and optimization of properties produced the most clinically advanced BACE inhibitor to date, **MK-8931** (verubecestat) [69]. This compound dramatically lowered CSF A β levels both in healthy volunteers [70] and in AD patients [33] in phase 1 clinical trials. Based on positive feedback from a planned interim safety analysis by their Data Monitoring Committee [71], MK-8931 initiated two phase 3 trials in 2013, one in mild-to-moderate AD patients [72] and one in patients with prodromal AD [73].

AstraZeneca arrived at iminopyrimidinone **3** from a very different starting point, in their case from isocytosine fragment hit **13** (Figure 14.3b) [43,44].

Deplanarization and removal of rotatable bonds from this hit gave C6-phenyl iminopyrimidinone **14**. X-ray crystallography of this compound with BACE1 showed that the sp^3 nature of the C5 and C6 centers enabled the C6-phenyl group to occupy the S1 subpocket, albeit via an energetically disfavored pseudoaxial conformation. Quaternization of the C6 center through introduction of a methyl group afforded compound **15** and imparted modest potency gains through stabilization of this conformation. Finally, derivatization of N3 with a methyl group based on the SAR from the planar isocytosine series gave core **16** with significant and ligand-efficient potency gains, and subsequent elaboration of the S1 phenyl to an S1–S3 biaryl ultimately produced **3**.

Guided by their X-ray data, they further modified **3** to more fully occupy the S1–S3 subsites. To that end, reintroduction of the rotatable bonds present in their initial hit **13** afforded analog **17**. The methoxybiphenyl portion of this compound did indeed sit deeper in the S1–S3 pockets with the iminopyrimidinone core tilted toward the prime side while maintaining productive contacts with the catalytic aspartates. This modification afforded a fourfold boost in BACE1 potency with no loss in ligand efficiency.

AstraZeneca subsequently pursued scaffold hopping in designing their core-modified inhibitors **18–20** [34,37,68], all of which retained key pharmacophore **1**. Interestingly, the Wyeth group independently discovered a bicyclic amidine scaffold similar to **18** through their own HTS campaign and optimized to very similar chemical space [74], highlighting the sometimes convergent nature of efforts in this arena. Compound **20** potentially lowered central A β levels in preclinical species [35], and it was advanced into phase 1 clinical trials as **AZD-3839** [36,75] but was ultimately halted. AstraZeneca has since partnered with Eli Lilly to develop **AZD-3293/LY-3314814**, which recently entered phase 2/3 clinical trials [76].

In their dihydrothiazine work, scientists at Eli Lilly also pursued a strategy of deplanarization, in this case of screening hit **21** [38] to give core **22** similar to lead **4** reported by Roche [54]. Compound **22** was optimized along similar lines as iminopyrimidinone **16**, building into the S3 subsite by elaborating the S1 phenyl into a *meta*-biaryl. With introduction of an S3 pyrimidinyl group to afford **23**, they identified a ligand efficient submicromolar BACE1 inhibitor lead that, with property-based optimization, ultimately led to identification of their first clinical compound **LY-2811376 (24)**. This compound afforded significant reductions in CSF A β levels in healthy volunteers following single doses, but its development was discontinued due to preclinical toxicity findings unrelated to inhibition of BACE1 [38]. Lilly subsequently turned to a related tetrahydrofuran-fused dihydrothiazine core, also investigated extensively by Eisai [66], from which they identified their second clinical candidate, **LY-2886721 (25)** [39]. Development of this compound was stopped in phase 2 due to abnormal liver function, which they reported as unrelated to inhibition of BACE1 [77].

In addition to the case studies described above, a number of other companies are or have been in phase 1 clinical trials with BACE1 inhibitors, including Eisai/Biogen (**E2609**) [78], Shionogi/Janssen (**JNJ-54861911**) [79], Boehringer-

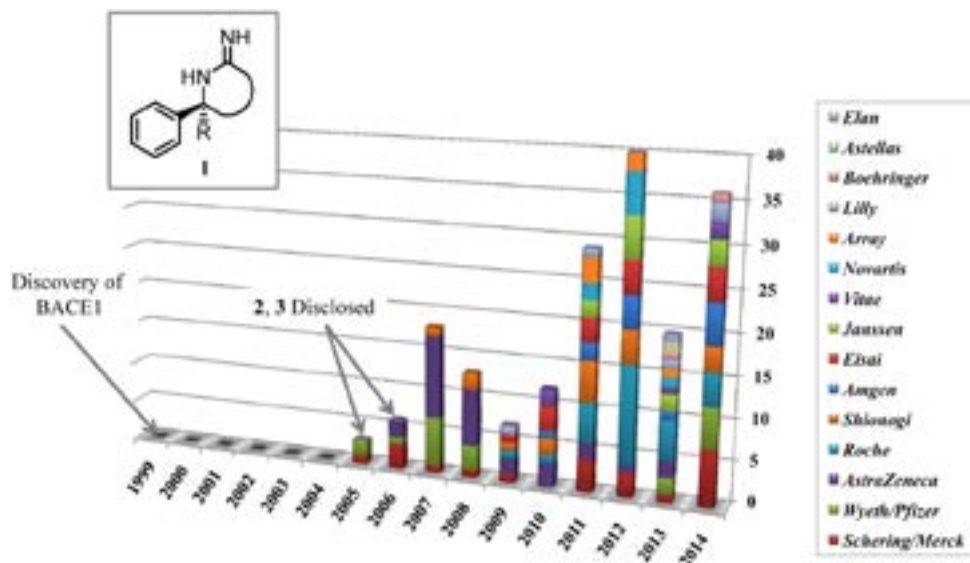


Figure 14.4 Survey of small molecule BACE1 inhibitor patent applications disclosing structures that contain key pharmacophore **1**. For each year, the bars are colored by company. After an initial period with relatively few

applications and limited companies working in this space, the number of applications and diversity of companies significantly increased beginning in 2011.

Ingelheim/Vitae (**BI1181181**, discontinued) [80], and Roche (**RG7129**, discontinued) [81]. While the structures of these compounds have not been disclosed, a review of the patent literature shows that, despite a wide array of structural differences, most if not all of the possible candidates contain the minimal pharmacophore **1** or a close variant thereof. More broadly, a recent review by Oehlrich *et al.* elegantly summarized the extensive diversity of cyclic nonplanar amidines that have been explored across the field (see Figure 30 in Ref. [40]). Looking at BACE1 inhibitor patent applications over time, Figure 14.4 represents a survey of those applications that have employed key pharmacophore **1**. Following its first disclosure in 2005 [59], there was an incubation period before a significant increase in prevalence is seen beginning in 2011 as more researchers recognized the value of this structural motif, particularly given the challenges of finding tractable, brain-penetrant chemical matter when pursuing other chemotypes. It is striking to note that from the first iminoheterocycle disclosures, it took 8 years to start the first phase 3 clinical trials with a BACE1 inhibitor in 2013, reflective of the extensive development and optimization of inhibitors that was still required to identify chemical matter suitable for long-term trials.

Finally, while a number of different hits exemplifying pharmacophore **1** were identified through FDBB and served as launching points for numerous BACE1 inhibitor discovery programs, this amidine moiety has created its own drug discovery challenges. As was found early on by the Schering-Plough group, the

amidine must be protonated for productive interactions with the catalytic dyad, and this basic center contributed to hERG affinity and P-gp susceptibility of the molecules. Several companies have published on their approaches to these issues (e.g [7,40,62,82].), reflecting the specific facets of their advanced chemical matter. More broadly, though, a general focus on ligand efficiency and maintenance of CNS drug-like physicochemical properties [83] appears to be important for achieving high brain BACE1 occupancy *in vivo* while minimizing off-target liabilities.

14.3

Conclusions

The emergence of BACE1 as a therapeutic target for the development of disease-modifying treatments for Alzheimer's disease has fueled intensive drug discovery efforts in which fragment-based approaches have played a key role. From several independent starting points identified through FBDD, a variety of design approaches provided a diverse set of lead structures that shared the nonplanar cyclic amidine minimal pharmacophore represented by general iminoheterocycle structure **1**. This novel chemotype for aspartyl protease inhibition provided direct, ligand-efficient access to both the contiguous S1–S3 subpockets and the non-prime side of BACE1. Even with key pharmacophore **1** as a foundation, there have been a number of innovative approaches to further optimization that have produced many structurally diverse inhibitors, as exemplified by compounds **12**, **20**, and **25**. It should be noted, however, that all of the disclosed compounds that have progressed into advanced preclinical testing or into clinical trials have remained relatively lean, occupying only two subsites of BACE1 with minimal rotatable bonds. Adherence to these design principles was critical for achieving high brain BACE1 occupancy *in vivo*, as evidenced by reduction of central A β levels in animal models. In this way, discovery of the iminoheterocycle class of BACE1 inhibitors transformed the field and, after a great deal of persistence and a high tolerance for setbacks, will now enable the most definitive test of the amyloid hypothesis to date in the clinic. The entry of multiple BACE1 inhibitors, all of which have likely arisen from or been influenced by fragment-based design, into clinical trials by several organizations is a testament to the progress of FBDD and its potential to impact the development of drugs for critical unmet medical needs.

References

- 1 Hardy, J. and Selkoe, D.J. (2002) The amyloid hypothesis of Alzheimer's disease: progress and problems on the road to therapeutics. *Science*, **297**, 353–356.
- 2 Karran, E., Mercken, M., and De Strooper, B. (2011) The amyloid cascade hypothesis for Alzheimer's disease: an appraisal for the development of therapeutics. *Nature Reviews Drug Discovery*, **10**, 698–711.

- 3 Vassar, R., Kuhn, P.-H., Haass, C., Kennedy, M.E., Rajendran, L., Wong, P.C., and Lichtenthaler, S.F.J. (2014) Function, therapeutic potential and cell biology of BACE proteases: current status and future prospects. *Journal of Neurochemistry*, **130**, 4–28.
- 4 Lemere, C.A. (2013) Immunotherapy for Alzheimer's disease: hoops and hurdles. *Molecular Neurodegeneration*, **8**, 36–41.
- 5 Biogen Idec Presents Positive Interim Results from Phase 1B Study of Investigational Alzheimer's Disease Treatment Aducanumab (BIIB037) at 2015 AD/PD™ Conference. <http://media.biogen.com/press-release/corporate/biogen-idec-presents-positive-interim-results-phase-1b-study-investigational> (accessed 3 May 2015).
- 6 Yan, R. and Vassar, R. (2014) Targeting the β secretase BACE1 for Alzheimer's disease therapy. *Lancet Neurology*, **13**, 319–329.
- 7 Yuan, J., Venkatraman, S., Zheng, Y., McKeever, B.M., Lawrence, W., Dillard, L.W., and Singh, S.B. (2013) Structure-based design of β -site APP cleaving enzyme 1 (BACE1) inhibitors for the treatment of Alzheimer's disease. *Journal of Medicinal Chemistry*, **56**, 4156–4180.
- 8 Vassar, R., Bennett, B.D., Babu-Khan, S., Kahn, S., Mendiaz, E.A., Denis, P., Teplow, D.B., Ross, S., Amarante, P., Loeloff, R., Luo, Y., Fisher, S., Fuller, J., Edenson, S., Lile, J., Jarosinski, M.A., Biere, A.L., Curran, E., Burgess, T., Louis, J.-C., Collins, F., Treanor, J., Rogers, G., and Citron, M. (1999) β -secretase cleavage of Alzheimer's amyloid precursor protein by the transmembrane aspartic protease BACE. *Science*, **286**, 735–741.
- 9 Yan, R., Bienkowski, M.J., Shuck, M.E., Miao, H.Y., Tory, M.C., Pauley, A.M., Brashler, J.R., Stratman, N.C., Mathews, W.R., Buhl, A.E., Carter, D.B., Tomasselli, A.G., Parodi, L.A., Heinrichson, R.L., and Gurney, M.E. (1999) Membrane-anchored aspartyl protease with Alzheimer's disease β -secretase activity. *Nature*, **402**, 533–537.
- 10 Sinha, S., Anderson, J.P., Barbour, R., Basi, G.S., Caccavello, R., Davis, D., Doan, M., Dovey, H.F., Frigon, N., Hong, J., Jacobson-Croak, K., Jewett, N., Keim, P., Knops, J., Lieberburg, I., Power, M., Tan, H., Tatsuno, G., Tung, J., Schenk, D., Seubert, P., Suomensaa, S.M., Wang, S., Walker, D., Zhao, J., McConlogue, L., and John, V. (1999) Purification and cloning of amyloid precursor protein β -secretase from human brain. *Nature*, **402**, 537–540.
- 11 Hussain, I., Powell, D., Howlett, D.R., Tew, D.G., Meek, T.D., Chapman, C., Gloger, I.S., Murphy, K.E., Southan, C.D., Ryan, D.M., Smith, T.S., Simmons, D.L., Walsh, F.S., Dingwall, C., and Christie, C. (1999) Identification of a novel aspartic protease (Asp 2) as β -secretase. *Molecular and Cellular Neurosciences*, **14**, 419–427.
- 12 Lin, X., Koelsch, G., Wu, S., Downs, D., Dashti, A., and Tang, J. (2000) Human aspartic protease memapsin 2 cleaves the β -secretase site of β -amyloid precursor protein. *Proceedings of the National Academy of Sciences of the United States of America*, **97**, 1456–1460.
- 13 Roberds, S.L., Anderson, J., Basi, G., Bienkowski, M.J., Branstetter, D.G., Chen, K.S., Freedman, S.B., Frigon, N.L., Games, D., Hu, K., Johnson-Wood, K., Kappenman, K.E., Kawabe, T.T., Kola, I., Kuehn, R., Lee, M., Liu, W., Motter, R., Nichols, N.F., Power, M., Robertson, D.W., Schenk, D., Schoor, M., Shopp, G.M., Shuck, M.E., Sinha, S., Svensson, K.A., Tatsuno, G., Tintrup, H., Wijsman, J., Wright, S., and McConlogue, L. (2001) BACE knockout mice are healthy despite lacking the primary β -secretase activity in brain: implications for Alzheimer's disease therapeutics. *Human Molecular Genetics*, **10**, 1317–1324.
- 14 Mullan, M., Crawford, F., Axelman, K., Houlden, H., Lilius, L., Winblad, B., and Lannfelt, L. (1992) A pathogenic mutation for probable Alzheimer's disease in the APP gene at the N-terminus of β -amyloid. *Nature Genetics*, **1**, 345–347.
- 15 Haass, C., Lemere, C.A., Capell, A., Citron, M., Seubert, P., Schenk, D., Lannfelt, L., and Selkoe, D.J. (1995) The Swedish mutation causes early-onset Alzheimer's disease by β -secretase cleavage within the secretory pathway. *Nature Medicine*, **1**, 1291–1296.

- 16 Jonsson, T., Atwal, J.K., Steinberg, S., Snaedal, J., Jonsson, P.V., Bjornsson, S., Stefansson, H., Sulem, P., Gudbjartsson, D., Maloney, J., Hoyte, K., Gustafson, A., Liu, Y., Lu, Y., Bhargale, T., Graham, R.R., Huttenlocher, J., Bjornsdottir, G., Andreassen, O.A., Jonsson, E.G., Palotie, A., Behrens, T.W., Magnusson, O.T., Kong, A., Thorsteinsdottir, U., Watts, R.J., and Stefansson, K. (2012) A mutation in APP protects against Alzheimer's disease and age-related cognitive decline. *Nature*, **488**, 96–99.
- 17 Hong, L., Koelsch, G., Lin, X., Wu, S., Terzyan, S., Ghosh, A.K., Zhang, X.C., and Tang, J. (2000) Structure of the protease domain of memapsin 2 (β -secretase) complexed with inhibitor. *Science*, **290**, 150–153.
- 18 Hong, L., Turner, R.T. 3rd, Koelsch, G., Shin, D., Ghosh, A.K., and Tang, J. (2002) Crystal structure of memapsin 2 (β -secretase) in complex with an inhibitor OM00-3. *Biochemistry*, **41**, 10963–10967.
- 19 Tamamura, H., Kato, T., Otaka, A., and Fujii, N. (2003) Synthesis of potent β -secretase inhibitors containing a hydroxyethylamine dipeptide isostere and their structure–activity relationship studies. *Organic and Biomolecular Chemistry*, **1**, 2468–2473.
- 20 Stachel, S.J., Coburn, C.A., Steele, T.G., Jones, K.G., Loutzenhiser, E.F., Gregro, A.R., Rajapakse, H.A., Lai, M.T., Crouthamel, M.C., Xu, M., Tugusheva, K., Lineberger, J.E., Pietrak, B.L., Espeseth, A.S., Shi, X.P., Chen-Dodson, E., Holloway, M.K., Munshi, S., Simon, A.J., Kuo, L., and Vacca, J.P. (2004) Structure-based design of potent and selective cell-permeable inhibitors of human β -secretase (BACE-1). *Journal of Medicinal Chemistry*, **47**, 6447–6450.
- 21 Ghosh, A.K. and Osswald, H.L. (2014) BACE1 (β -secretase) inhibitors for the treatment of Alzheimer's disease. *Chemical Society Reviews*, **43**, 6765–6813.
- 22 Hopkins, A.L., Groom, C.R., and Alex, A. (2004) Ligand efficiency: a useful metric for lead selection. *Drug Discovery Today*, **9**, 430–431.
- 23 Sankaranarayanan, S., Holahan, M.A., Colussi, D., Crouthamel, M.C., Devanarayan, V., Ellis, J., Espeseth, A., Gates, A.T., Graham, S.L., Gregro, A.R., Hazuda, D., Hochman, J.H., Holloway, K., Jin, L., Kahana, J., Lai, M.T., Lineberger, J., McGaughey, G., Moore, K.P., Nantermet, P., Pietrak, B., Price, E.A., Rajapakse, H., Stauffer, S., Steinbeiser, M.A., Seabrook, G., Selnick, H.G., Shi, X.P., Stanton, M.G., Swestock, J., Tugusheva, K., Tyler, K.X., Vacca, J.P., Wong, J., Wu, G., Xu, M., Cook, J.J., and Simon, A.J. (2009) First demonstration of cerebrospinal fluid and plasma A β lowering with oral administration of a β -site amyloid precursor protein-cleaving enzyme 1 inhibitor in nonhuman primates. *Journal of Pharmacology and Experimental Therapeutics*, **328**, 131–140.
- 24 Lerchner, A., Machauer, R., Betschart, C., Veenstra, S., Rueeger, H., McCarthy, C., Tintelnot-Blomley, M., Jatou, A.-L., Rabe, S., Desrayaud, S., Enz, A., Staufenbiel, M., Paganetti, P., Rondeau, J.-M., and Neumann, U. (2010) Macrocyclic BACE-1 inhibitors acutely reduce A β in brain after po application. *Bioorganic and Medicinal Chemistry Letters*, **20**, 603–607.
- 25 Dineen, T.A., Weiss, M.M., Williamson, T., Acton, P., Babu-Khan, S., Bartberger, M.D., Brown, J., Chen, K., Cheng, Y., Citron, M., Croghan, M.D., Dunn, R.T., Esmay, J., Graceffa, R.F., Harried, S.S., Hickman, D., Hitchcock, S.A., Horne, D.B., Huang, H., Imbeah-Ampiah, R., Judd, T., Kaller, M.R., Kreiman, C.R., La, D.S., Li, V., Lopez, P., Louie, S., Monenschein, H., Nguyen, T.T., Pennington, L.D., Miguel, T.S., Sickmier, E.A., Vargas, H.M., Wahl, R.C., Wen, P.H., Whittington, D.A., Wood, S., Xue, Q., Yang, B.H., Patel, V.F., and Zhong, W. (2012) Design and synthesis of potent, orally efficacious hydroxyethylamine derived β -site amyloid precursor protein cleaving enzyme (BACE1) inhibitors. *Journal of Medicinal Chemistry*, **55**, 9025–9044.
- 26 Kaller, M.R., Halrried, S.S., Albrecht, B., Amarante, P., Babu-Khan, S., Bartberger, M.D., Brown, J., Brown, R., Chen, K., Cheng, Y., Citron, M., Croghan, M.D., Graceffa, R., Hickman, D., Judd, T.,

- Kriemen, C., La, D., Li, V., Lopez, P., Luo, Y., Masse, C., Monenschein, H., Nguyen, T., Pennington, L.D., Miguel, T.S., Sickmier, E.A., Wahl, R.C., Weiss, M.M., Wen, P.H., Williamson, T., Wood, S., Xue, M., Yang, B., Zhang, J., Patel, V., Zhong, W., and Hitchcock, S. (2012) A potent and orally efficacious, hydroxyethylamine-based inhibitor of β -secretase. *ACS Medicinal Chemistry Letters*, **3**, 886–891.
- 27 Weiss, M.M., Williamson, T., Babu-Khan, S., Bartberger, M.D., Brown, J., Chen, K., Cheng, Y., Citron, M., Croghan, M.D., Dineen, T.A., Esmay, J., Graceffa, R.F., Harried, S.S., Hickman, D., Hitchcock, S.A., Horne, D.B., Huang, H., Imbeah-Ampiah, R., Judd, T., Kaller, M.R., Kreiman, C.R., La, D.S., Li, V., Lopez, P., Louie, S., Monenschein, H., Nguyen, T.T., Pennington, L.D., Rattan, C., San Miguel, T., Sickmier, E.A., Wahl, R.C., Wen, P.H., Wood, S., Xue, Q., Yang, B.H., Patel, V.F., and Zhong, W. (2012) Design and preparation of a potent series of hydroxyethylamine containing β -secretase inhibitors that demonstrate robust reduction of central β -amyloid. *Journal of Medicinal Chemistry*, **55**, 9009–9024.
- 28 Congreve, M., Aharony, D., Albert, J., Callaghan, O., Campbell, J., Carr, R.A.E., Chessari, G., Cowan, S., Edwards, P.D., Fredrickson, M., McMenamin, R., Murray, C.W., Patel, S., and Wallis, N. (2007) Application of fragment screening by X-ray crystallography to the discovery of aminopyridines as inhibitors of β -secretase. *Journal of Medicinal Chemistry*, **50**, 1124–1132.
- 29 Patel, S., Vuillard, L., Cleasby, A., Murray, C. W., and Yon, J. (2004) Apo and inhibitor complex structures of BACE (β -secretase). *Journal of Molecular Biology*, **343**, 407–416.
- 30 Stachel, S.J. (2009) Progress toward the development of a viable BACE-1 inhibitor. *Drug Development Research*, **70**, 101–110.
- 31 Probst, G. and Xu, Y.-Z. (2012) Small-molecule BACE1 inhibitors: a patent literature review (2006–2011). *Expert Opinion on Therapeutic Patents*, **22**, 511–540.
- 32 Baker, M. (2013) Fragment-based lead discovery grows up. *Nature Reviews Drug Discovery*, **12**, 5–7.
- 33 Forman, M., Kleijn, H.-J., Dockendorf, M., Palcza, J., Tseng, J., Canales, C., Egan, M., Kennedy, M., Laterza, O., Ma, L., Scott, J., Tanen, M., Apter, J., Backonja, M., Ereshefsky, L., Gevorkyan, H., Jhee, S., Rynders, R., Zari, A., Bryan, E., Wagner, J., Troyer, M., and Stone, J. (2013) The novel BACE inhibitor MK-8931 dramatically lowers CSF beta-amyloid in patients with mild-to-moderate Alzheimer's disease. *Alzheimer's and Dementia*, **9** (4), Supplement P139.
- 34 Swahn, B.-M., Kolmodin, K., Karlström, S., von Berg, S., Söderman, P., Holenz, J., Berg, S., Lindström, J., Sundström, M., Turek, D., Kihlström, J., Slivo, C., Andersson, L., Pyring, D., Rotticci, D., Öhberg, L., Kers, A., Bogar, K., von Kieseritzky, F., Bergh, M., Olsson, L.-L., Janson, J., Eketjäll, S., Georgievskaya, B., Jeppsson, F., and Färling, J. (2012) Design and synthesis of β -secretase (BACE1) inhibitors with *in vivo* brain reduction of β -amyloid peptides. *Journal of Medicinal Chemistry*, **55**, 9346–9361.
- 35 Jeppsson, F., Eketjäll, S., Janson, J., Karlström, S., Gustavsson, S., Olsson, L.-L., Radesäter, A.-C., Ploeger, B., Cebers, G., Kolmodin, K., Swahn, B.-M., von Berg, S., Bueters, T., and Färling, J. (2012) Discovery of AZD3839, a potent and selective BACE1 clinical candidate for the treatment of Alzheimer's disease. *Journal of Biological Chemistry*, **287**, 41245–41257.
- 36 Quartino, A., Huledal, G., Sparve, E., Lüttgen, M., Bueters, T., Karlsson, P., Olsson, T., Paraskos, J., Maltby, J., Claeson-Bohnstedt, K., Lee, C.-M., Alexander, R., Färling, J., and Paulsson, B. (2014) Population pharmacokinetic and pharmacodynamic analysis of plasma A β 40 and A β 42 following single oral doses of the BACE1 inhibitor AZD3839 to healthy volunteers. *Clinical Pharmacology in Drug Development*, **3**, 396–405.
- 37 Gravenfors, Y., Viklund, J., Blid, J., Ginman, T., Karlstrom, S., Kihlstrom, J., Kolmodin, K., Lindstrom, J., von Berg, S., von Kierseritzky, F., Slivo, C., Swahn, B.-M., Olsson, L.-L., Johansson, P., Eketjäll, S., Färling, J., Jeppsson, F., Strömberg, K., Janson, J., and Rahm, F.

- (2012) New aminoimidazoles as β -secretase (BACE-1) inhibitors showing amyloid- β (A β) lowering in brain. *Journal of Medicinal Chemistry*, **55**, 9297–9311.
- 38 May, P.C., Dean, R.A., Lowe, S.L., Martenyi, F., Sheehan, S.M., Boggs, L.N., Monk, S.A., Mathes, B.M., Mergott, D.J., Watson, B.M., Stout, S.L., Timm, D.E., Smith LaBell, E., Gonzales, C.R., Nakano, M., Jhee, S.S., Yen, M., Ereshefsky, L., Lindstrom, T.D., Calligaro, D.O., Cocke, P.J., Hall, D.G., Friedrich, S., Citron, M., and Audia, J.E. (2011) Central reduction of amyloid- β in humans with an orally available, non-peptidic β -secretase inhibitor. *Journal of Neuroscience*, **31**, 16507–16516.
- 39 May, P.C., Willis, B.A., Lowe, S.L., Dean, R.A., Monk, S.A., Cocke, P.J., Audia, J.E., Boggs, L.N., Borders, A.R., Brier, R.A., Calligaro, D.O., Day, T.A., Ereshefsky, L., Erickso, J.A., Gevorkyan, H., Gonzales, C.R., James, D.E., Jhee, S.S., Komjathy, S.F., Li, L., Lindstrom, T.D., Mathe, B.M., Martenyi, F., Sheehan, S.M., Stout, S.L., Timm, D.E., Vaught, G.M., Watson, B.M., Winneroski, L.L., Yang, Z., and Mergott, D.J. (2015) The potent BACE1 inhibitor LY2886721 elicits robust central A β pharmacodynamic responses in mice, dogs, and humans. *Journal of Neuroscience*, **35**, 1199–1210.
- 40 Oehlrich, D., Prokopcova, H., and Gijsen, H.J.M. (2014) The evolution of amidine-based brain penetrant BACE1 inhibitors. *Bioorganic and Medicinal Chemistry Letters*, **24**, 2033–2045.
- 41 Menting, K.W. and Claassen, J.A.H.R. (2014) β -secretase inhibitor; a promising novel therapeutic drug in Alzheimer's disease. *Frontiers in Aging Neuroscience*, **6**, 165.
- 42 Murray, C.W., Callaghan, O., Chessari, G., Cleasby, A., Congreve, M., Frederickson, M., Hartshorn, M.J., McMenamin, R., Patel, S., and Wallis, N. (2007) Application of fragment screening by X-ray crystallography to β -secretase. *Journal of Medicinal Chemistry*, **50**, 1116–1123.
- 43 Geschwindner, S., Olsson, L.-L., Albert, J.S., Deinum, J., Philip, D., Edwards, P.D., de Beer, T., and Folmer, R.H.A. (2007) Discovery of a novel warhead against β -secretase through fragment-based lead generation. *Journal of Medicinal Chemistry*, **50**, 5903–5911.
- 44 Edwards, P.D., Albert, J.S., Sylvester, M., Aharony, D., Andisik, D., Callaghan, O., Campbell, J.B., Carr, R.A., Chessari, G., Congreve, M., Frederickson, M., Folmer, R.H.A., Geschwindner, S., Koether, G., Kolmodin, K., Krumrine, J., Mauger, R.C., Murray, C.W., Olsson, L.-L., Patel, S., Spear, N., and Tian, G. (2007) Application of fragment-based lead generation to the discovery of novel, cyclic amidine β -secretase inhibitors with nanomolar potency, cellular activity, and high ligand efficiency. *Journal of Medicinal Chemistry*, **50**, 5912–5925.
- 45 Kuglstatte, A., Stahl, M., Peters, J., Huber, W., Stihle, M., Schlatter, D., Benz, J., Ruf, A., Roth, D., Enderle, T., and Hennig, M. (2008) Tyramine fragment binding to BACE-1. *Bioorganic and Medicinal Chemistry Letters*, **18**, 1304–1307.
- 46 Yang, W., Fucini, R.V., Fahr, B.T., Randal, M., Lind, K.E., Lam, M.B., Lu, W., Lu, Y., Cary, D.R., Romanowski, M.J., Colussi, D., Pietrak, B., Allison, T.J., Munshi, S.K., Penny, D.M., Pham, P., Sun, J., Thomas, A.E., Wilkinson, J.M., Jacobs, J.W., McDowell, R.S., and Ballinger, M.D. (2009) Fragment-based discovery of nonpeptidic BACE-1 inhibitors using tethering. *Biochemistry*, **48**, 4488–4496.
- 47 Godemann, R., Madden, J., Joachim Krämer, J., Smith, M., Fritz, U., Hestekamp, T., Barker, J., Höppner, S., Hallett, D., Cesura, A., Ebnet, A., and Kemp, J. (2009) Fragment-based discovery of BACE1 inhibitors using functional assays. *Journal of Medicinal Chemistry*, **48**, 10743–10751.
- 48 Madden, J., Dod, J.R., Godemann, R., Kraemer, J., Smith, M., Biniszkiwicz, M., Hallett, D.J., Barker, J., Dyekjaer, J.D., and Hestekamp, T. (2010) Fragment-based discovery and optimization of BACE1 inhibitors. *Bioorganic and Medicinal Chemistry Letters*, **20**, 5329–5333.
- 49 Wang, Y.-S., Strickland, C., Voigt, J.H., Kennedy, M.E., Beyer, B.M., Senior, M.M., Smith, E.M., Nechuta, T.L., Madison, V.S., Czarniecki, M., McKittrick, B.A., Stamford, A.W., Parker, E.M., Hunter, J.C., Greenlee, W.J., and Wyss, D.F. (2010)

- Application of fragment-based NMR screening, X-ray crystallography, structure-based design, and focused chemical library design to identify novel μ M leads for the development of nM BACE-1 (β -site APP cleaving enzyme 1) inhibitors. *Journal of Medicinal Chemistry*, **53**, 942–950.
- 50 Zhu, Z., Sun, Z.-Y., Ye, Y., Voigt, J., Strickland, C., Smith, E.M., Cumming, J., Wang, L., Wong, J., Wang, Y.-S., Wyss, D.F., Chen, X., Kuvelkar, R., Kennedy, M.E., Favreau, L., Parker, E., McKittrick, B.A., Stamford, A., Czarniecki, M., Greenlee, W., and Hunter, J.C. (2010) Discovery of cyclic acylguanidines as highly potent and selective β -site amyloid cleaving enzyme (BACE) inhibitors. Part I. Inhibitor design and validation. *Journal of Medicinal Chemistry*, **53**, 951–965.
 - 51 Cheng, Y., Judd, T.C., Bartberger, M.D., Brown, J., Chen, K., Freneau, R.T., Jr., Hickman, D., Hitchcock, S.A., Jordan, B., Li, V., Lopez, P., Louie, S.W., Luo, Y., Michelsen, K., Nixey, T., Powers, T.S., Rattan, C., Sickmier, E.A., St. Jean, D.J. Jr., Wahl, R.C., Wen, P.H., and Wood, S. (2011) From fragment screening to *in vivo* efficacy: optimization of a series of 2-aminoquinolines as potent inhibitors of beta-site amyloid precursor protein cleaving enzyme 1 (BACE1). *Journal of Medicinal Chemistry*, **54**, 5836–5857.
 - 52 Efremov, I.V., Vajdos, F.F., Borzilleri, K.A., Capetta, S., Chen, H., Dorff, P.H., Dutra, J.K., Goldstein, S.W., Mansour, M., McColl, A., Noell, S., Oborski, C.E., O'Connell, T.N., O'Sullivan, T.J., Pandit, J., Wang, H., Wei, B.Q., and Withka, J.M. (2012) Discovery and optimization of a novel spiropyrrolidine inhibitor of β -secretase (BACE1) through fragment-based drug design. *Journal of Medicinal Chemistry*, **55**, 9069–9088.
 - 53 Gerritz, S.W., Zhai, W., Shi, S., Zhu, S., Toyn, J.H., Meredith, J.E., Jr., Iben, L.G., Burton, C.R., Albright, C.F., Good, A.C., Tebben, A.J., Muckelbauer, J.K., Camac, D.M., Metzler, W., Cook, L.S., Padmanabha, R., Lentz, K.A., Sofia, M.J., Poss, M.A., Macor, J.E., and Thompson, L.A., III (2012) Acyl guanidine inhibitors of β -secretase (BACE-1): optimization of a micromolar hit to a nanomolar lead via iterative solid- and solution-phase library synthesis. *Journal of Medicinal Chemistry*, **55**, 9208–9223.
 - 54 Woltering, T.J., Wostl, W., Hilpert, H., Rogers-Evans, M., Pinard, E., Mayweg, A., Göbel, M., Banner, D.W., Benz, J., Travagli, M., Pollastrini, M., Marconi, G., Gabellieri, E., Guba, W., Mauser, H., Andreini, M., Jacobsen, H., Power, E., and Narquizian, R. (2013) BACE1 inhibitors: a head group scan on a series of amides. *Bioorganic and Medicinal Chemistry Letters*, **23**, 4239–4243.
 - 55 Hilpert, H., Guba, W., Woltering, T.J., Wostl, W., Pinard, E., Mauser, H., Mayweg, A.V., Rogers-Evans, M., Humm, R., Krummenacher, D., Muser, T., Schnider, C., Jacobsen, H., Ozmen, L., Bergadano, A., Banner, D.W., Hochstrasser, R., Kuglstatter, A., David-Pierson, P., Fischer, H., Polara, A., and Narquizian, R. (2013) β -Secretase (BACE1) inhibitors with high *in vivo* efficacy suitable for clinical evaluation in Alzheimer's disease. *Journal of Medicinal Chemistry*, **56**, 3980–3995.
 - 56 Baxter, E.W., Conway, K.A., Kennis, L., Bischoff, F., Mercken, M.H., De Winter, H.L., Reynolds, C.H., Tounge, B.A., Luo, C., Scott, M.K., Huang, Y., Braeken, M., Pieters, S.M.A., Berthelot, D.J.C., Masure, S., Bruinzeel, W.D., Jordan, A.D., Parker, M.H., Boyd, R.E., Qy, J., Alexander, R.S., Brenneman, D.E., and Reitz, A.B. (2007) 2-Amino-3,4-dihydroquinazolines as inhibitors of BACE-1 (β -site APP cleaving enzyme): use of structure based design to convert a micromolar hit into a nanomolar lead. *Journal of Medicinal Chemistry*, **50**, 4261–4264. PDB: 2Q15.
 - 57 Stamford, A. and Strickland, C. (2013) Inhibitors of BACE for treating Alzheimer's disease: a fragment-based drug discovery story. *Current Opinion in Chemical Biology*, **17**, 320–328.
 - 58 Cumming, J.N., Smith, E.M., Wang, L., Misiaszek, J., Durkin, J., Pan, J., Iserloh, U., Wu, Y., Zhu, Z., Strickland, C., Voigt, J., Chen, X., Kennedy, M.E., Kuvelkar, R., Hyde, L.A., Cox, K., Favreau, L., Czarniecki, M.F., Greenlee, W.J., McKittrick, B.A., Parker, E.M., and

- Stamford, A.W. (2012) Structure based design of iminohydantoin BACE1 inhibitors: identification of an orally available, centrally active BACE1 inhibitor. *Bioorganic and Medicinal Chemistry Letters*, **22**, 2444–2449.
- 59 Zhu, Z., McKittrick, B., Sun, Z.-Y., Ye, Y.C., Voigt, J.H., Strickland, C., Smith, E.M., Stamford, A., Greenlee, W.J., Wu, Y., Iserloh, U., Mazzola, R., Caldwell, J., Cumming, J., Wang, L., Guo, T., Le, T.X.H., Saionz, K.W., Babu, S.D., and Hunter, R.C. (2005) Preparation of heterocyclic aspartyl protease inhibitors for treating various diseases. *PCT Int. Appl. PATN WO 2005058311 A1*.
 - 60 Wyss, D.F., Wang, Y.-S., Eaton, H.L., Strickland, C., Voigt, J.H., Zhu, Z., and Stamford, A.W. (2012) Combining NMR and X-ray crystallography in fragment-based drug discovery: discovery of highly potent and selective BACE-1 inhibitors. *Topics in Current Chemistry*, **317**, 83–114.
 - 61 Stamford, A.W., Scott, J.D., Li, S.W., Babu, S., Tadesse, D., Hunter, R., Wu, Y., Misiaszek, J., Cumming, J.N., Gilbert, E.J., Huang, C., McKittrick, B.A., Hong, L., Guo, T., Zhu, Z., Strickland, C., Orth, P., Voigt, J.H., Kennedy, M.E., Chen, X., Kuvelkar, R., Hodgson, R., Hyde, L.A., Cox, K., Favreau, L., Parker, E.M., and Greenlee, W.J. (2012) Discovery of an orally available, brain penetrant BACE1 inhibitor that affords robust CNS A β reduction. *ACS Medicinal Chemistry Letters*, **3**, 897–902.
 - 62 Mandal, M., Zhu, Z., Cumming, J.N., Liu, X., Strickland, S., Mazzola, R.D., Caldwell, J.P., Leach, P., Grzelak, M., Hyde, L., Zhang, Q., Terracina, G., Zhang, L., Chen, X., Kuvelkar, R., Kennedy, M.E., Favreau, L., Cox, K., Orth, P., Buevich, A., Voigt, J., Wang, H., Kazakevich, I., McKittrick, B.A., Greenlee, W., Parker, E.M., and Stamford, A.W. (2012) Design and validation of bicyclic iminopyrimidinones as beta amyloid cleaving enzyme-1 (BACE1) inhibitors: conformational constraint to favor a bioactive conformation. *Journal of Medicinal Chemistry*, **55**, 9331–9345.
 - 63 Nowak, P., Cole, D.C., Aulabaugh, A., Bard, J., Chopra, R., Cowling, R., Fan, K.Y., Hu, B., Jacobsen, S., Jani, M., Jin, G., Lo, M.-C., Malamas, M.S., Manas, E.S., Narasimhan, R., Reinhart, P., Robichaud, A.J., Stock, J.R., Subrath, J., Svenson, K., Turner, J., Wagner, E., Zhou, P., and Ellingboe, J.W. (2010) Discovery and initial optimization of 5,5'-disubstituted aminohydantoins as potent β -secretase (BACE1) inhibitors. *Bioorganic and Medicinal Chemistry Letters*, **20**, 632–635.
 - 64 Malamas, M.S., Robichaud, A., Erdei, J., Quagliato, D., Solvibile, W., Zhou, P., Morris, K., Turner, J., Wagner, E., Fan, K., Olland, A., Jacobsen, S., Reinhart, P., Riddell, D., and Menelas, P. (2010) Design and synthesis of aminohydantoins as potent and selective human b-secretase (BACE1) inhibitors with enhanced brain permeability. *Bioorganic and Medicinal Chemistry Letters*, **20**, 6597–6605.
 - 65 Kobayashi, N., Ueda, K., Itoh, N., Suzuki, S., Sakaguchi, G., Kato, A., Yukimasa, A., Hori, A., Koriyama, Y., Haraguchi, H., Yasui, K., and Kanda, Y. (2007) Preparation of 2-aminodihydrothiazine derivatives as beta-secretase inhibitors. *PCT Int. Appl. WO 2007049532 A1*.
 - 66 Suzuki, Y., Motoki, T., Kaneko, T., Takaishi, M., Ishida, T., Takeda, K., Kita, Y., Yamamoto, N., Khan, A., and Dimopoulos, P. (2009) Condensed aminodihydrothiazine derivative. *PCT Int. Appl. WO 2009091016 A1*.
 - 67 Audia, J.E., Mergott, D.J., Sheehan, S.M., and Watson, B.M. (2009) Aminodihydrothiazine derivatives as bace inhibitors for the treatment of Alzheimer's disease. *PCT Int. Appl. WO 2009134617 A1*.
 - 68 Swahn, B.-M., Holenz, J., Kihlstrom, J., Kolmodin, K., Lindstrom, J., Plobeck, N., Rottici, D., Sehgelmeble, F., Sundstrom, M., von Berg, S., Färling, J., Georgievsk, B., Gustavsson, S., Neelissen, J., Ek, M., Olsson, L.-L., and Berg, S. (2012) Aminoimidazoles as BACE-1 inhibitors: the challenge to achieve *in vivo* brain efficacy. *Bioorganic and Medicinal Chemistry Letters*, **22**, 1854–1859.
 - 69 Cumming, J.N., Scott, J.D., Li, S.W., Cartwright, M., Chen, X., Cox, K., Forman, M., Gilbert, E.J., Hodgson, R., Hyde, L., Jin, Y., Kazakevich, I., Kuvelkar, R., Liang, X., Mei, H., Misiaszek, J., Orth, P., Stone, J.,

- Strickland, C., Voigt, J.H., Wang, H., Werner, B., Wong, J., Parker, E.M., Greenlee, W.J., Kennedy, M.E., and Stamford, A.W. (2015) Discovery of MK-8931: a BACE inhibitor in phase 3 clinical development for Alzheimer's disease. *Abstract MEDI 246 at 249th ACS National Meeting, Denver, CO, March 22–26, 2015*.
- 70 Forman, M., Tseng, J., Palcza, J., Leempols, J., Ramael, S., Krishna, G., Ma, L., Wagner, J., and Troyer, M. (2013) The novel BACE inhibitor MK-8931 dramatically lowers CSF A β peptides in healthy subjects: results from a rising single dose study. *Neurology*, **78**. doi: 10.1212/WNL.78.1_MeetingAbstracts.PL02.004.
 - 71 Merck Advances Development Program for Investigational Alzheimer's Disease Therapy, MK-8931. <http://www.mercknewsroom.com/news-release/prescription-medicine-news/merck-advances-development-program-investigational-alzheimer> (accessed 3 May 2015).
 - 72 An Efficacy and Safety Trial of MK-8931 in Mild to Moderate Alzheimer's Disease (P07738) (EPOCH). <http://www.clinicaltrials.gov/ct2/show/NCT01739348> (accessed 3 May 2015).
 - 73 Efficacy and Safety Trial of MK-8931 in Participants With Prodromal Alzheimer's Disease (MK-8931-019) (APECS). <http://www.clinicaltrials.gov/ct2/show/NCT01953601> (accessed 3 May 2015).
 - 74 Malamas, M., Erdei, J., Gunawan, I., Barnes, K., Johnson, M., Hui, Y., Turner, J., Hu, Y., Wagner, E., Fan, K., Olland, A., Bard, J., and Robichaud, A.J. (2009) Aminoimidazoles as potent and selective human β -secretase (BACE1) inhibitors. *Journal of Medicinal Chemistry*, **52**, 6314–6323.
 - 75 Assessment of Safety, Tolerability and Blood Concentrations of Single Doses of AZD3839 in Healthy Volunteers. <http://www.clinicaltrials.gov/ct2/show/NCT01348737> (accessed 3 May 2015).
 - 76 AZD3293 – Alzforum. <http://www.alzforum.org/therapeutics/azd3293-0> (accessed 22 July 2015).
 - 77 Lilly Voluntarily Terminates Phase II Study for LY2886721, a Beta Secretase Inhibitor, Being Investigated as a Treatment for Alzheimer's Disease. investo.lilly.com/releasedetail.cfm?ReleaseID=771353 (accessed 3 May 2015).
 - 78 E2609 – Alzforum. <http://www.alzforum.org/therapeutics/e2609> (accessed 22 July 2015).
 - 79 JNJ-5486191 – Alzforum. <http://www.alzforum.org/therapeutics/jnj-5486191> (accessed 22 July 2015).
 - 80 BACE Inhibitor Trial Put on Hold. <http://www.alzforum.org/news/research-news/bace-inhibitor-trial-put-hold> (accessed 3 May 2015).
 - 81 RG7129 – Alzforum. <http://www.alzforum.org/therapeutics/rg7129> (accessed 22 July 2015).
 - 82 Dineen, T.A., Chen, K., Cheng, A.C., Derakhchan, K., Epstein, O., Esmay, J., Hickman, D., Kreiman, C.E., Marx, I.E., Wahl, R.C., Wen, P.H., Weiss, M.M., Whittington, D.A., Wood, S., Freneau J Jr., R.T., White, R.D., and Patel, V.F. (2014) Inhibitors of β -site amyloid precursor protein cleaving enzyme (BACE1): identification of (S)-7-(2-fluoropyridin-3-yl)-3-((3-methyloxetan-3-yl)ethynyl)-5'-H-spiro[chromeno[2,3-b]pyridine-5,4'-oxazol]-2'-amine (AMG-8718). *Journal of Medicinal Chemistry*, **57**, 9811–9831.
 - 83 Wager, T.T., Chandrasekaran, R.Y., Hou, X., Troutman, M.D., Verhoest, P.R., Villalobos, A., and Will, Y. (2010) Defining desirable central nervous system drug space through the alignment of molecular properties, *in vitro* ADME, and safety attributes. *ACS Chemical Neuroscience*, **1**, 420–434.